DOE/METC-93/4113
(DE93000263)

Phased-Array Ultrasonic Surface Contour Mapping System

Technical Note

George E. Fasching
Wilma J. Loudin
David E. Paton
Nelson S. Smith, Jr.

November 1992

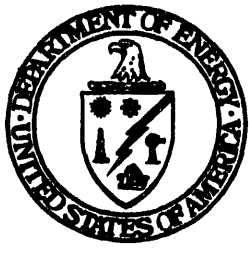

U.S. Department of Energy
Office of Fossil Energy
Morgantown Energy Technology Center
Morgantown, West Virginia

DISCLAIMER

DOE/METC-93/4113
(DE93000263)

Phased-Array Ultrasonic Surface Contour Mapping System

Technical Note

George E. Fasching
Wilma J. Loudin
David E. Paton
Nelson S. Smith, Jr.

U.S. Department of Energy
Office of Fossil Energy
Morgantown Energy Technology Center
P.O. Box 880
Morgantown, West Virginia 26507-0880

November 1992

Abstract

The development of reliable mechanistic models for prediction of conventional and fluidized-bed combustor and gasifier operation and solids flow behavior in silos or other solids handling and storage components requires knowledge of the contained solids flow characteristics. This knowledge is gained from dynamic experimental measurements of bed top surface contours in addition to measurements of bulk bed properties.

The surface contour mapping system (SCMS) provides a means of generating surface contour maps in real time with a unique, automatically focused, density-compensated, digital phased-array scanning, ultrasonic-range measurement system. The system is designed to operate in environments having gas temperatures up to 1,600 °F and pressures to 1,000 psig.

Computer simulation of several SCMS candidates and acoustic carrier modulation techniques indicates that a surface measurement resolution of ± 2 inches over a range of 5 to 20 feet distance between the transmit/receive (T/R) transducers and the bed surface can be expected. The simulation of a particular design, a 9-T/R, 25-pixel bed surface, in which the level of each pixel was randomly set between 5 and 7 feet below the plane of the T/R transducers, then measured using two different modulation techniques, produced excellent results. The simulation of this surface contour mapping system determined the value of the level of each of the 25 pixels to within ± 1 inch for over 95 percent of more than 100 test cases for one of the modulation techniques, and for over 99 percent of about 100 test cases for a second modulation technique. A hardware implementation of the design simulated but using only a two-T/R, three-pixel SCMS produced results very closely approximating those obtained during the simulation. During proof-of-concept tests of the two-T/R SCMS, the system output signal wave shapes used to produce the numerical value of pixel elevation were strikingly similar to the equivalent simulated wave shapes.

Contents

List of Figures

List of Figures
(Continued)

List of Figures
(Continued)

List of Tables

1 Introduction

The behavior of bulk materials stored in hoppers and silos and while being transferred into or out of storage in such vessels is of interest to those wanting to optimize the materials handling process. The behavior of materials in dynamic processing systems, such as combustors and fluidized beds, is important to those involved in the design, development, or operation of such systems. Such materials behavior has been studied using instrumentation designed to measure density (Almstedt 1987; Fasching and Smith 1991), particle velocities (Raso and Tirabasso 1983), circulation patterns (Lin, Chen, and Chao 1985; Merry and Davidson 1973), and other parameters within the bed of materials. This report deals with measurement of the behavior of the top surface of the material under both static and dynamic conditions. Knowledge of surface contours under static conditions would be useful for purposes such as materials inventory. Under dynamic conditions, control of the filling and emptying of hoppers, the fueling and ash removal processes for combustion/gasification vessels, and the monitoring and control of fluidized beds are candidates for application of the surface contour mapping system (SCMS).

The use of the SCMS in the harsh environment of a high-temperature reactor or a fluidized-bed combustor/gasifier is shown in Figure 1. The Transmit/Receive (T/R) phased-array section at the top of the vessel contains a set of acoustic transducers that are kept operable by the cooling water and the nitrogen purge illustrated in more detail in Figure 2. The transducers are used to generate a modulated, focused ultrasonic beam that scans the bed surface and to receive the beam after it has been reflected from the surface. The returned signals are processed to provide a three-dimensional measure of the elevation contour of the bed surface. The modulation placed upon the transmitted beam allows the efficient extraction of the elevation-determining signal from the noisy received signal.

2 Background

There are currently no known instruments existing that can provide the high-resolution, short-range, surface contour mapping capability of this system. An extensive on-line search of the technical literature for other non-radar contour mapping systems reported over the period from 1972 to the present yielded only seven fairly loosely related references. The researchers reporting in two of these references (Di Stefano et al. 1983; Merry and Davidson 1973) apply ultrasonic probes placed within an inch or less of the surface whose contour is to be measured. Redding (1982) describes the first known attempt at the application of radio-frequency techniques to ultrasonic measurement and imaging. Sackman (1981) uses reflected ultrasonic waves to generate three-dimensional contour maps of the ocean floor. The system uses a large number N of acoustic receivers, each appearing to be focused only on a portion of the floor, to generate an N-pixel representation of the contour map. Another ocean bed contour mapping system (Denbigh 1981) uses sidescan sonar to measure ocean depth correlated with range and direction measurements. Both of these ocean floor mapping systems appear to use long-range planar acoustic wavefronts as opposed to the short-range focused, converging acoustic beams used in the SCMS. Morgera (1973) developed an ocean bottom return signal model and a signal processor that showed promise of allowing wide swath ocean bottom mapping. Kujoory (1984) developed a laser-based range/elevation finder. The use of such an optical system would not be feasible in the dusty atmospheres of combustors and gasifiers where the SCMS is designed to function. The SCMS utilizes an automatically focused, digitally controlled, phased-array, ultrasonic transmitter/receiver system for surface contour measurement in high-temperature, high-pressure fluidized-bed environments.

3 System Description

3.1 Introduction

This section describes one particular SCMS design that was tested using computer simulation with two different ultrasonic signal modulation techniques and gives details on those subsystems where the circuit properties are critical to the attainment of accurate, high-resolution results. The design incorporates the usual resolution and accuracy-versus-cost tradeoffs. The number of transducers, each with its own transmit/receive channel of supporting electronics, is minimized to 9, and the number of bed surface pixels is maximized to 25. These compromise values were reached by the use of the simulation model described later in the Results of Simulation Tests section where the operation of the design is analyzed. It was found, by trying combinations of larger and smaller numbers of sensors and pixels than the 9 and 25 used, that acceptable values of range error and surface area resolution were obtained with these values.

In this section, we give a design for hardware implementation of a 9-ultrasonic T/R transducer array used with a 25-pixel, bed surface contour map. Other number combinations of transducers and pixels are possible, with more transducers requiring additional hardware and more pixels requiring additional transducers. However, a larger number of transducers allows a more narrow ultrasonic beam formation and, consequently, better resolution since a larger number of smaller pixels can be used.

3.2 Transmitter

Figure 1 shows the usual positioning of the SCMS T/R array at the top center of the monitored vessel. In this case, the vessel represents a fluidized-bed combustor or gasifier or other high-temperature process. The cooling water and cooling/dust-purging nitrogen necessary for transducer survival and operation are shown. These measures are not needed for a clean, low-temperature application. The T/R transducers (or elements) are ceramic piezoelectric crystals having a resonant frequency near 39 kHz for the design described herein. Other resonant frequencies may be used with appropriate changes in the system electronic circuitry and in the clock frequency. The cross-sectional view of the array shows details on the thermal-protection means provided for the transducers. Rubber cushions in the pressure containment cavity of the water-cooled, flange-mounted assembly provide vibration and thermal isolation of the T/R transducers. Nitrogen provides direct convection cooling of the transducers as well as dust-removal purging of the perforated sound baffles that serve as radiation shields. Castable ceramic foam insulation provides additional thermal protection.

Figures 3 and 4 show the layout of the 9 flange-mounted transducers and the 25 regions that define the pixel map of the surface of the bed material. The relative orientation of the transducers and the surface map is set such that the center of transducer 2 lies directly above the radial line that bisects pixel number 2.

The 9 T/R elements are shown in Figure 5 as a cross-section taken through the centers of transducers 1, 2, and 4. (See Figure 3.) Transducers 5, 6, and 9, although also shown in Figure 3, actually are in front of the cross section shown, and transducers 3, 7, and 8 are behind this cross section. Using the known transducer spacings and an assumed bed level 72 inches below the transducers, the distances from each transducer to the center of pixel 19, designated as point x, were found as indicated in Figure 5. Using a nominal value of 1,080 feet per second for the velocity of the ultrasonic wave, the wave travel time from each transducer to point x was found. These time values were used to determine the time delay to be applied to the excitation of each transducer assuming that those farthest away from point x (6 and 7) are excited at t = 0. These delay times are shown as the values in microseconds in Figure 5. These time relationships are shown more clearly in Figure 6, where the time delay values for the 9-cycle acoustical tone-burst transmission of modulation technique A (MTA) are also shown in terms of the number of system clock cycles. The same time delays are applied to the signals of modulation technique B (MTB) described in the next paragraph. The delay time calculations were done for each of the 25 pixels at each of 32 levels spaced at 0.5 foot intervals between the 5- and 20-foot elevations. The stored transmit delay times were then used to focus the beam upon each pixel. Upon reaching point x, the ultrasonic beam is reflected back to the nine transducers and reaches them in the order E, D, C, B, and A. Therefore, to recombine the signals properly in time, those signals traveling the shorter distances from point x to their transducers must be delayed at the input to the receiver circuitry relative to the signals traveling the greater distances. The electrical signals, produced by the echoes, exciting the B, C, D, and E transducers are stored serially as received until the A transducers are excited at the time defined as t = 0, then the signals are combined serially in time. For example, the B signal having arrived 63.3 μs ahead of t = 0 is delayed 63.3 μs before being released to be combined with the stored signals of the C, D, and E transducers and the just-arrived A signals. The corresponding delay times for each of the other 24 pixels are found (and stored as described later in the section) in like fashion.

A block diagram of one of the nine ultrasonic array element transmitter circuits is illustrated in Figure 7. The 39.0625 kHz sine-wave tone burst is generated by reading 8,192 digital values at the 10.0-MHz clock rate in sequence from an EPROM memory, so that when the values are converted to an analog signal by a digital-to-analog (D/A) converter and then passed through a bandpass filter, they form a synthesized N-cycle burst for modulation technique A (MTA). The synthesized 9-cycle tone burst is amplitude modulated by a low frequency sinusoid (such as the 1.30 kHz used here). Both the ultrasonic carrier and the modulation frequencies are linearly frequency modulated at different rates to provide unwanted (out-of-focus) echo signal rejection. Figure 6 shows only the MTA tone bursts appropriately delayed for each transducer. The second modulation scheme, MTB, is illustrated in Figure 8. Each of the four 4-cycle chips making up a 16-cycle tone burst starts with an initial phase shift of 0 °, ± 180 °, + 90 °, and - 90 °, respectively, as shown. The 16-cycle tone burst is then generated repetitively. In addition to the phase modulation shown, each of the chips is frequency modulated by a 1.30-kHz signal for producing a more distinct signature, making easier extraction from a noisy received signal. Each of the nine transducers is repetitively excited by the properly delayed tone bursts of MTA or MTB.

To provide the necessary phase delay for each array element's transmitted tone burst, the delay counter in Figure 7 is preset with the digital 1's complement values of the required delay supplied by the delay/phase EPROM. The delay/phase EPROM is programmed with 32 blocks of 32 phase values. Each block provides a set of phase values corresponding to 1 of 32 different average surface autofocusing levels, i.e., 5.0, 5.5, 6.0, 6.5, ..., 20.0 feet. The values within each block provide, from scan counter addressing, up to 32 scan points at each of the 0.5-foot increments. Density compensation is added to the phase delay by means of the density EPROM and adder. The density EPROM is programmed to correct the phase delay for changes in sound velocity with internal gas density according to the relationship:

$$\text{Phase delay} \propto \frac{1}{v} \propto \sqrt{d},$$

where d is the gas density, v is the sound velocity in gas, and α indicates proportionality. Amplitude control of the transmit tone-burst for array beam shaping is accomplished by means of an 8-bit by 8-bit digital multiplier and an amplitude EPROM that is programmed with 32 amplitude multipliers, one for each scan position. The EPROM is addressed by the 5-bit scan counter output.

The number of ultrasonic, full sine-wave cycles for MTA can be set at 2 or 4, then 8, 9, 10, ..., 16, and then 32, with a selector switch on the output of the sine-wave/pulse counter to reset flip-flop 2 (FF2). No provisions are made for selecting the number of cycles in each chip or of the number of chips in each tone burst for the MTB illustrated in Figure 7. These are fixed as shown in Figure 8.

A START pulse from the control and timing circuit in Figure 9 to all transmitter circuits initiates the array tone-burst transmission. The tone-burst phase delay for each array element is individually controlled digitally by its respective delay/phase EPROMs. Flip-flop 1 (FF1) in Figure 7 is set by START at all array transmitters simultaneously, and reset individually by each of their respective delay counters as they time out (count up to zero). As each one times out, they also set FF2, which then enables a 10.0-MHz clock gate to the sine-wave/pulse counter, starting the tone burst for the corresponding array transmitter. The tone burst is terminated when FF2 is reset by the sine-wave/pulse counter through the cycles-per-tone burst selector switch.

The analog tone burst developed by the D/A converter in Figure 7 is bandpass filtered and then applied to the power amplifier. The power amplifier is designed to boost the tone-burst level to about 100 V p-p at the transmit/antitransmit (TR/ATR) device transmitter input (T) shown in Figure 10.

3.3 Receiver/Range Processor

The echo signal R from each array element is routed by its TR/ATR device (see Figure 10) to its receiver, where it is amplified and filtered. The resulting high level (nominal 2 V p-p) is converted by the 8-bit A/D converter to digital sample values at up to the 10.0-Mhz clock rate. These values are amplitude modified for beam shape by the 8-bit by 8-bit multiplier, which gets its multiplicand from the programmed EPROM. The values stored in the amplitude EPROM correspond to the desired beam shape as the beam is scanned over the bed surface. The amplitude-adjusted digital signal values are next stored in alternating memories (receiver Memories A and B) to allow continuous receiving and processing of received echo signals. Memory A stores digital echo signals during receiver Period A while data previously stored in Memory B is being read and processed for range determination. The reverse takes place during receiver Period B on alternate tone-burst echo signals. The Store Memory Counter provides addressing for the memory that is on a "store" period. That address counter starts at a fixed time delay from the transmit start signal (Figure 9) and advances the address at the 10.0-Mhz rate in order to store digital samples from the A/D converter that are taken at the same clock rate. The 8k samples of the echo signal are stored during this period. During the next period, the 8k samples are read from that memory at the 10.0-Mhz rate, but the start of the read sequence is delayed by a Delay counter to provide the appropriate phase delay for that T/R element's echo to receive focusing, based on the distance from the surface target scan "spot" to that particular T/R element. The delay EPROM provides the 1's complement delay values, which are modified by the addition of the gas density compensation, to the preset input of the Delay counter. The Delay EPROM has 32 blocks of 32 scan delay values that are selected by a 7-bit autofocusing input to correspond to an average "spot" range from 5 to 20 feet for each 0.5 foot increment. START READ begins a read from memory by setting FF3, and STOP READ terminates a memory read by resetting FF4, while Reset 3, which occurs at the end of a read delay, resets FF3. The timing of these signals is given in Figure 11.

The delayed digital echo signals from all nine receivers of the T/R array are summed by receiver array adders such that they combine in phase as received after being reflected from the selected scan "spot" on the bed surface. This combined signal is then processed to find the onset of the received tone burst echo to determine the two-way sound wave travel time and, from that, the range to the "spot" using the density-corrected sound velocity. A 7-bit autofocusing signal is developed from the computed average range for a complete scan of the surface. The 32 ranges to the scanned "spots" on the surface are stored for alternate scans in range Memories A and B. The stored values are alternately read from these memories, and a display signal is generated for presenting a real-time, three-dimensional surface contour map on a video monitor.

3.4 Calibration/Standardization

Calibration/standardization, for a particular set of gas temperature, pressure, entrained dust, and other like conditions, is accomplished by periodically deploying a standardization target as shown in Figure 1, focusing on the target and then correcting the range and focus calibration accordingly.

4 Results of Simulation Tests

This section describes the computer simulation of the candidate SCMS presented in the System Description section and gives the results obtained for multiple tests of the capability of the SCMS in accurately producing surface contour maps. These results are presented and discussed for both MTA and MTB.

Figure 12 shows a simplified block diagram of the SCMS that was designed to include 9 T/R transducers and a 60-inch diameter bed surface divided into 25 pixels. Other designs using different numbers of transducers and pixels and expected to give comparable results are possible. Although not explicitly shown, provisions have been made for adding random fluctuations to the signal in the receiver subsystem to account for noise and other variations that would naturally occur in practical electronic circuits, and to account for reflected signals from the vessel walls and from out-of-focus points on the bed surface due to surface variations. This noise is introduced as variations in the amplitude of the received signals. These variations are the sum of the amplitude change produced by a random ± 1.5 inch variation in the pixel elevation during the time of signal reflection, and a ± 15 percent random change in the received signal amplitude to account for other sources of noise. The two modulation techniques, MTA and MTB, which are briefly described in the System Description section, are each used to produce pixel elevation values using a computer simulation of the SCMS.

The carrier sinusoid used in MTA and shown in Figure 12 has a frequency that is varied linearly from 39.0625 kHz at the beginning of a nine-cycle tone burst to a value (1 + 0.05) times its initial frequency at the end of the tone burst. The sinusoidal modulating signal has a frequency that is varied linearly from 1.30 kHz at the beginning of the tone burst to a value 1.50 times its initial frequency at the end of the tone burst. The frequency-modulated carrier is amplitude modulated with a modulation factor larger than 100 percent by the 1.30 kHz frequency-modulated wave. The phase-modulated acoustical signal used in MTB is illustrated in Figure 8 where details of one of the repetitive tone bursts are given. The 16-cycle tone burst is composed of four 4-cycle chips. The first chip consists of four cycles of the 39.0625 kHz acoustical sinusoidal signal starting at the beginning of the chip with zero phase shift. The sinusoid in Chip 2 starts with 180 ° phase shift immediately following the signal in Chip 1. Similarly, the sinusoid in Chip 3, starting with a phase shift of + 90 °, follows the sinusoid in Chip 2. Then the sinusoid in Chip 4 starts with a phase shift of - 90 ° and immediately follows the signal comprising Chip 3. The frequency of the 4-cycle sinusoid in each chip is increased linearly from 39.0625 kHz at the beginning of each chip to a value 2 percent higher at the end of the chip. These modulation schemes produce frequency spectra that can be processed to extract accurate transducer-to-pixel range values in the presence of extremely noisy echo signals. The modulated carrier for MTA is processed to produce nine (16 for MTB) cycle bursts of the carrier signal, with the starting time of each burst for both MTA and MTB appropriately delayed such that the ultrasonic signal produced by one T/R transducer adds in phase at the focus range with each of the similarly-processed signals from the other eight transducers at the center of the pixel being scanned. This process is repeated

for each of the other 24 pixels. Figure 3 shows the arrangement of the transducers used in the SCMS simulation work.

The transducers are mounted horizontally at the top center of a 5-foot diameter vertical vessel with a bed surface assumed, to simplify the simulation, to be limited to a range of 60 inches to 84 inches below the horizontal plane occupied by the transducers. The bed surface is divided into 25 pixels as shown in Figure 4, with transducer No. 2 in Figure 3 located directly above the angular center of pixel 2 and slightly displaced inward from its radial center. This specification of transducer-bed pixel orientation allows the calculation of the linear distance from the center of each transducer to the center of each bed-surface pixel. These distances together with the velocity of sound in the gas, corrected for conditions including gas specific gravity, temperature, and pressure, determine the relative delay times associated with the transmitted and received acoustic signals of each transducer.

The appropriately delayed tone burst for each transducer is increased in voltage level to the transducer rating in the power amplifier shown in Figure 12. The TR/ATR circuit directs this high-level signal to the transducer, while keeping it out of the receiver system. The transducer transmits an N-cycle (N = 9 or 16, depending on the modulation technique used) burst of acoustic waves, which, upon combining with the acoustic waves from the eight other transducers, are focused upon the pixel being examined. The reflected wave is returned to the transducer from which it was emitted as well as to the other eight transducers. The electrical return signal produced by a typical transducer receiving its own echo signal and the echoes caused by the other eight transducers is directed by the TR/ATR circuit to the preamplifier/ amplifier circuit of the receiver system. The one-transducer amplified range signal is appropriately time delayed and combined with the properly delayed range signals from the other eight transducers to produce the signal from which the bed level of the pixel being examined is extracted. After processing and A/D conversion, the combined range signal is stored for later analysis. The range signal is also passed on immediately to the Imaging System Processor matched filter, demodulator, and other circuits shown in Figure 12, where the equivalent range signals for each of the 25 pixels are used to generate bed-level information for the real-time display. The system also contains a specially designed custom filter, which accepts the range signal for each pixel and produces as an output a range estimate for the pixel that serves as the focus range on the next scan. This procedure is discussed in more detail beginning on the next page.

The filtering scheme that allows the extraction of the range signal from the noisy, combined sum of properly delayed echo signals from all nine transducers is illustrated in more detail in Figure 13. The results obtained using this filtering system with both MTA and MTB are discussed now. The positive attributes of the system for both modulation techniques are illustrated by omitting one or more of the filtering sections and showing the effects of these omissions upon signal wave shapes and pixel elevation values. The results are given first for MTA, then those for MTB follow in the next paragraph. Figures 14 through 17 show the signal waveforms for MTA at various points in the receiver system in Figure 13 for the beam directed at pixel 1, which has a true range of 60 inches, with a focus range of 60 inches. Figures 18 through 21 give the equivalent figures for the scanning of pixel 2, which has a true range of 83.92 inches (84 inches, nominally), with a beam focus range of

60 inches. Figures 14 and 18 show the combined delayed digital signals at the input to the first block, Matched Finite Impulse Response (FIR) filter, for the two illustrative cases. The use of the matched filter causes the signal-to-noise ratio at the output of the filter to be maximized. In each of Figures 14 through 21, the column of circle points marks the beam focus range used, and the column of square points indicates the random-valued, preset true range to the interrogated pixel. The horizontal line marks the 50 percent of full scale used as the threshold for valid range estimates. The seed number 9 in each of the figures discussed here denotes the input to the computer program random number generator that was used to select the random set of 25 pixel elevation values. While the simulation tests were run for a number of different pixel elevation sets, only that set derived using seed 9 is discussed here for ease of comparison of results. Figures 15 and 19 show the signal at the output of the second block, the Gaussian FIR low-pass filter, for the two cases. This signal is demodulated (squared) and smoothed with another low-pass filter. The signal waveform for each of the two cases at the output of this second low-pass filter is given in Figures 16 and 20. The signal at this point is then directed both to the range detector and to the input to the high-pass custom FIR filter. The range detector uses the 50 percent threshold and takes the largest peak above this threshold. The 50 percent threshold was chosen arbitrarily, and other values could be chosen to obtain the estimate of the range to the scanned pixel for this step of the range determination process. Early in the MTA simulation studies, it was noted that the ultrasonic signal modulation scheme caused a closely spaced pair of large peaks, evident in Figures 16 and 20, to appear near the true range value. The custom filter was designed to emphasize these dual peaks relative to the other signals present that would predict incorrect range values. Figures 17 and 21 show the resultant signals at the output of the custom filter. This output is processed by a peak detector, where the value of the range to the pixel is determined as the range value at the largest signal peak. This range value is then used as the focus range to the scanned pixel on the next set of 25 pixel range measurements. For those cases where the surface elevation map changes by less than several inches between scans, the focus range is then optimum for accurate range determination, as will be shown next.

Figures obtained using MTB that are equivalent to Figures 14 through 21, that showed signal waveforms throughout the receiver subsystem for MTA, are now discussed. It should be noted that the two sets of figures are not exactly equivalent since pixel 1, having a true range of 60 inches, was scanned using a focus range of 60 inches for MTA but with a focus range of 72 inches for MTB. For pixel 2, which had a true nominal range of 84 inches, a focus range of 60 inches was used for MTA and 72 inches for MTB. Figures 22 though 25 for pixel 1 and Figures 26 through 29 for pixel 2 show the MTB signal at selected points in the signal-processing receiver subsystem. Figures 22 and 26 shows the received signal at the input to the matched filter, Figures 23 and 27 at the output of the matched filter and the input to the first low-pass (LP) smoothing filter, Figures 24 and 28 at the output of the first LP filter and the input to the second LP filter, and Figures 25 and 29 at the output of the second LP filter. The column of circle points again marks the beam focus range used, and the column of square points marks the true range of the pixel being examined. The threshold indicated by the horizontal line was taken for MTB as 99 percent of full scale. As discussed for MTA, the output of the second LP filter is processed by a peak-catching circuit to produce the estimate of the range to, or the elevation of, the pixel being sonified. This signal serves also as the input to the custom filter, which produces the estimate of pixel range to be used as the focus for this pixel on the next set of 25-pixel scans.

As a means of showing the positive attributes of the SCMS electronic design for both MTA and MTB, a series of measurements of the same randomly assigned pixel elevation values (seed 9) were simulated with the system as designed having all filters included for signal processing. The simulated measurements were then repeated for the same surface contour with the input matched filter removed. This removes the signal-to-noise ratio maximization action of the filter and allows noise to contribute more to error in pixel range estimation. The simulated measurements were then run a third time for the same surface contour, with both the input matched filter and both of the low-pass FIR filters removed. These measurements lose the advantages of both signal smoothing and noise bandwidth reduction provided by the low-pass filters and the signal-to-noise maximization of the matched filter.

The measured pixel elevation values obtained using MTA are now discussed and compared to the randomly selected, known values set by seed number 9. The measured results obtained for the same set of known elevation values using MTB then follow. Figures 30 through 32 show the 25-pixel true and measured levels for fixed, focused ranges of 60, 72, and 84 inches, for the system complete with all filters. The system then selected the largest range signal from the 60-, 72-, and 84-inch trials and used its range prediction as the pixel level for each of the 25 pixels. These results are presented in Figure 33. This procedure simulates operation upon startup with an unknown bed contour. The focus range for each pixel would be randomly selected for each consecutive scan until the custom filter output provides a focus range close to the measured range. An alternate procedure for an expected bed range of 5 to 20 feet would be to scan the bed surface at range intervals of 2 to 3 feet and to use the largest returned signals as the first trial focus range. Once this zeroing in on each pixel level has been attained, the individual focus ranges are updated by using the output of the custom filter from scan to scan.

Figures 34 through 36 give the actual range values and the range measurement error for each of the 25 pixels at focus ranges of 60, 72, and 84 inches with the signal-to-noise maximization action of the matched filter removed. Then Figure 37 shows the true range values and the measured range values for each pixel for this case. The measured range value was found using the range taken as predicted by the largest signal peak appearing at the input to the custom filter. The results compared to those in Figures 30 through 32 show the value of signal-to-noise ratio optimization at the front end of the combined signal processing system.

The value of the combined action of the matched filter and the two low-pass signal-smoothing filters at the input and output of the demodulator section is illustrated in Figures 38 through 40. The measurement errors resulting when determining the same preset pixel levels with the effects of all three of these filters removed are illustrated in these figures and indicates the value of the collective action of all three filters. Figure 41 gives the results when the largest range signal appearing at the input of the range detector of the 60-, 72-, and 84-inch focus range trials is used to define the measured range.

Measurements of one set of pixel elevations using MTB are now discussed. The elevation set corresponding to seed number 9 is used so that the results using MTA and MTB can

be compared for the same set of elevations. The measured range (or elevation) values obtained for the SCMS complete with all filters are given in Figures 42 (focus range of 60 inches), 43 (focus range of 72 inches), and 44 (focus range of 84 inches). The known, randomly preset values of each of the pixel elevations are also shown on each of these figures for ease of evaluation of measurement error. The elevation values measured using the largest signal value (in the equivalent of Figure 24) for each pixel in Figures 42, 43, and 44 are given in Figure 45. The high degree of accuracy in determination of the surface contour elevation by the complete SCMS, pixel by pixel, is clearly evident in this figure. To illustrate this point more completely, the same pixel elevation set is measured with selected portions of the SCMS disabled.

First, Figures 46, 47, and 48 for focus ranges of 60, 72, and 84 inches, respectively, show the measured elevation values with the omission of the matched filter at the input to the receiver section of the SCMS. Then, Figure 49 shows the measured elevations using the highest processed received signal (the equivalent for each pixel of the peak signal in Figure 24) at the input to the custom filter. A comparison of the results shown in Figures 46 through 49 to those in the counterpart figures in Figures 42 through 45 illustrates the value of the signal-to-noise optimization properties of the matched filter.

A comparison of Figures 50 through 53, which were obtained without the matched filter and the two low-pass filters (at the input and the output of the demodulator), with the sets in Figures 46 through 49 and 42 through 45 shows the value of the filters included in the SCMS design in minimizing elevation measurement error.

Table 1 gives a summary of the root-mean-square (rms) error of the measurements presented in Figures 30 through 41 for MTA. These generally indicate the effectiveness of the system design incorporating signal enhancement filtering systems. The simulation also suggests in this summary that the implemented SCMS including all filters would have an average range determination error of around ± 0.25 to ± 0.35 inches for an expected bed level between 5 and 7 feet below the transducers. Assuming a linear relationship between range error and expected bed level range and including the effects of changes in variables such as temperature, gas density, and the like, an error of around ± 2 inches as our best estimate could be expected for a bed level range of 5 to 20 feet. The rms errors for the measurements shown in Figures 42 through 53 for MTB are given in Table 2. For the design that includes all filters, the error was about ± 0.6 to ± 0.9 inches for a bed level between 5 and 7 feet below the transducers, which would extrapolate to an expected error of around ± 3 inches for an expected bed level of 5 to 20 feet.

Although a general comparison of the error across Tables 1 and 2 shows MTA having less error than MTB, for many cases, with the reverse true in other cases, these tables give only a comparison of error between two randomly chosen MTA and MTB tests. An overall assessment of the more than 100 tests for each of the modulating techniques, showed the total error for MTB to be better than that for MTA for around 99 percent of the system conditions defined in each row of the tables. In addition, since only a few carrier modulating techniques were tried before selecting those of the MTA and MTB, it would be expected that other modulating techniques could be developed to improve the accuracy of range measurements.

Table 1. SCMS Simulation Elevation rms Errors Modulation Technique A

	At Input to Custom Filter				
	Center Pixel (Inches)	Inner Ring (Inches)	Outer Ring (Inches)	Total* (Inches)	System Condition and Focus Range Used All Filters Used
1	0.2720	9.1216	8.1557	8.3185	60 Inches
2	0.2150	0.3836	3.9697	3.1835	72 Inches
3	0.1860	2.7761	3.6066	3.2852	84 Inches
4	0.2720	0.3418	0.3546	0.3476	Best of 3 Matched Filter Removed
5	0.2720	1.3626	6.7560	5.4597	60 Inches
6	0.2150	1.1358	5.4072	4.3734	72 Inches
7	0.1860	1.2626	5.0133	4.0739	84 Inches
8	0.2720	1.2277	4.6620	3.7941	Best of 3 Matched and 2 Low-Pass Filters Removed
9	0.0420	15.1911	9.6907	11.5736	60 Inches
10	0.0130	8.1760	7.6243	7.6547	72 Inches
11	24.7260	2.6296	7.0827	7.6664	84 Inches
12	0.2720	4.4313	6.7093	5.9242	Best of 3

* The total error is the weighted average error over the 1 center pixel, the 8 inner-ring pixels, and the 16 outer-ring pixels. For example, the total error for this first row was found as:

$$\text{Total} = \left\{\frac{1}{25}\left[(0.2720)^2 \times 1 + (9.1216)^2 \times 8 + (8.1557)^2 \times 16\right]\right\}^{1/2} = 8.3185 \text{ inches}$$

Table 2. SCMS Simulation Elevation rms Errors
Modulation Technique B

	At Input to Custom Filter				At Output of Custom Filter				System Condition and Focus Used
	Center Pixel (Inches)	Inner Ring (Inches)	Outer Ring (Inches)	Total* (Inches)	Center Pixel (Inches)	Inner Ring (Inches)	Outer Ring (Inches)	Total* (Inches)	All Filters Used
1	1.3200	0.8956	6.5601	5.2791	1.6050	1.4749	4.8713	3.9982	60 Inches
2	0.6200	0.7616	0.5692	0.6390	1.5270	1.4987	1.2540	1.3485	72 Inches
3	0.5430	0.9690	2.2853	1.9117	1.4760	1.5027	1.8225	1.7133	84 Inches
4	0.6200	0.9072	0.5633	0.6941	1.5270	1.4972	1.2947	1.3724	Best of 3
									Matched Filter Removed
5	1.8680	1.0693	5.8418	4.7272	0.3610	0.5677	5.9278	4.7537	60 Inches
6	0.6500	2.9856	5.7600	4.9095	0.3650	2.6651	4.9139	4.2110	72 Inches
7	1.2780	4.6217	5.7904	5.3255	0.4170	2.2631	3.4726	3.0600	84 Inches
8	0.6500	4.6949	5.8038	5.3505	0.3650	2.6808	5.2695	4.4807	Best of 3
									Matched and 2 Low-Pass Filters Removed
9	0.9350	13.9039	7.4943	9.8915	0.2090	13.4679	7.9272	9.9128	60 Inches
10	24.9630	7.4504	7.8671	9.0719	24.0810	8.8398	5.9702	8.4269	72 Inches
11	21.0490	11.2540	8.7162	10.3380	25.4030	11.1914	8.6854	10.6851	84 Inches
12	0.9350	8.2449	7.0218	7.3037	0.2090	8.1736	6.4951	6.9555	Best of 3

* The total error is defined under Table 1.

5 Experimental Results

To verify the capability of a practical hardware SCMS to produce the results predicted by the computer simulation, an effective two-transducer T/R system using MTB was constructed. For these preliminary tests, the two transmit/receive systems were bread-boarded, not installed, on more stable printed-circuit boards. To minimize crosstalk between the transmitter and receiver circuits, two transducers were used to produce an effective one-transducer T/R element. One of these transducers was connected at the output of the transmitter subsystem (with the TR/ATR subsystem disconnected), and the other transducer, mounted below and within an inch of the first transducer, was connected at the input to the receiver subsystem. A second two-transducer set was mounted a horizontal distance of 16 inches from the first set. The two T/R transducer pairs were pointed toward three acoustically reflective vertical surfaces facing the T/R elements. The three surfaces represented three, 1-foot square pixels, each located at different distances (± 3 to ± 5 inches) from the transducers at a nominal distance of about 66 inches. Preliminary tests showed that the two-T/R SCMS system was able to scan the three pixels, and the system was able to process the returned signal for range estimates. While these estimates were not as accurate as predicted by the nine T/R simulation, the measurements indicated to us that when seven more T/R devices are added, the signal-to-noise ratio will be improved to the point where the range measurement error will be within the simulation-predicted range. In addition, the signal at the input to the custom filter, when displayed on an oscilloscope, looked strikingly close to those obtained during simulation tests. (For example, see Figure 24.)

6 Summary

The SCMS design described in this paper includes features to allow for operation in the face of the effects of the high-temperature, dust-filled environments encountered in coal handling and utilization systems. The signal generation and processing circuits implement designs based upon principles utilized to permit extraction of surface elevation information from acoustic signals collected by the transducer array as echoes from the surface in this environment. The echo signal collected by one of the transducers contains noise produced by gas temperature, pressure, and density fluctuations, sharp irregularities in the bed surface, reflections from the vessel walls, and the reception of echoes produced by transmissions from all of the other eight transducers.

The system design includes:

- A T/R phased array of acoustic transducers provided with thermal radiation shielding and insulation, water cooling, and nitrogen purging to protect the T/R transducers from the devastating effects of the 1,600°F fluidized-bed temperatures and from entrained ash and dust.

- Gas density correction of range calculations to compensate for ultrasonic wave velocity variation with density.

- An ultrasonic frequency tunable by single adjustment of the master clock frequency. For example, use of a 6.4-MHz clock for a 25-kHz ultrasonic signal frequency or use of a 10.24-MHz clock to produce a 40-kHz ultrasonic wave.

- Single step adjustment of the pulse width of the ultrasonic tone burst by selection of an integer number multiple (2, 4, 8, 9, 10, ..., 15, 16, and 32) of the number of periods of the ultrasonic sinusoid to appear in the tone burst.

- Rapid surface scanning and control of ultrasonic beam shape by use of multiple ultrasonic T/R transducers coupled to individual digital amplitude and phase controllers for both transmit and receive functions.

- Digital control of amplitude and phase of transmitted and received ultrasonic signals to provide repeatable and precise amplitude to within ± 0.5 percent and phase to within ± 1.41 degrees.

- Application of wave propagation velocity correction for variations in gas medium temperature, pressure, and composition to the transmit- and receive-phase controllers to maintain adequate focusing over a wide range of gas conditions.

- Incorporation of autofocusing by computing the estimated range to the bed surface for each pixel and employing a feedback adjustment to the phase of the transmitted and received signals.

- Periodic deployment of a calibration target of known range and position to provide frequent calibration standardization.

- Use of pairs of alternating receiving memories and range memories to avoid loss of alternate scan signals, thus maximizing scan rate.

- Enhancement of the rejection of out-of-focus and other interfering signals by incorporation of amplitude-, phase-, and frequency-modulated tone-burst transducer excitation signals.

- Maximization of signal-to-noise ratio in the received-signal processing system by use of matched filters.

- Optimization of the combined, received-signal, conversion-to-range value process through dual signal peak emphasis in the custom high pass filter.

The SCMS offers unique measurement and monitoring capabilities to the utility and chemical industries, and to materials handling processes where surface contour maps are required. These contour maps could be used for flow monitoring and for bed level determination for material inventory in bins, hoppers, silos and stockpiles, and for gasifier- and fluidized-bed studies and operation. This system can also provide measurements to characterize the flow of solids in silos, hoppers, and lines in support of fossil energy research for the generation of a mechanistic solids flow modeling data base.

7 References

Almstedt, A.E. 1987. Distribution of the Gas Flow in Fluidized Beds With a Slugging Behavior. *Chemical Engineering Science* 42(3):581-590.

Denbigh, P.N. 1981. Stereoscopic Visualization and Contour Mapping of the Sea Bed Using BASS, 191-311. Conference on Electronics for Ocean Technology. IERE, London.

Di Stefano, T.H., R. Hammer, R.L. Hollis, and V.B. Jipson. 1983. Acoustic Contour Mapping. *IBM Technical Disclosure Bulletin* 25(10):5103-8.

Fasching, G.E., and N.S. Smith. 1991. A Capacitive System for Three-Dimensional Imaging of Fluidized Beds. *Rev. Sci. Instrum.* 62(9):2243-2251.

Kujoory, M.A. 1984. Real-Time Range and Evaluation Finder. *Proceedings of the IEEE* 72(12):1821-1822.

Lin, J.S., M.M. Chen, and B.T. Chao. 1985. A Novel Radioactive Particle Tracking Facility For Measurement of Solids Motion in Gas Fluidized Beds. *AIChE Journal* 31(3):465-473.

Merry, J.M.D., and J.F. Davidson. 1973. "Gulf Stream" Circulation in Shallow Fluidized Beds. *Trans. Instn. Chem. Engrs.* 51:361-368.

Morgera, S.D. 1973. Signal Processing for Precise Ocean Mapping. IEEE International Conference on Engineering in the Ocean Environment, 118-23. IEEE, N.Y.

Raso, G., and G. Tirabasso. 1983. An Impact Probe for Local Analysis of Gas-Solid Flow. *Powder Technology* 34(2):151-159.

Redding, R.J. 1982. Acoustic Imaging. In *Proceedings of the Tenth International Symposium on Acoustical Imaging*, 143-9. Plenum, N.Y.

Sackman, G.L. Ultrasonic Image System. September 1981. U.S. Patent 4288866.

8 Bibliography

Carlin, B. 1960. *Ultrasonics.* New York: McGraw-Hill Book Company, Incorporated.

Embree, P.M., and B. Kimble. 1991. *C Language Algorithms for Digital Signal Processing.* Englewood Cliffs, New Jersey: Prentice Hall.

Dixon, R.C. 1984. *Spread Spectrum Systems.* New York: John Wiley and Sons.

Kinser, L.E., and A.R. Frey. 1962. *Fundamentals of Acoustics.* New York: John Wiley and Sons.

Kraus, J.D. 1950. *Antennas.* New York: McGraw-Hill Book Company, Incorporated.

Lee, K.F. 1984. *Principles of Antenna Theory.* New York: John Wiley and Sons.

Reintjes, J.F., and G.T. Coate. 1952. *Principles of Radar.* New York: McGraw-Hill Book Company, Incorporated.

Schoenwald, J.S., M.S. Black, J.F. Martin, G.A. Arnold, and T.A. Allison. 1987. Acoustic Range Sensing Servo Control: Improved Robot Positioning and Trajectory. *IEEE Transactions on Ultrasonics, Ferroelectrics and Frequency Control.* UFFC-34(2):225-231.

Szilard, J. 1982. *Ultrasonic Testing.* New York: John Wiley and Sons.

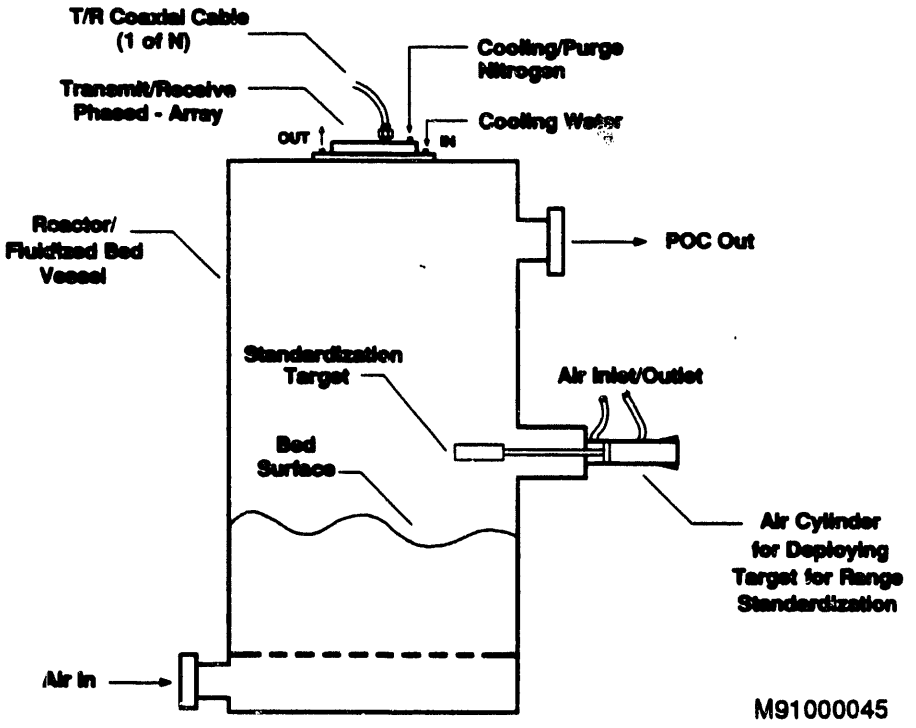

Figure 1. Application of Surface Contour Mapping System

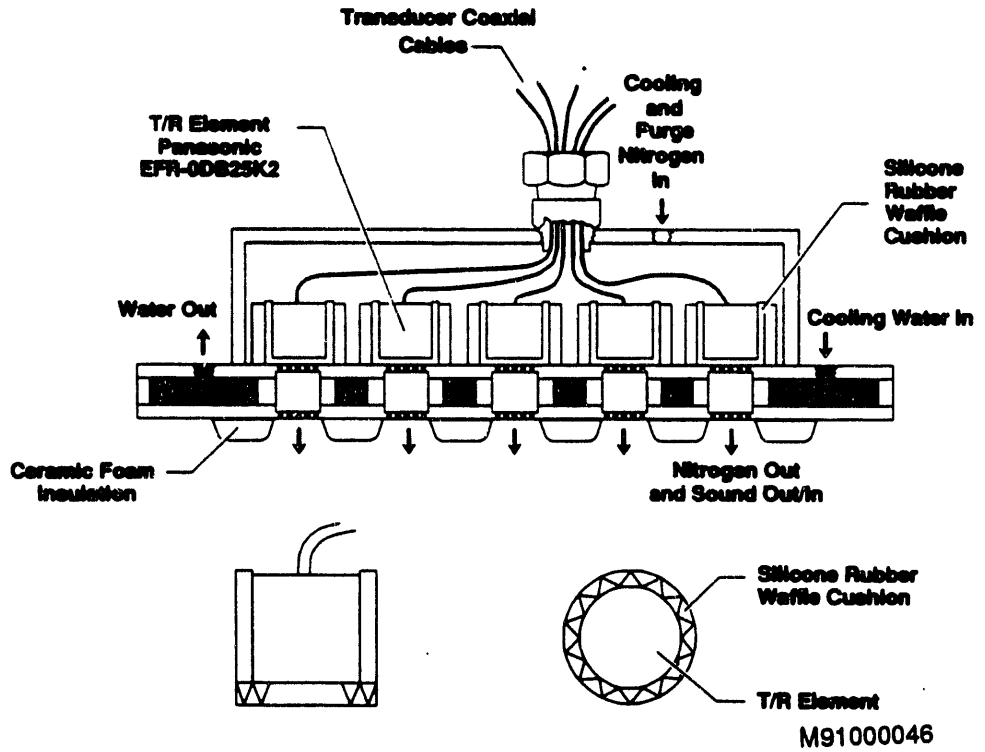

Figure 2. Transmit/Receive Array

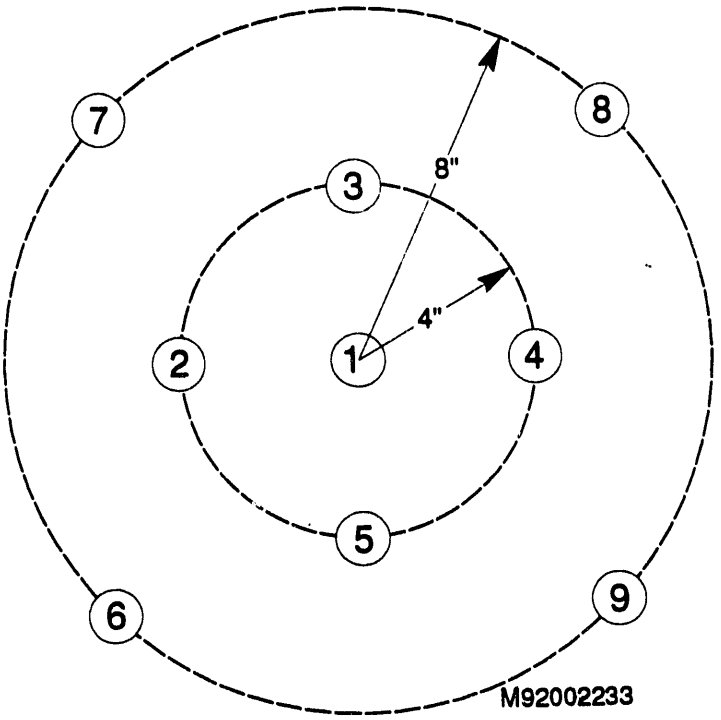

Figure 3. Transmit/Receive Transducer Layout

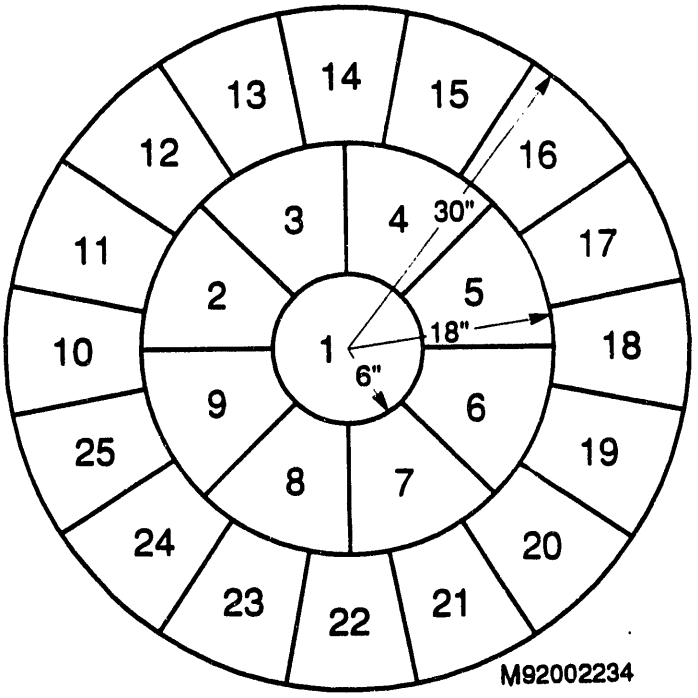

Figure 4. Bed Surface Pixel Designation

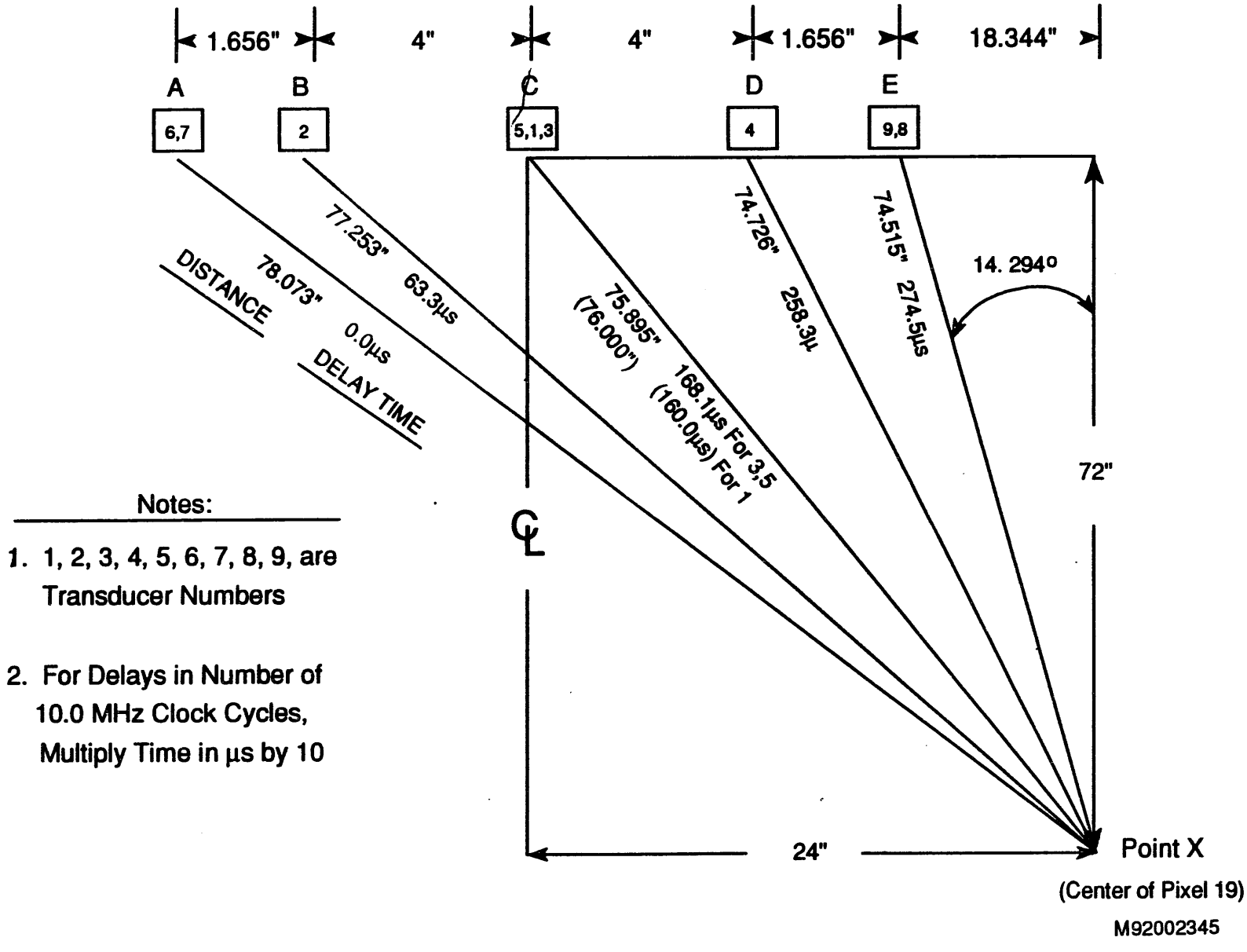

Figure 5. Time Delay for Beam Focusing

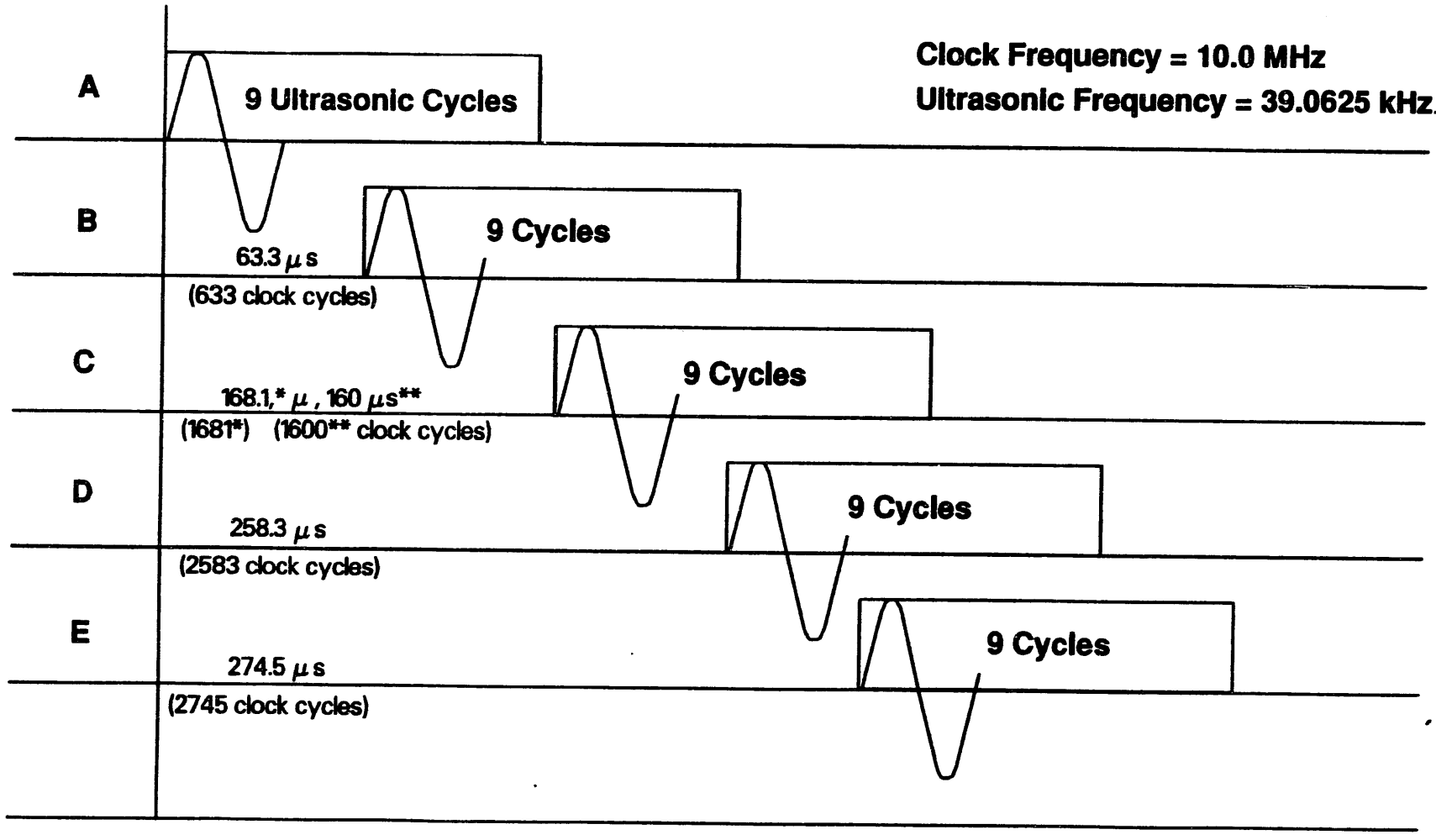

*For Transducer No. 1

**For Transducer Numbers 3 and 5

M91000048

Figure 6. Tone Burst Transmission Delay

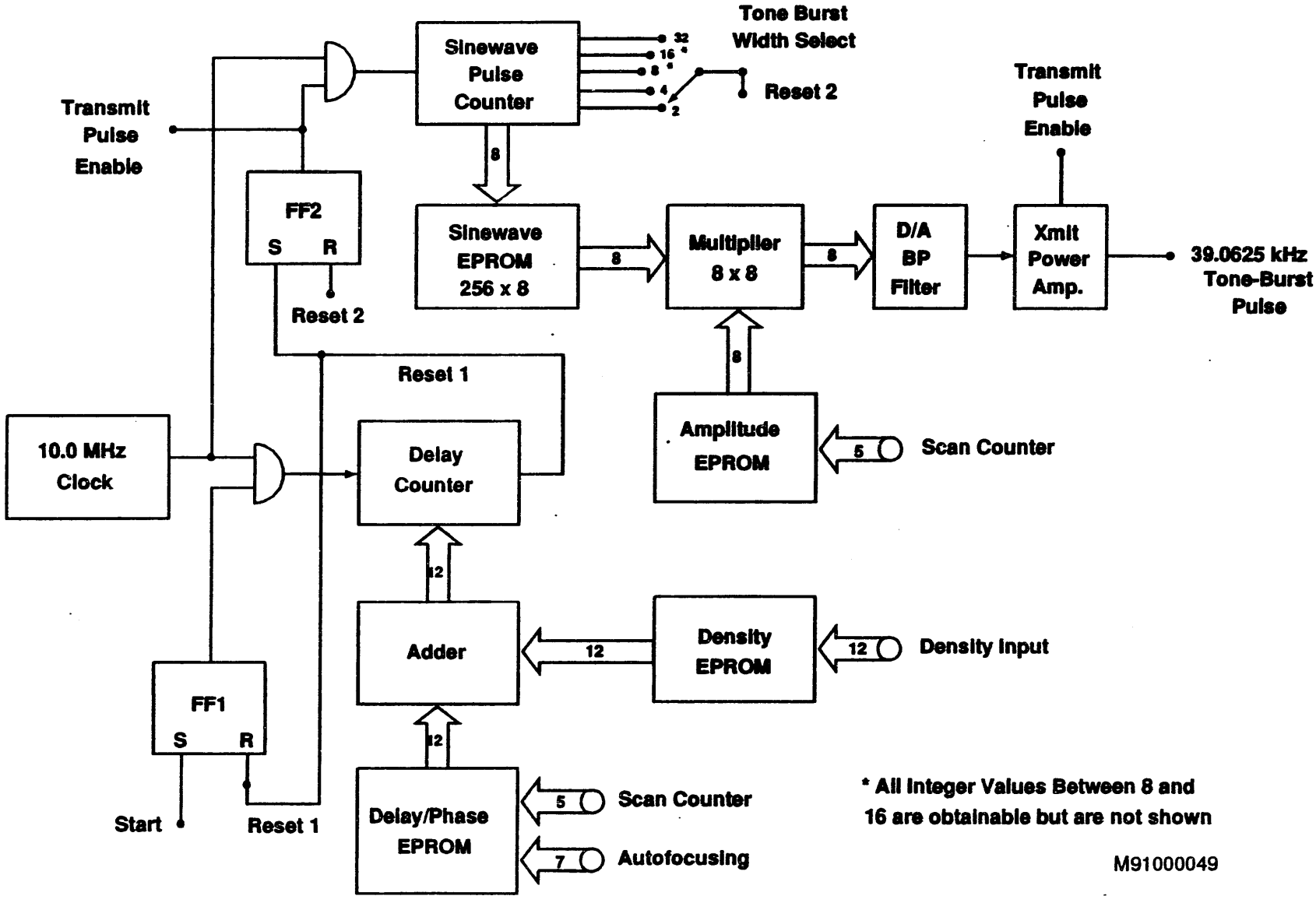

Figure 7. Transmitter Diagram

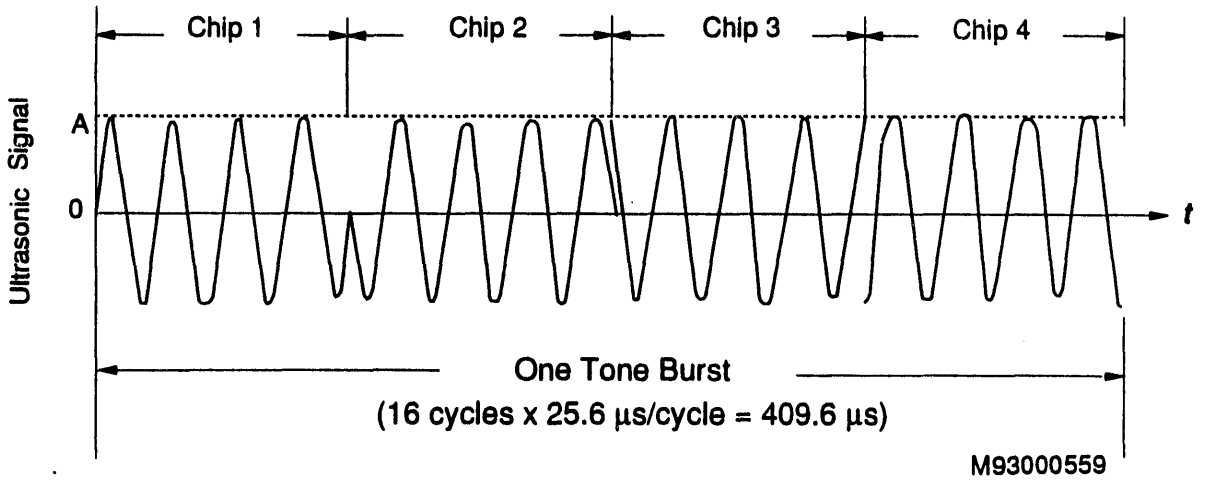

Figure 8. Tone Burst Using Modulation Technique B (MTB)

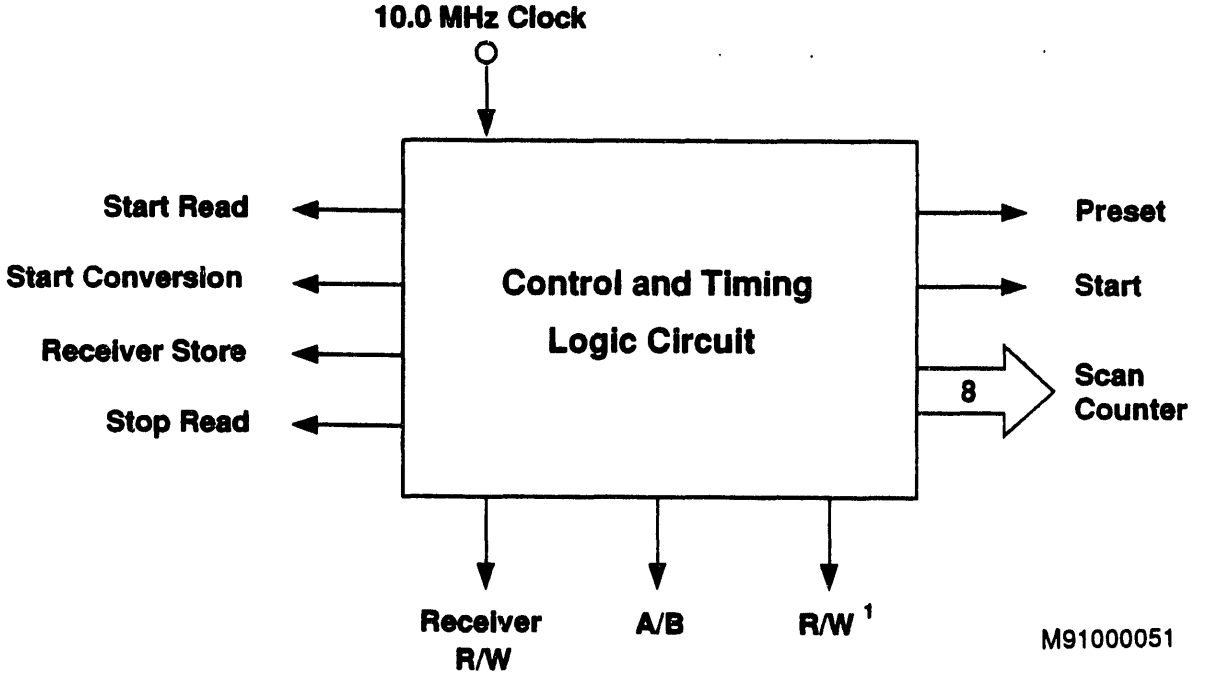

Figure 9. Control and Timing Logic Circuit

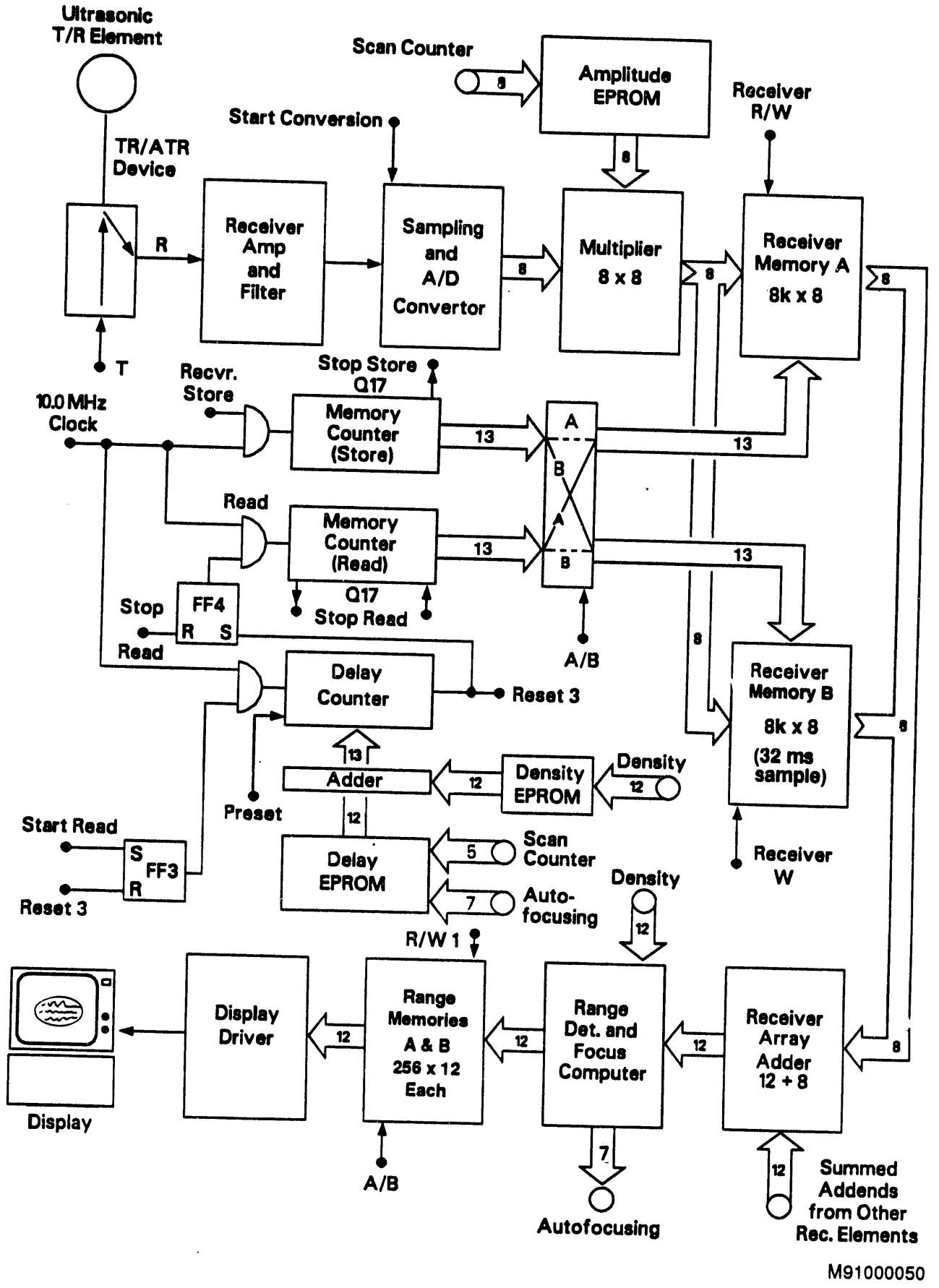

Figure 10. Receiver Diagram

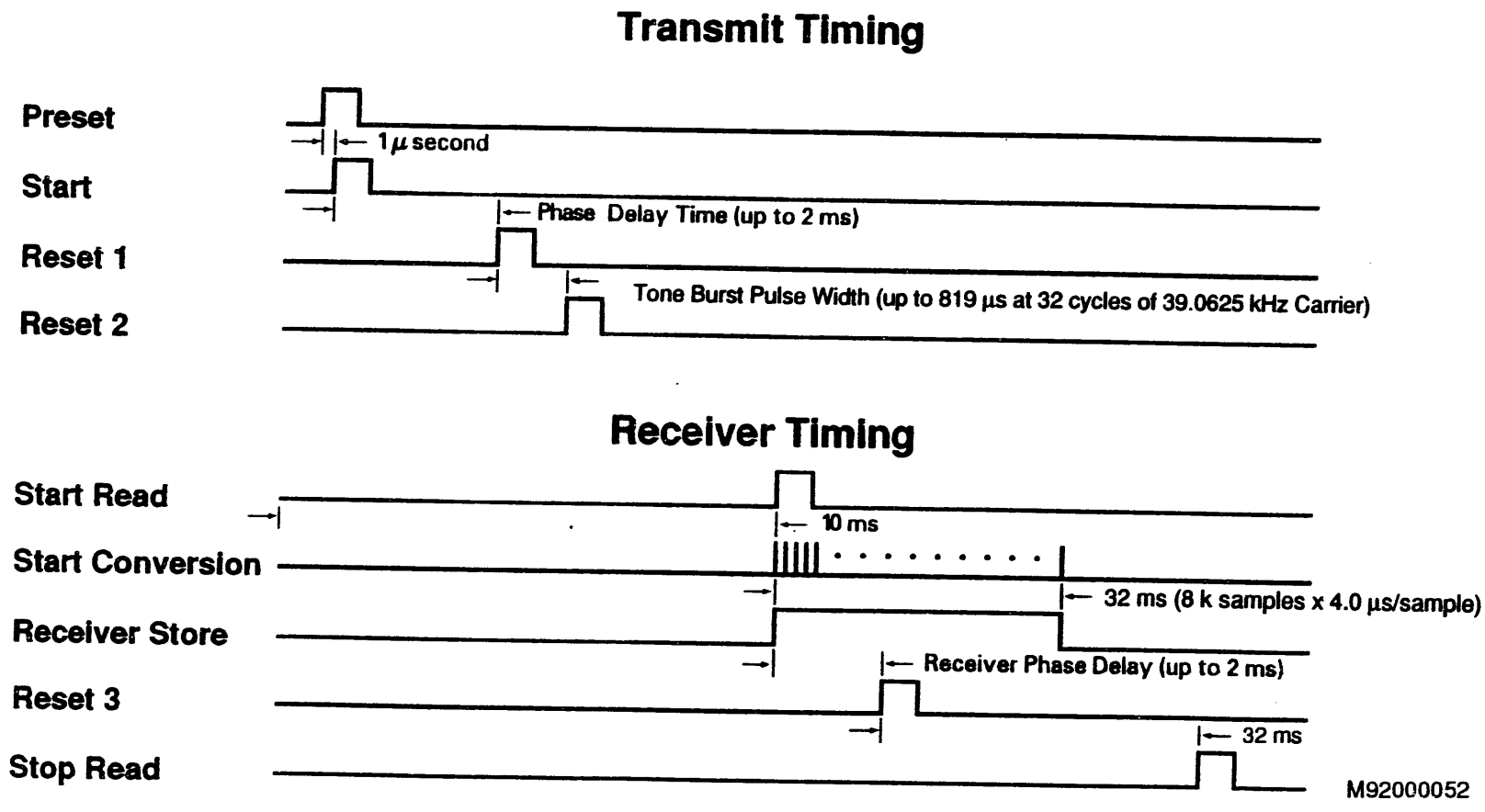

Figure 11. Timing Diagrams

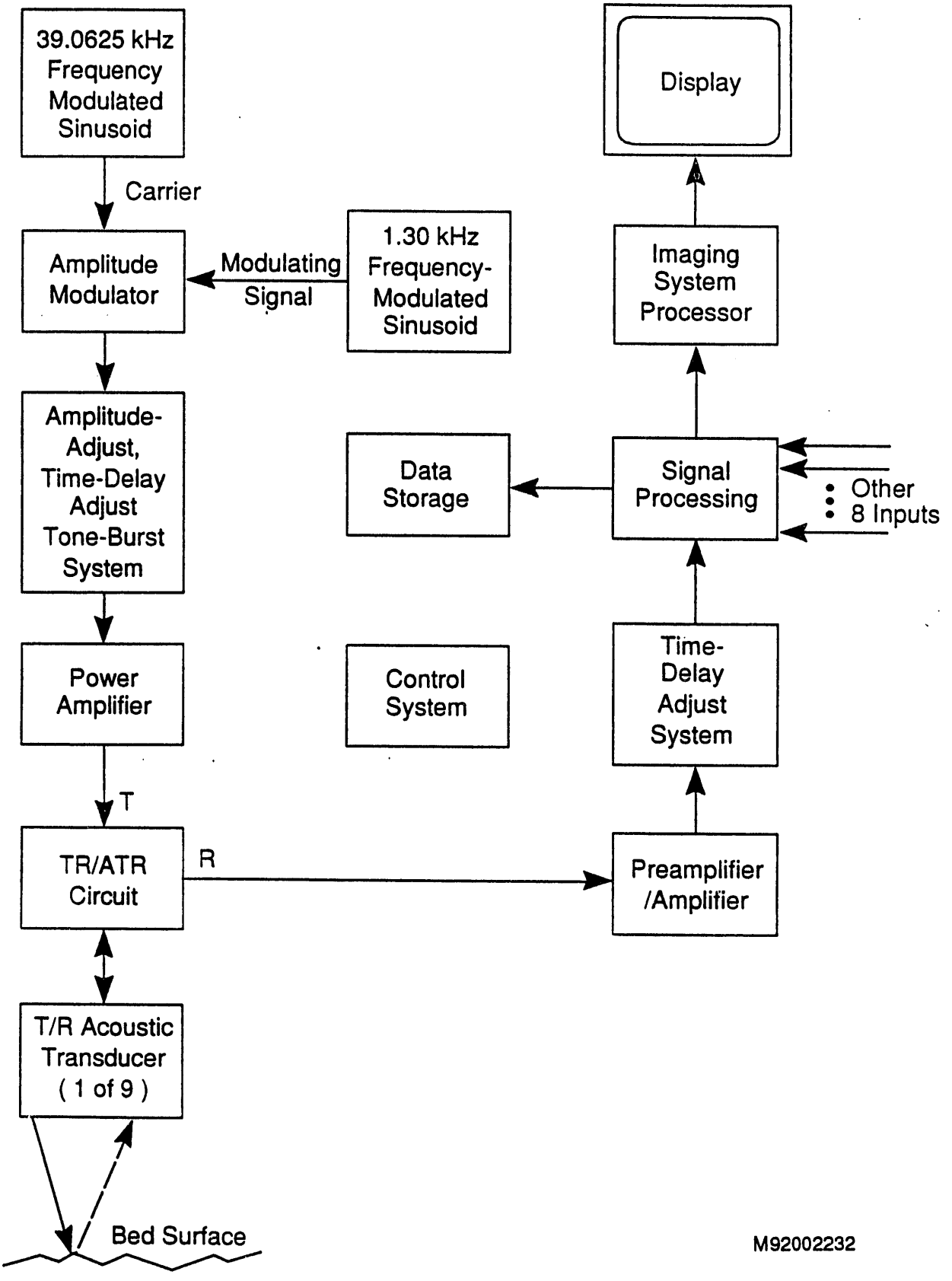

Figure 12. Surface Contour Mapping System Block Diagram

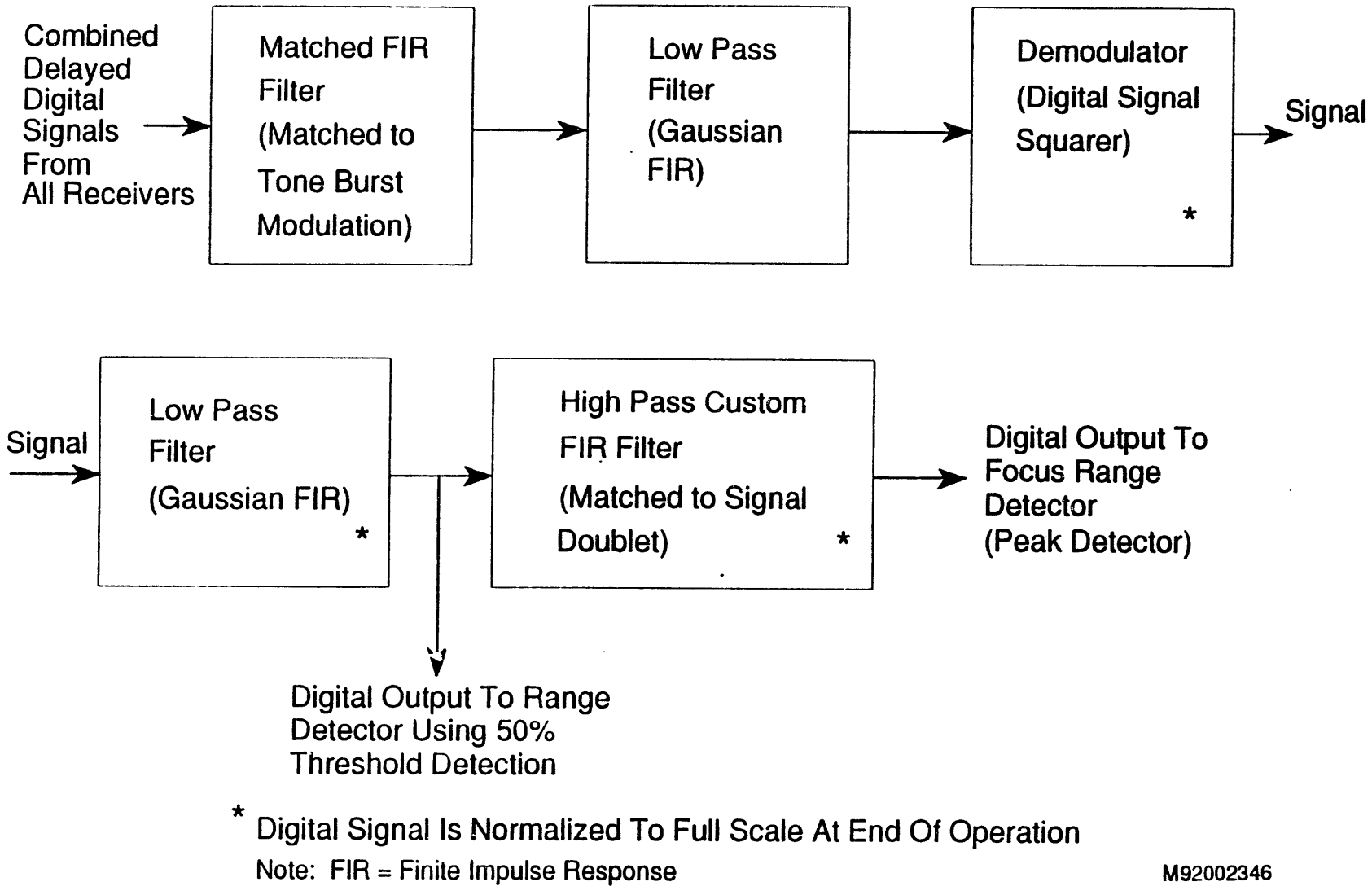

Figure 13. Signal Processing Block Diagram

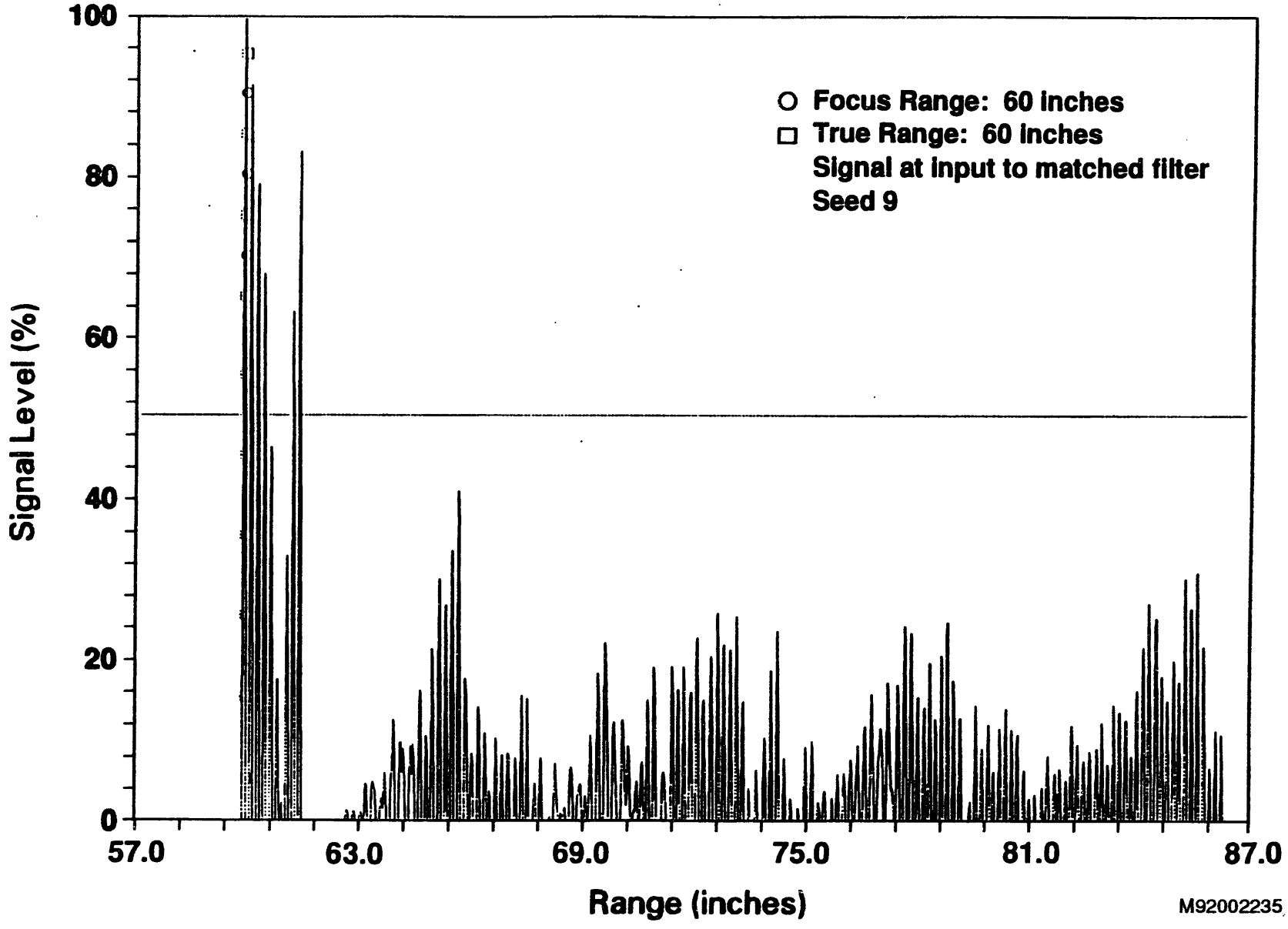

Figure 14. SCMS Receiver Signal, Pixel No. 1, MTA Signal at Input to Matched Filter

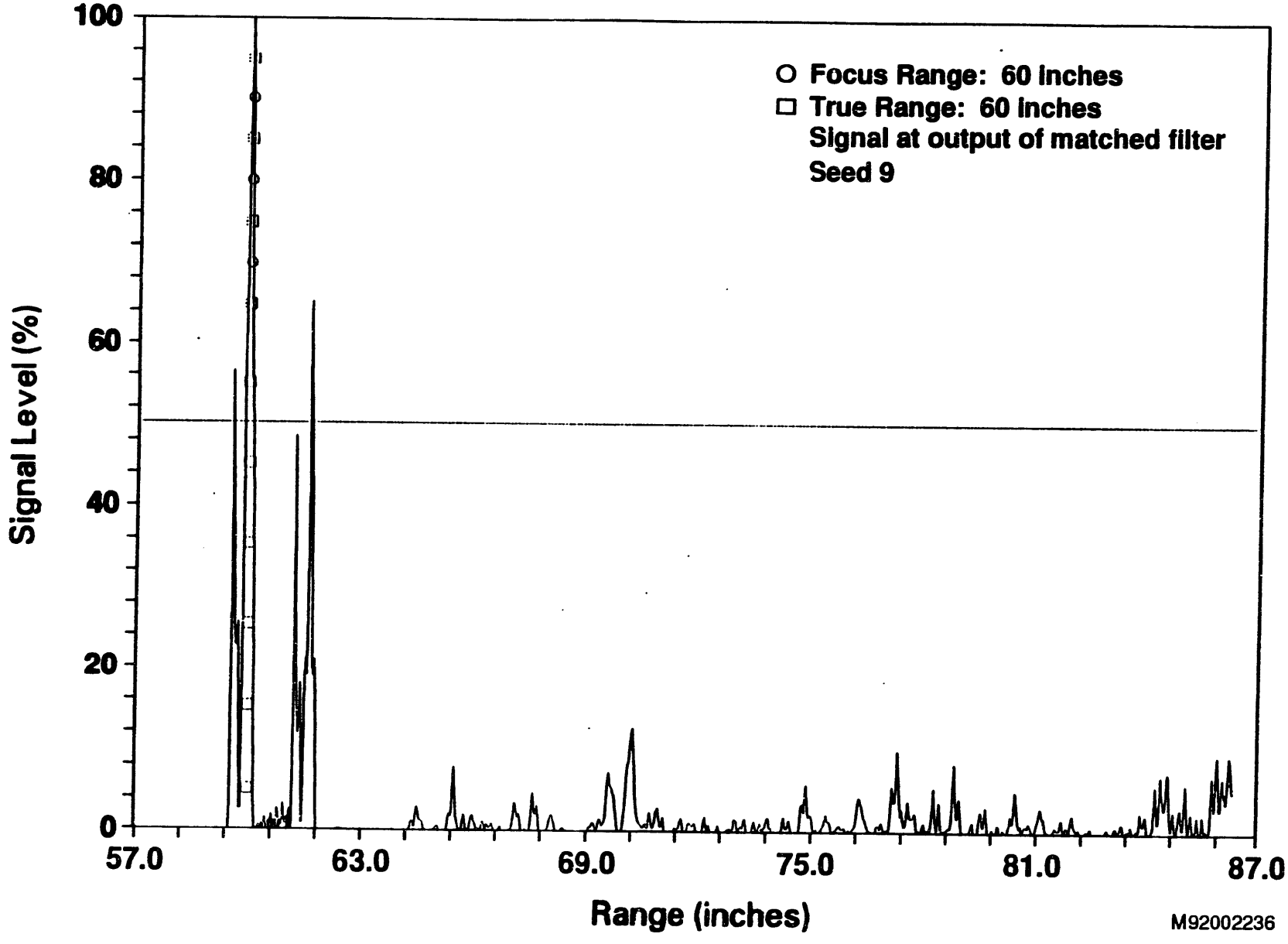

Figure 15. SCMS Receiver Signal, Pixel No. 1, MTA Signal at Output of Matched Filter

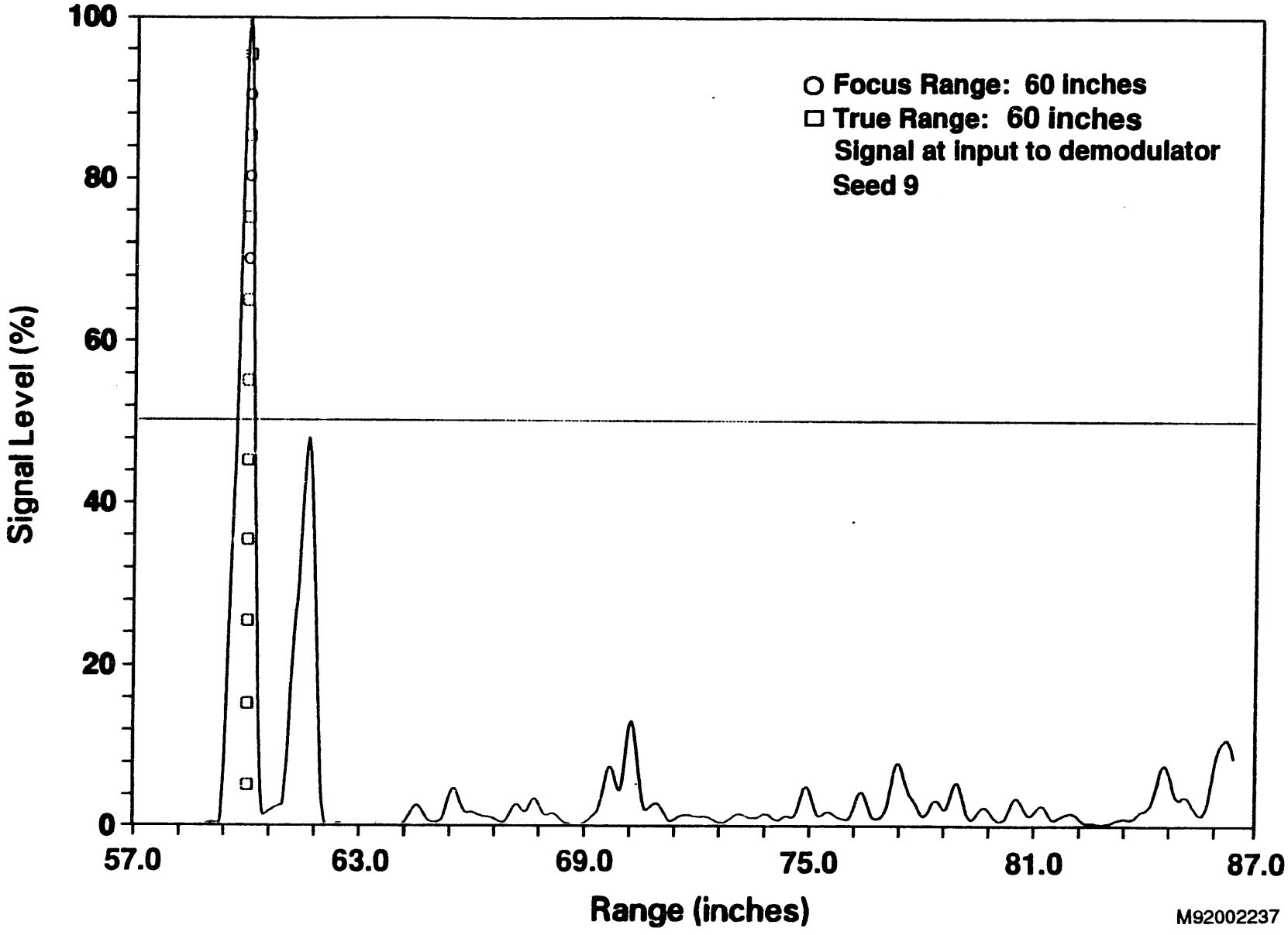

Figure 16. SCMS Receiver Signal, Pixel No. 1, MTA Signal at Input to Demodulator

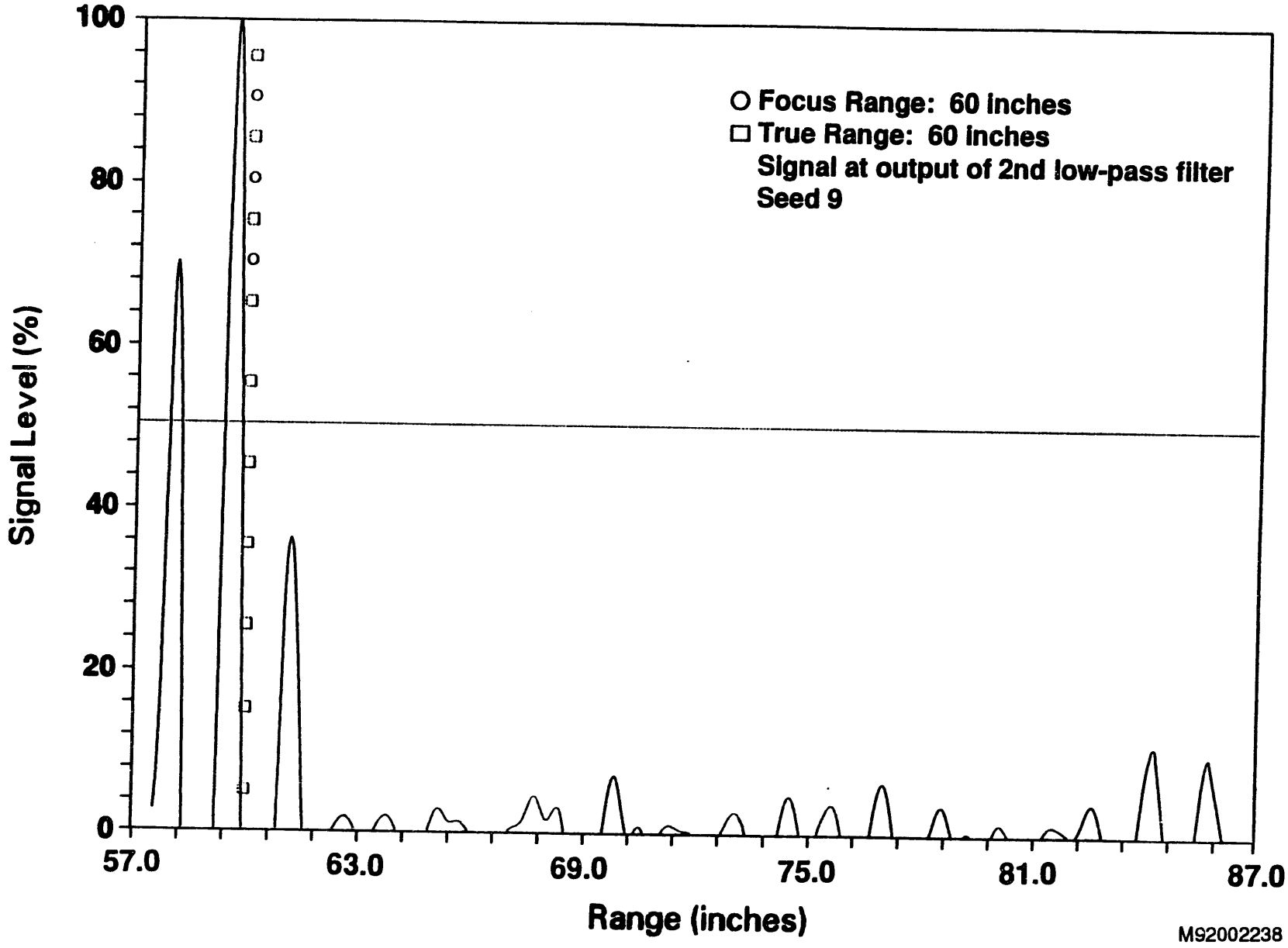

Figure 17. SCMS Receiver Signal, Pixel No. 1, MTA Signal at Output of 2nd Low-Pass Filter

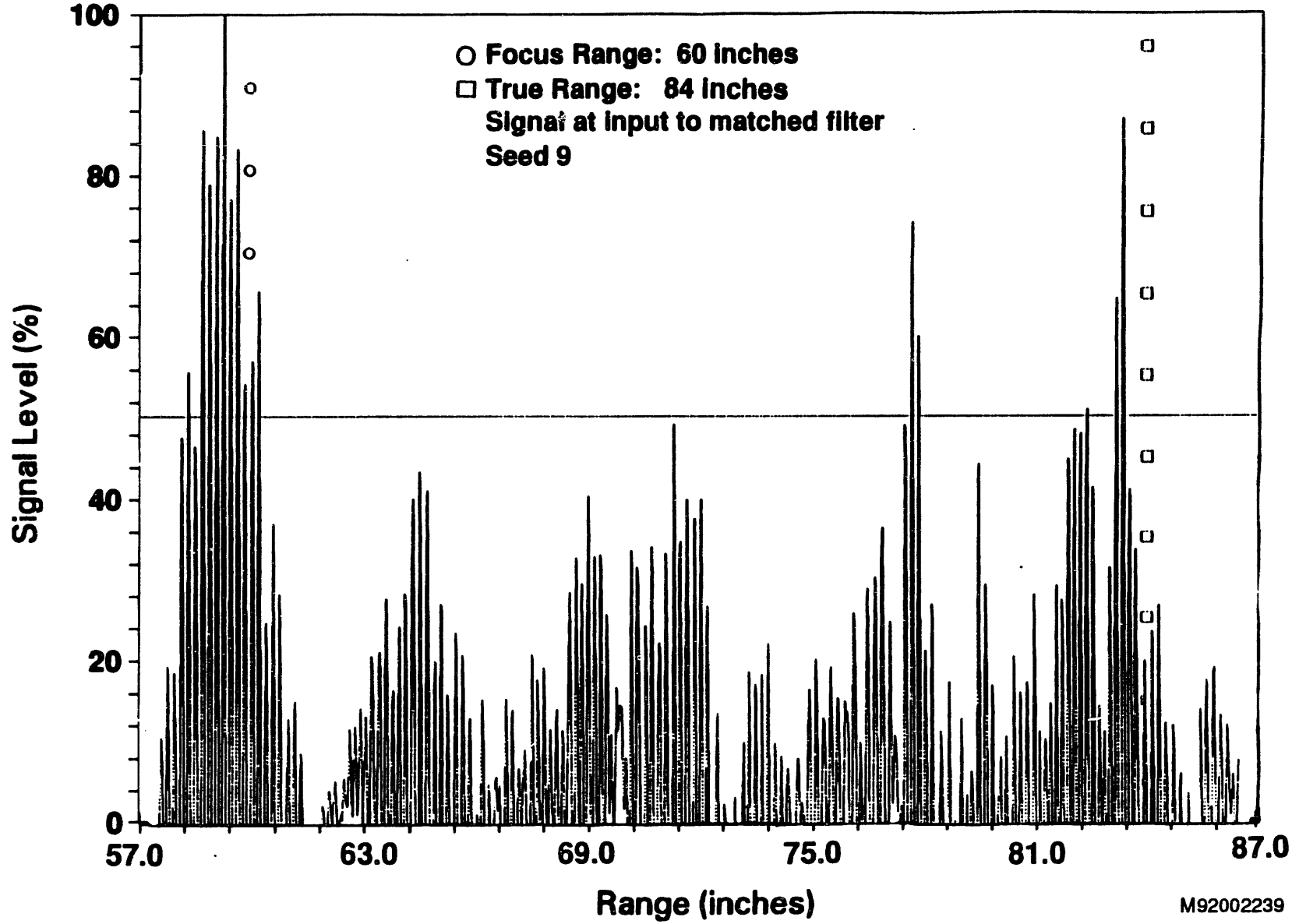

Figure 18. SCMS Receiver Signal, Pixel No. 2, MTA Signal at Input to Matched Filter

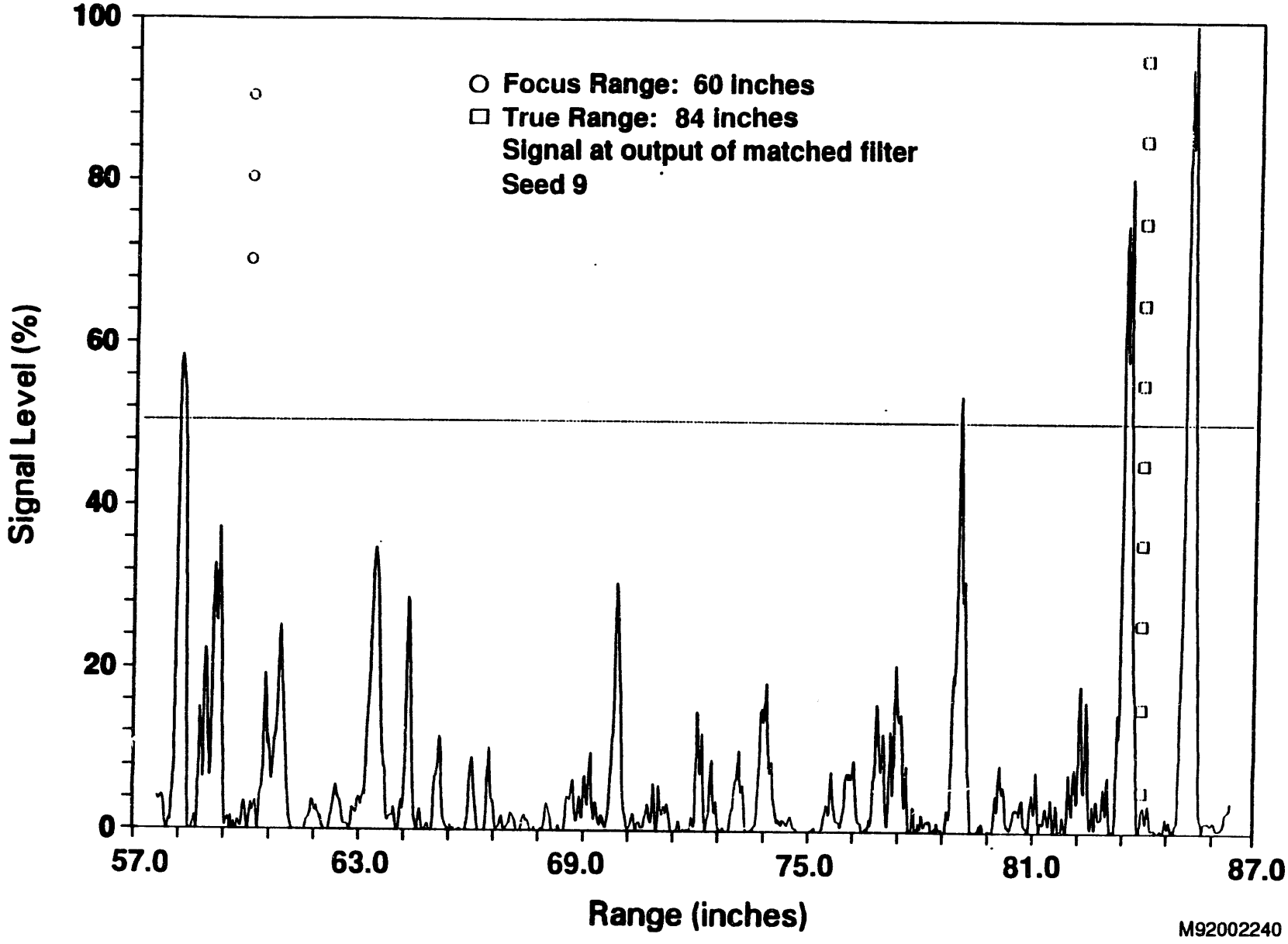

Figure 19. SCMS Receiver Signal, Pixel No. 2, MTA Signal at Output of Matched Filter

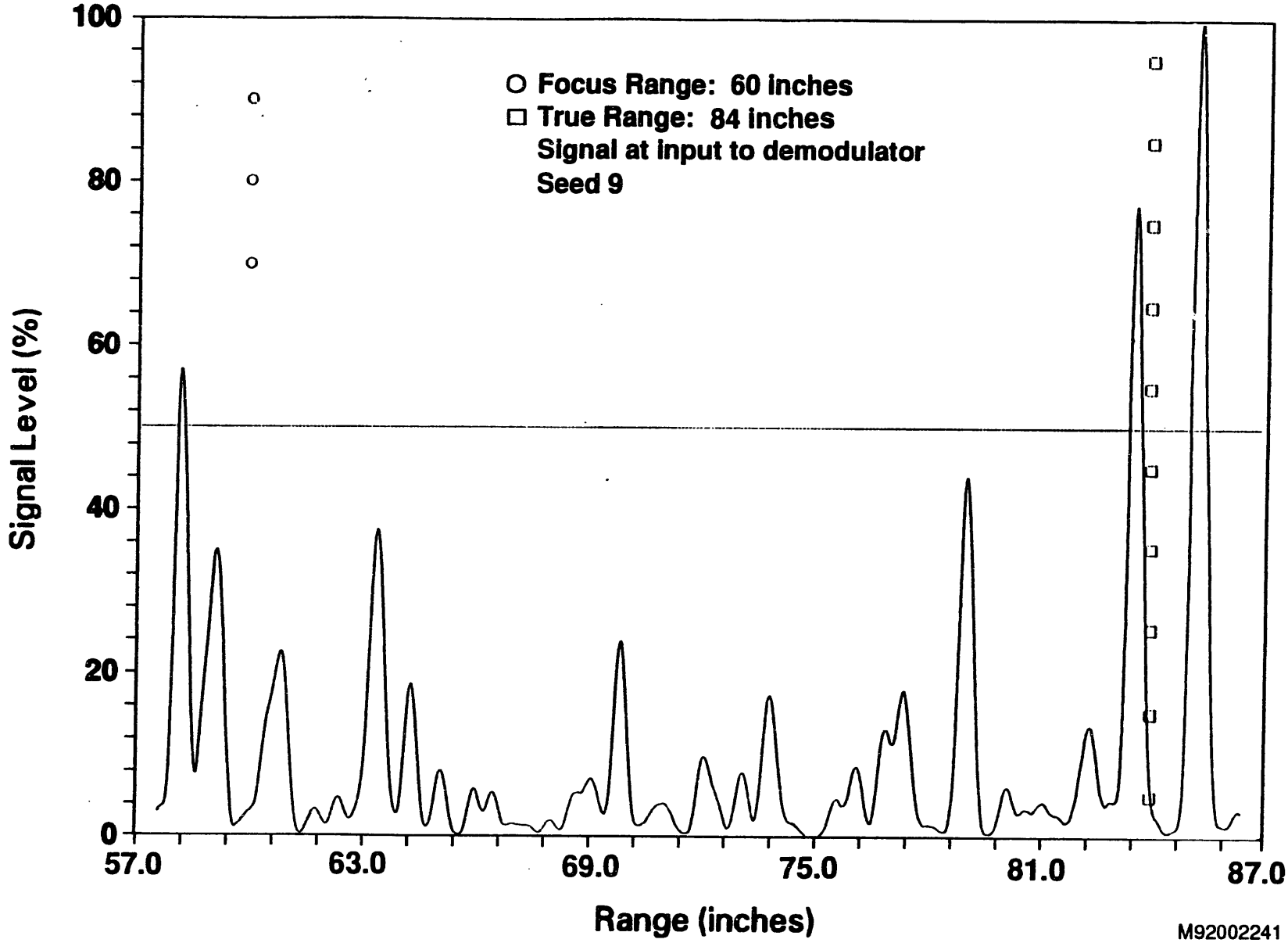

Figure 20. SCMS Receiver Signal, Pixel No. 2, MTA Signal at Input to Demodulator

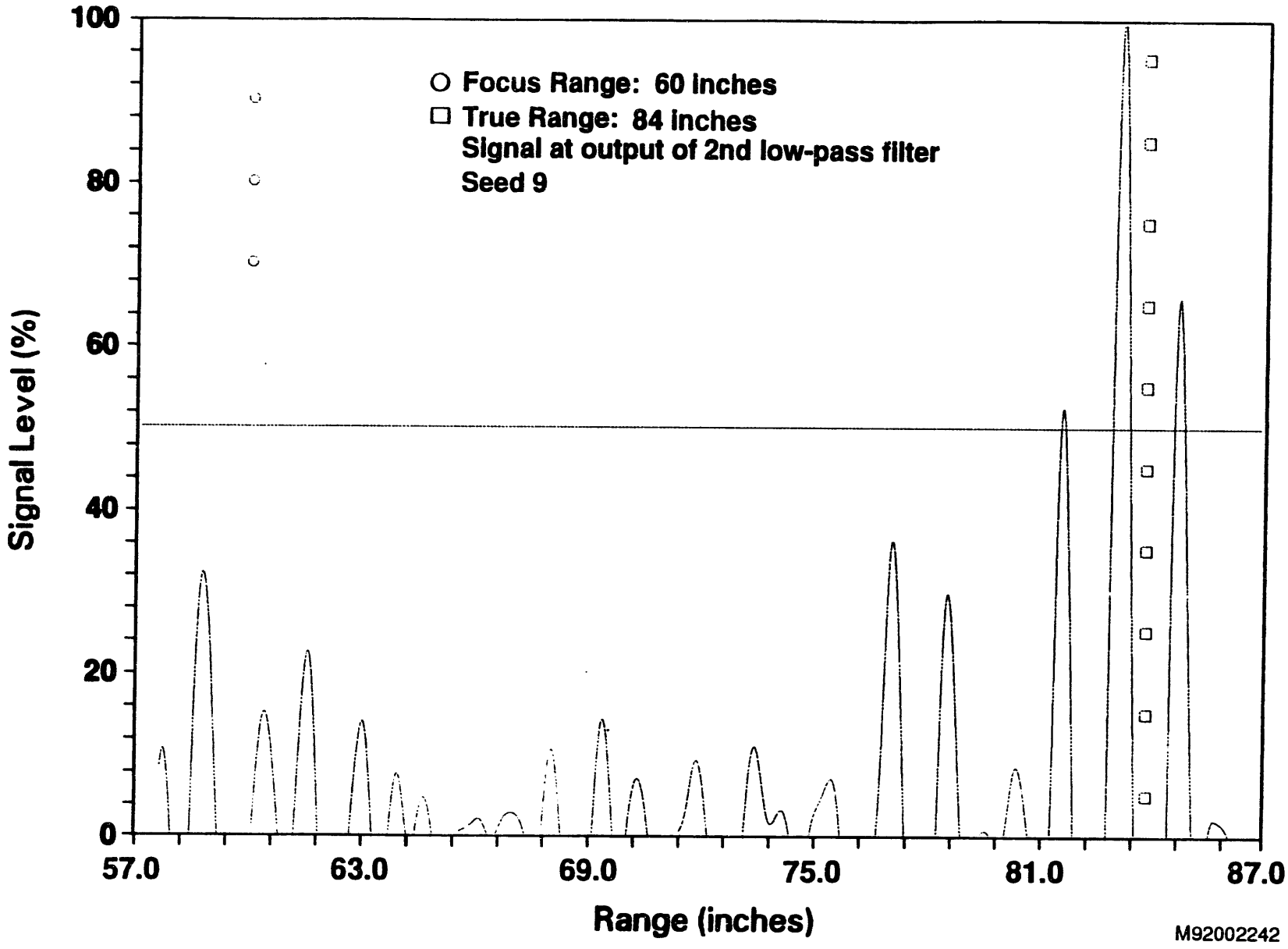

Figure 21. SCMS Receiver Signal, Pixel No. 2, MTA Signal at Output of 2nd Low-Pass Filter

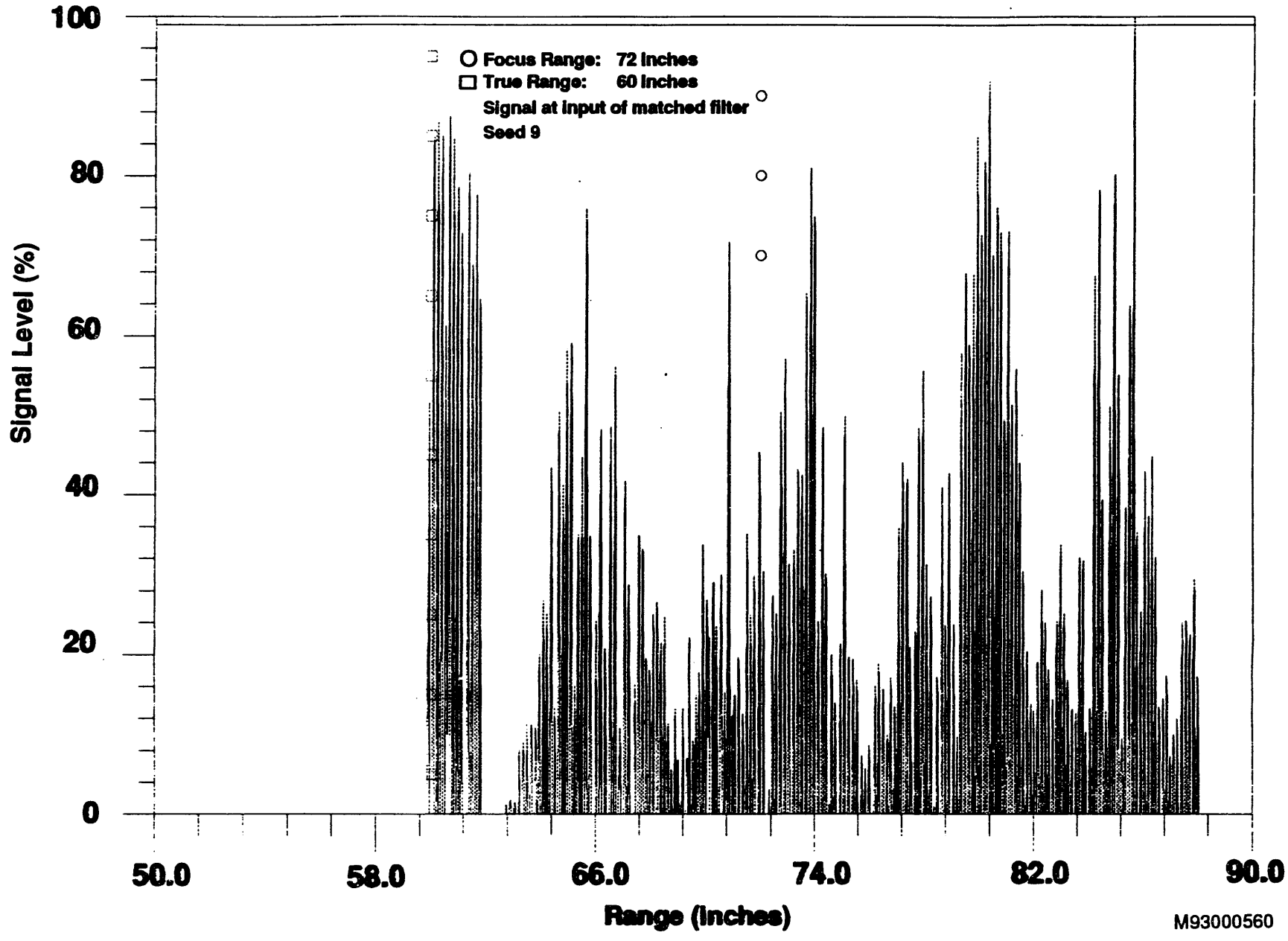

Figure 22. SCMS Receiver Signal, Pixel No. 1, MTB Signal at Input of Matched Filter

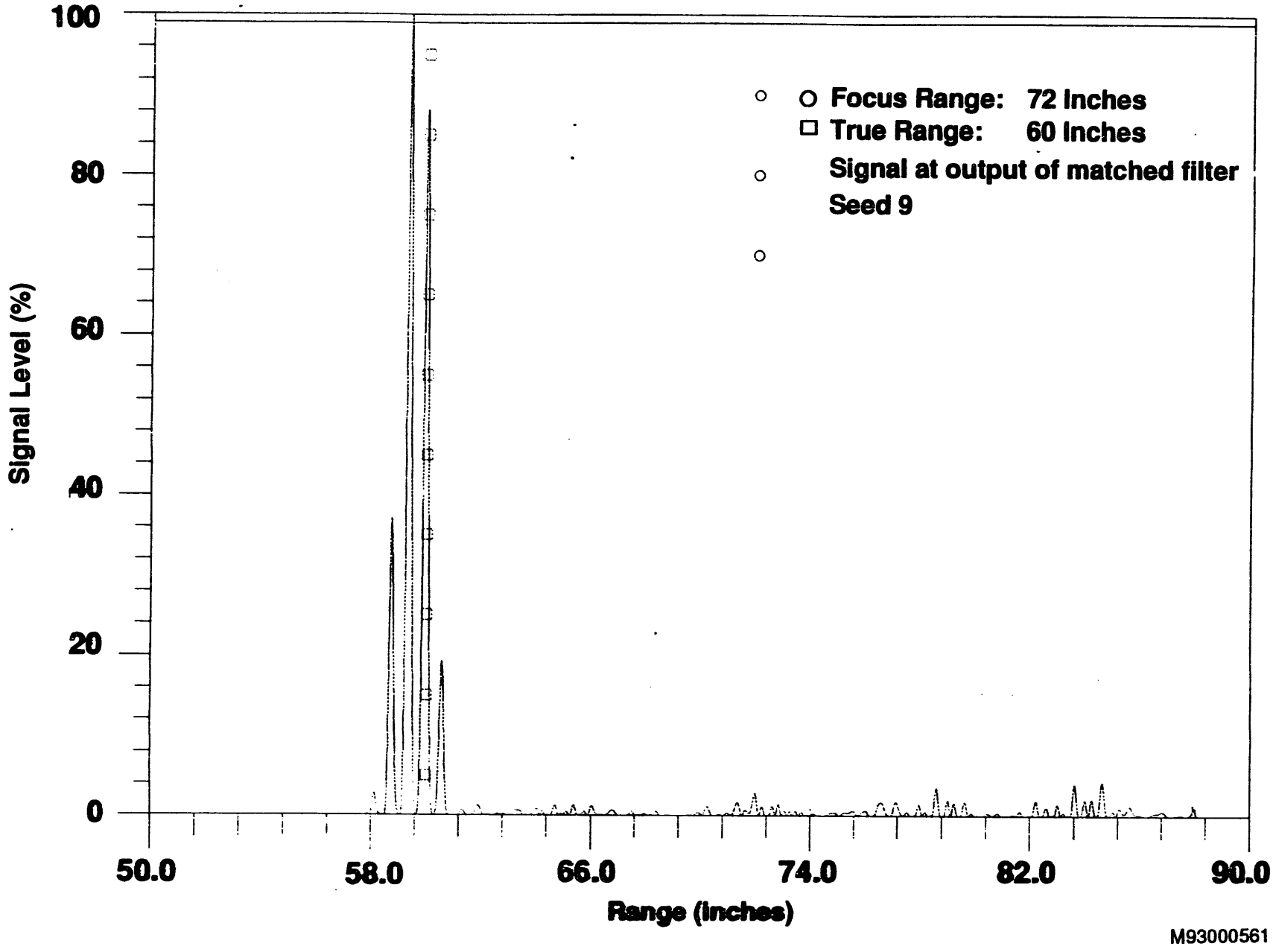

Figure 23. SCMS Receiver Signal, Pixel No. 1, MTB
Signal at Output of Matched Filter

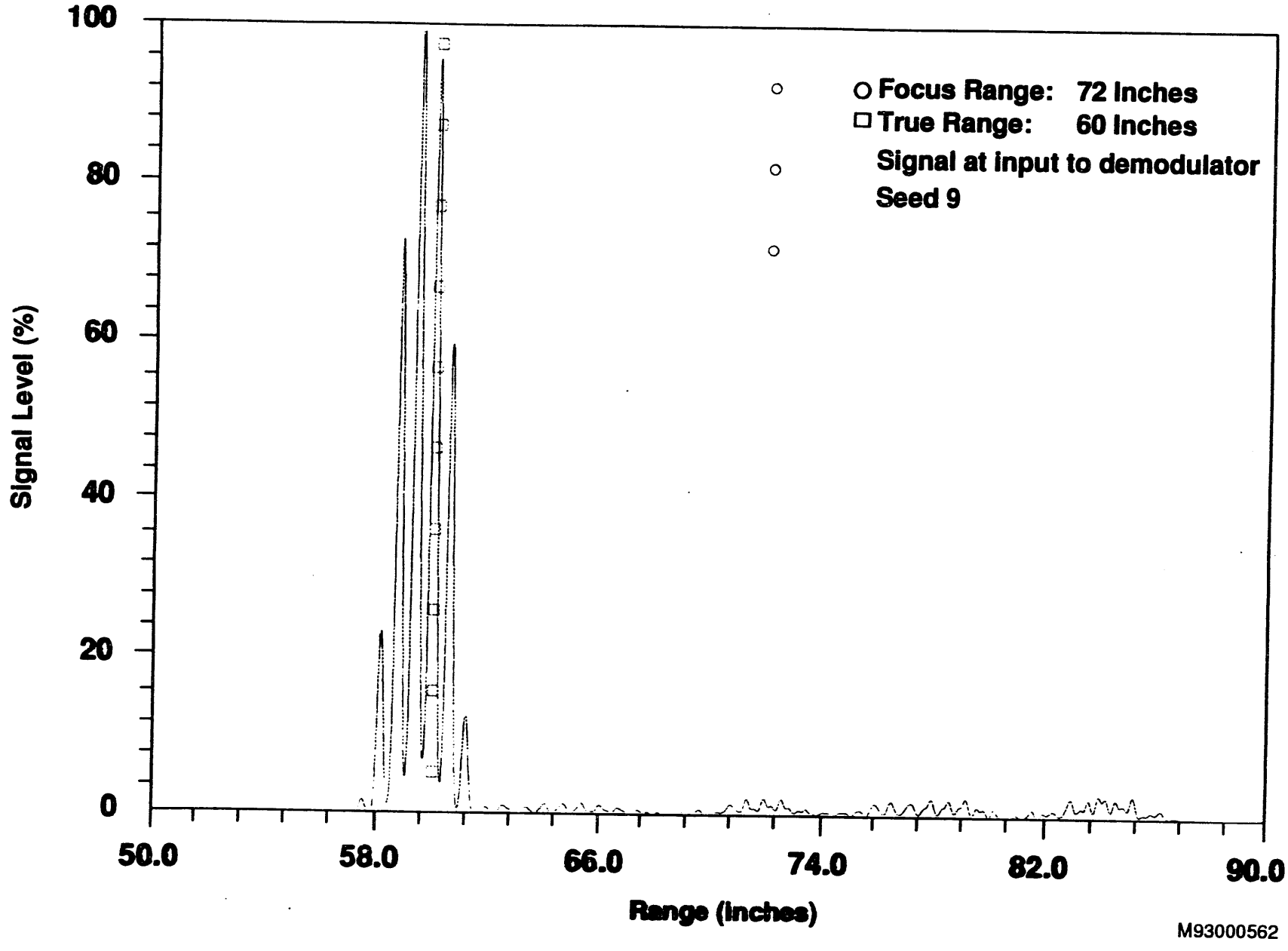

Figure 24. SCMS Receiver Signal, Pixel No. 1, MTB
Signal at Input to Demodulator

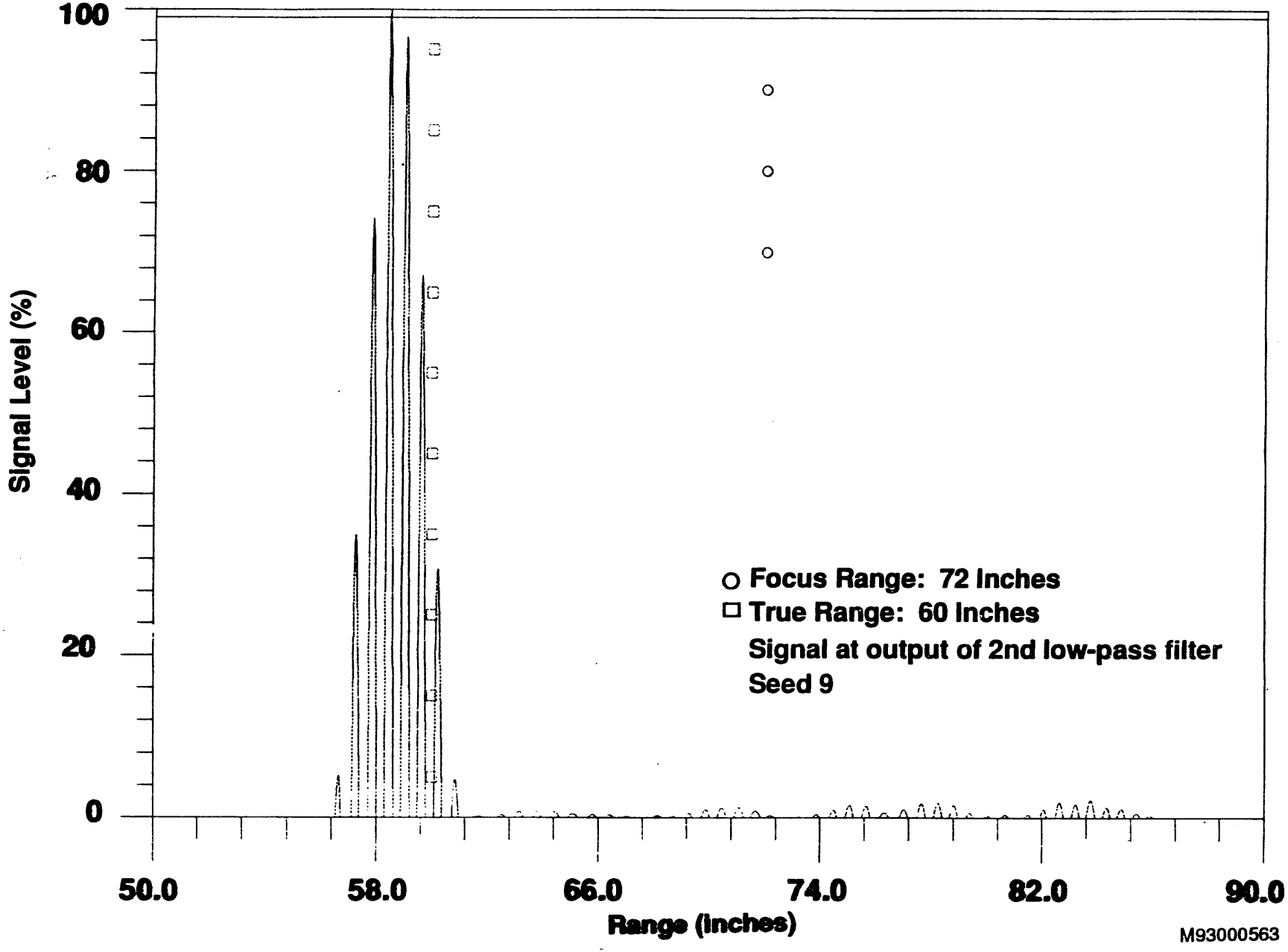

Figure 25. SCMS Receiver Signal, Pixel No. 1, MTB
Signal at Output of 2nd Low-Pass Filter

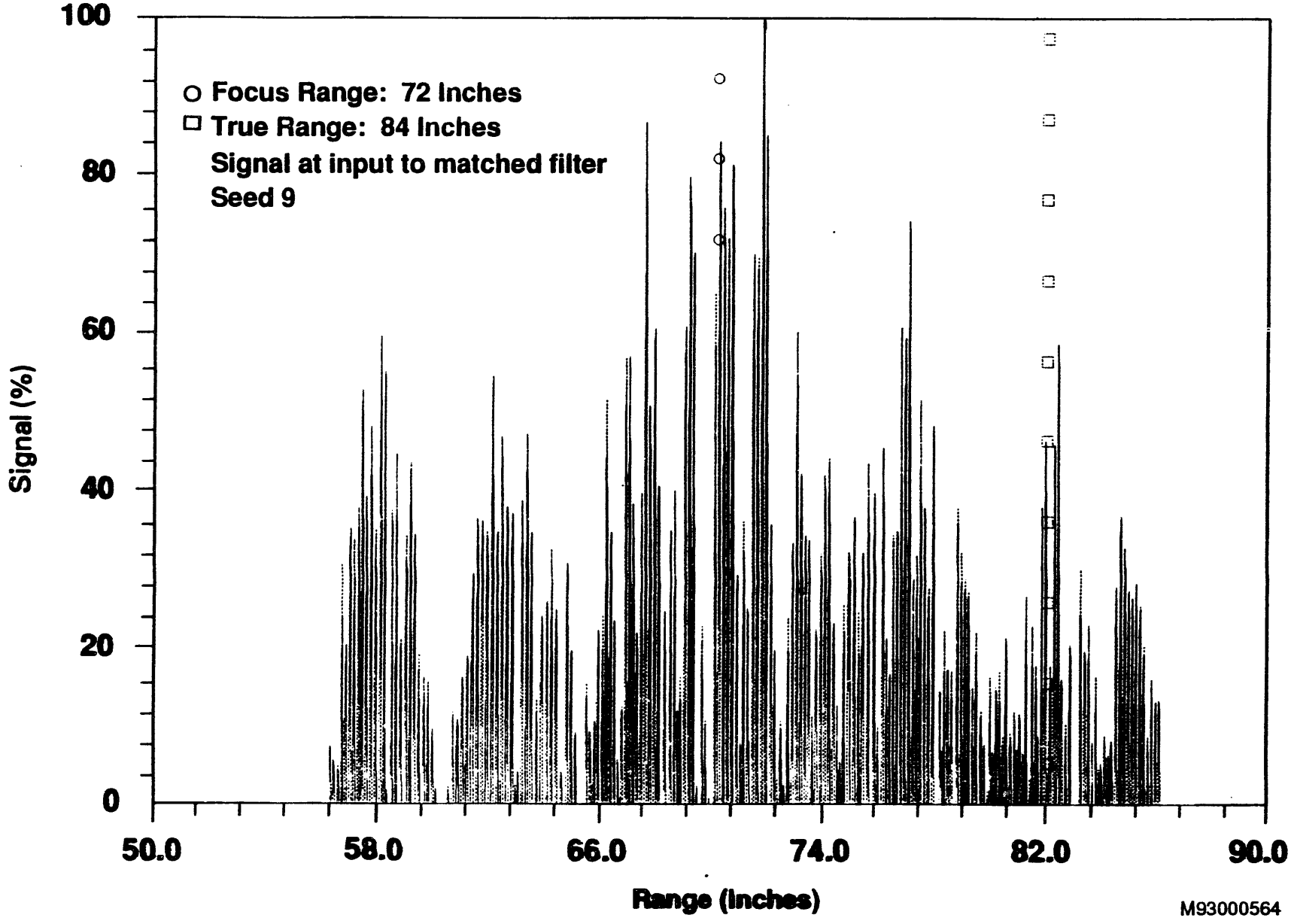

Figure 26. SCMS Receiver Signal, Pixel No. 2, MTB Signal at Input to Matched Filter

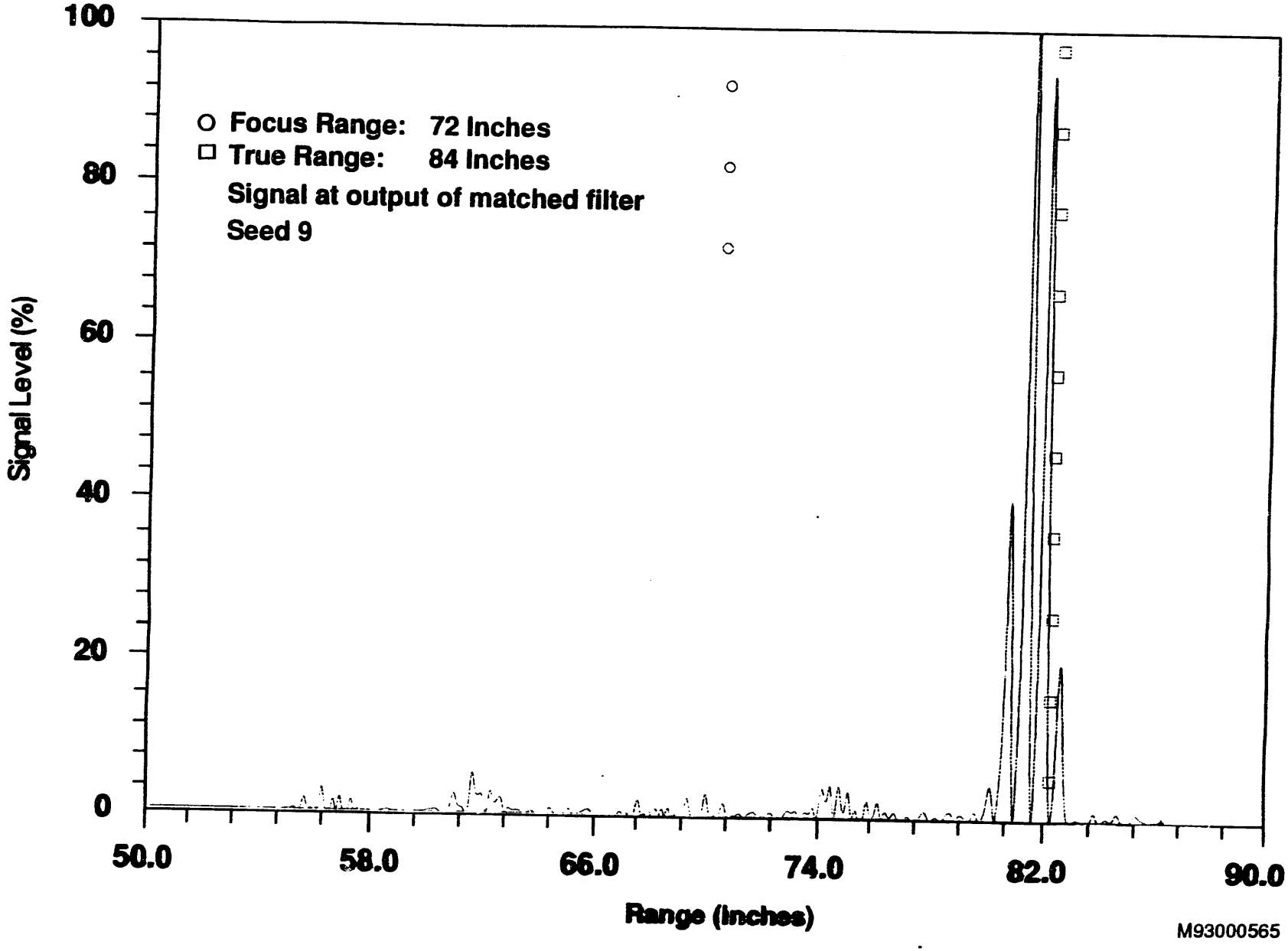

Figure 27. SCMS Receiver Signal, Pixel No. 2, MTB
Signal at Output of Matched Filter

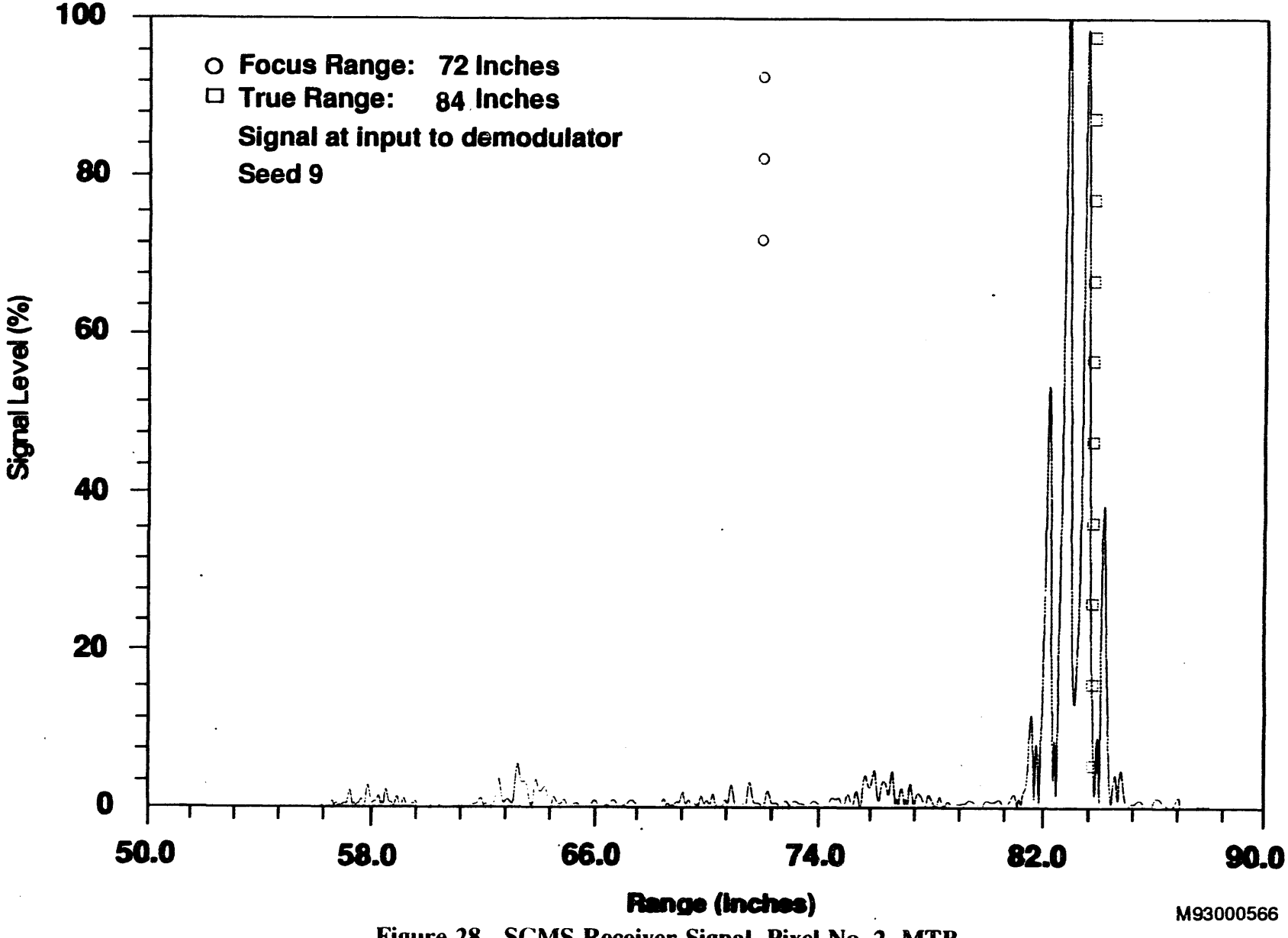

Figure 28. SCMS Receiver Signal, Pixel No. 2, MTB
Signal at Input to Demodulator

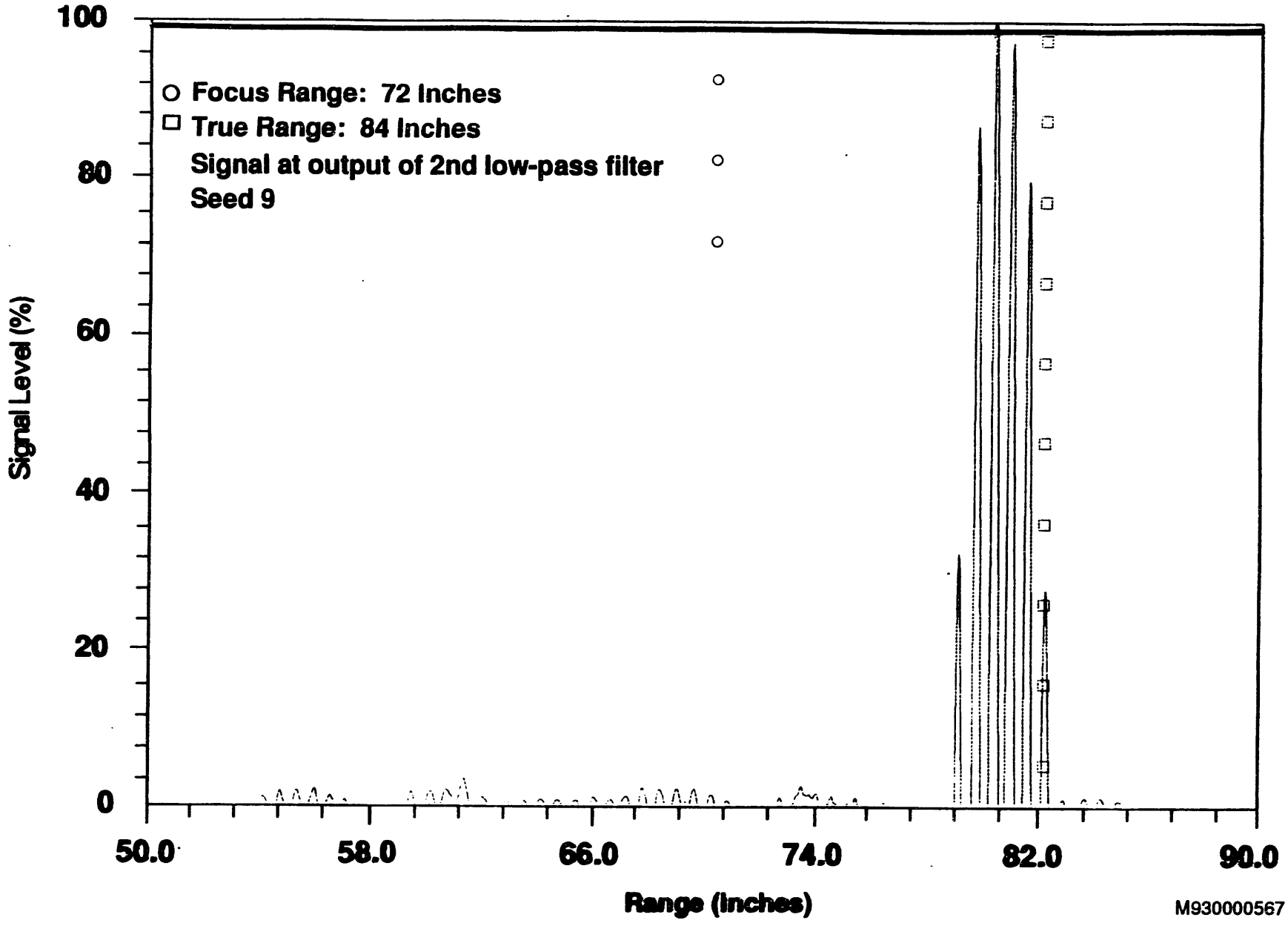

Figure 29. SCMS Receiver Signal, Pixel No. 2, MTB
Signal at Output of 2nd Low-Pass Filter

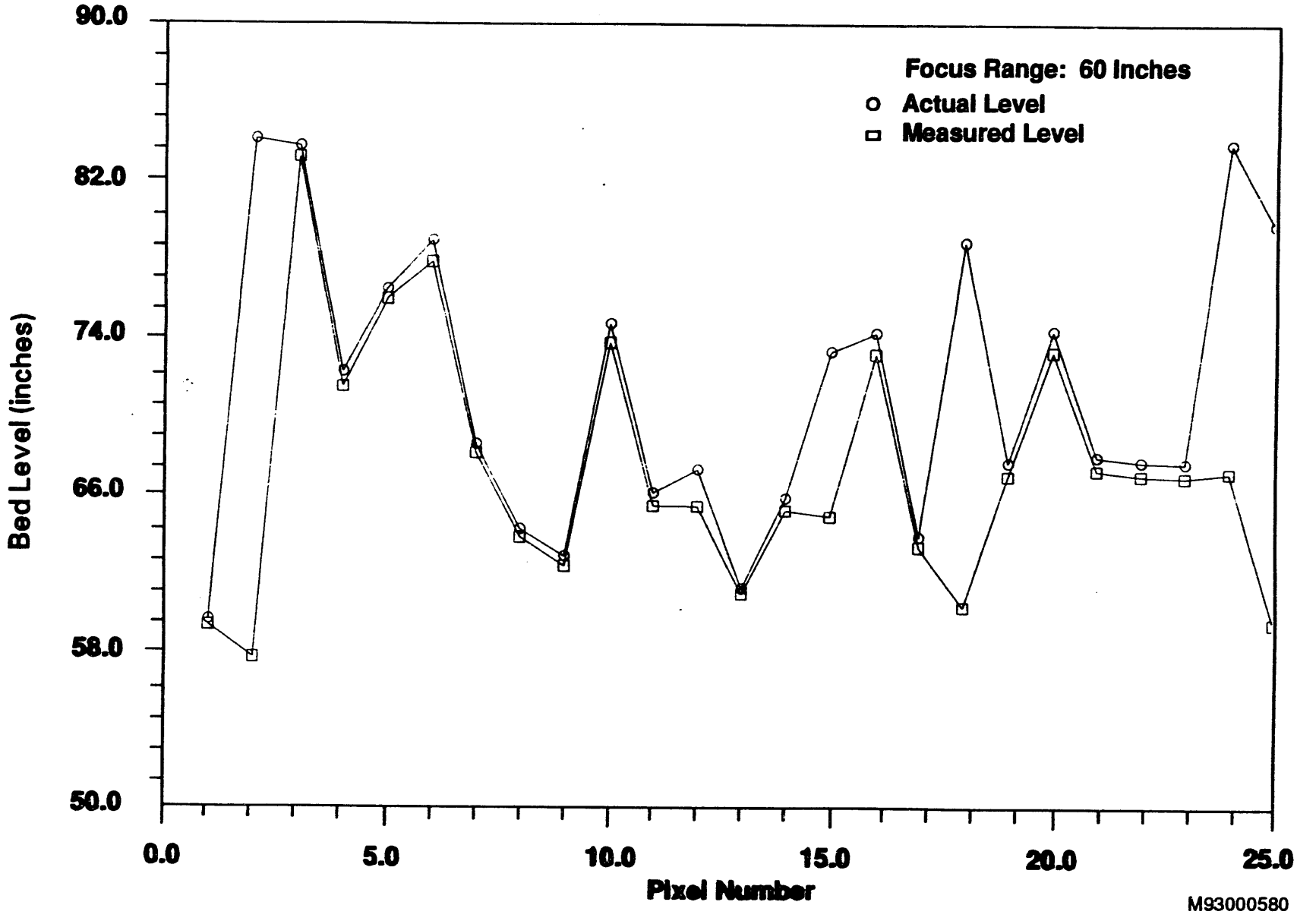

Figure 30. Actual and Measured Bed Levels, All Filters Used, MTA Focus Range: 60 Inches

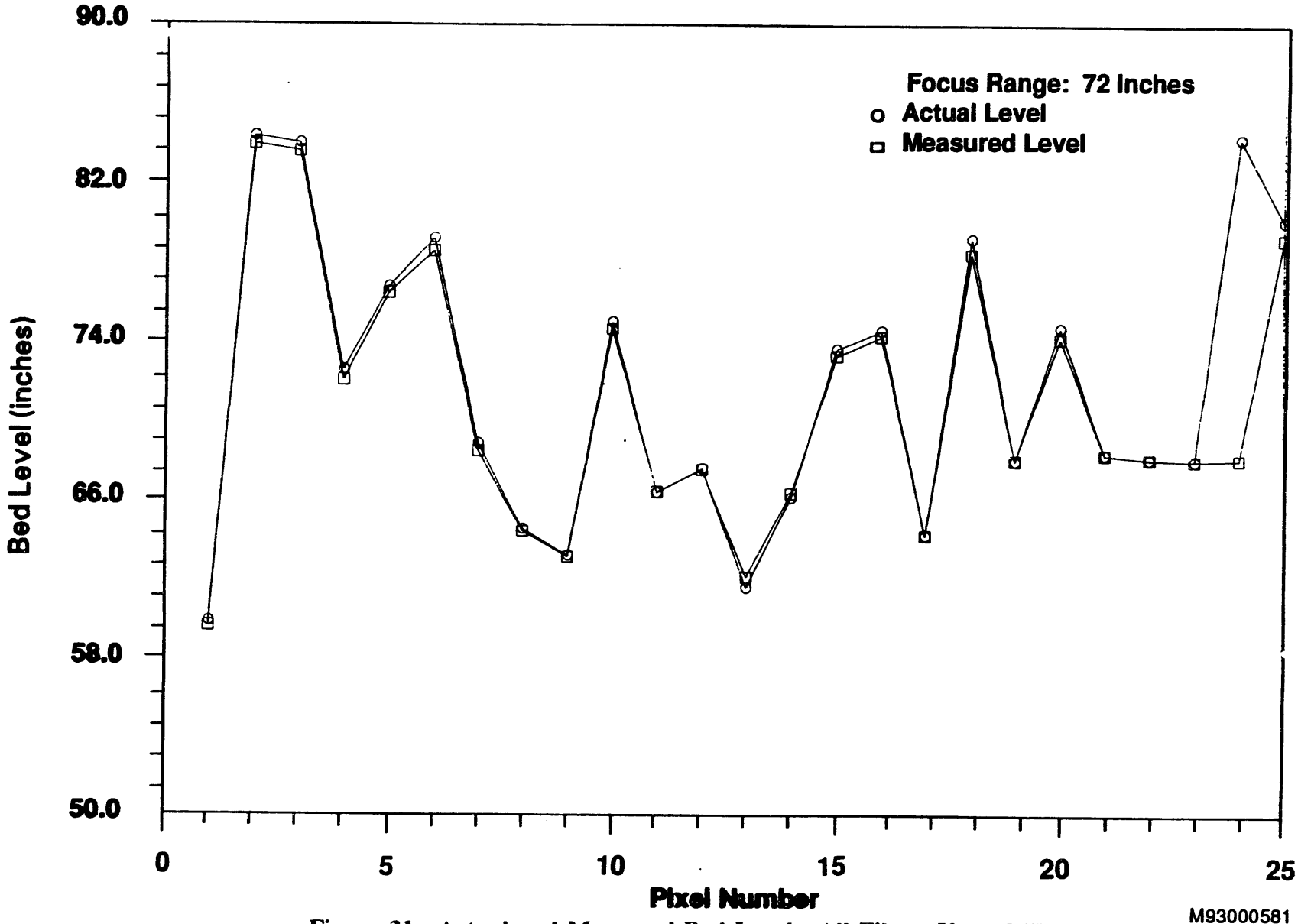

Figure 31. Actual and Measured Bed Levels, All Filters Used, MTA Focus Range: 72 Inches

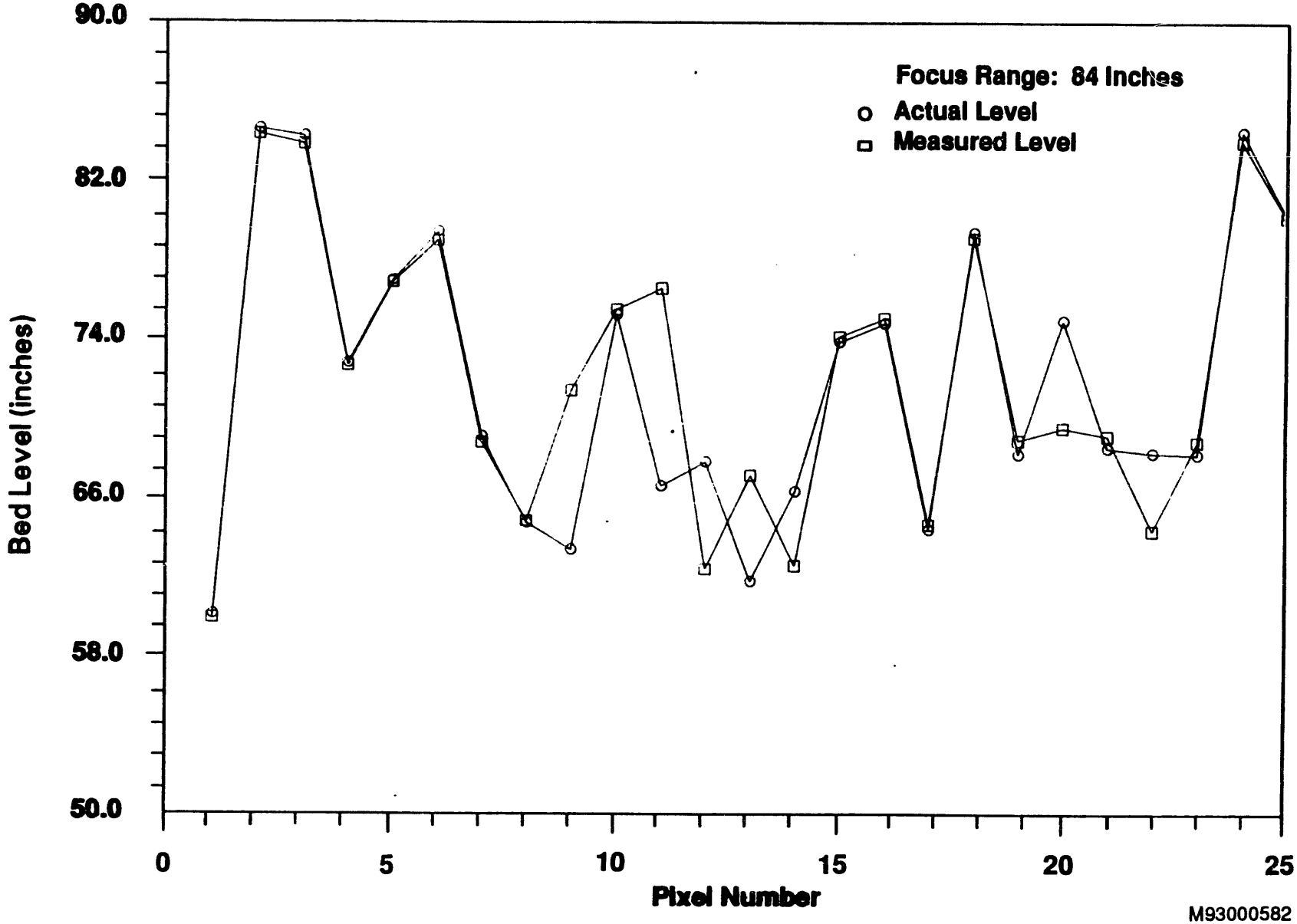

Figure 32. Actual and Measured Bed Levels, All Filters Used, MTA
Focus Range: 84 Inches

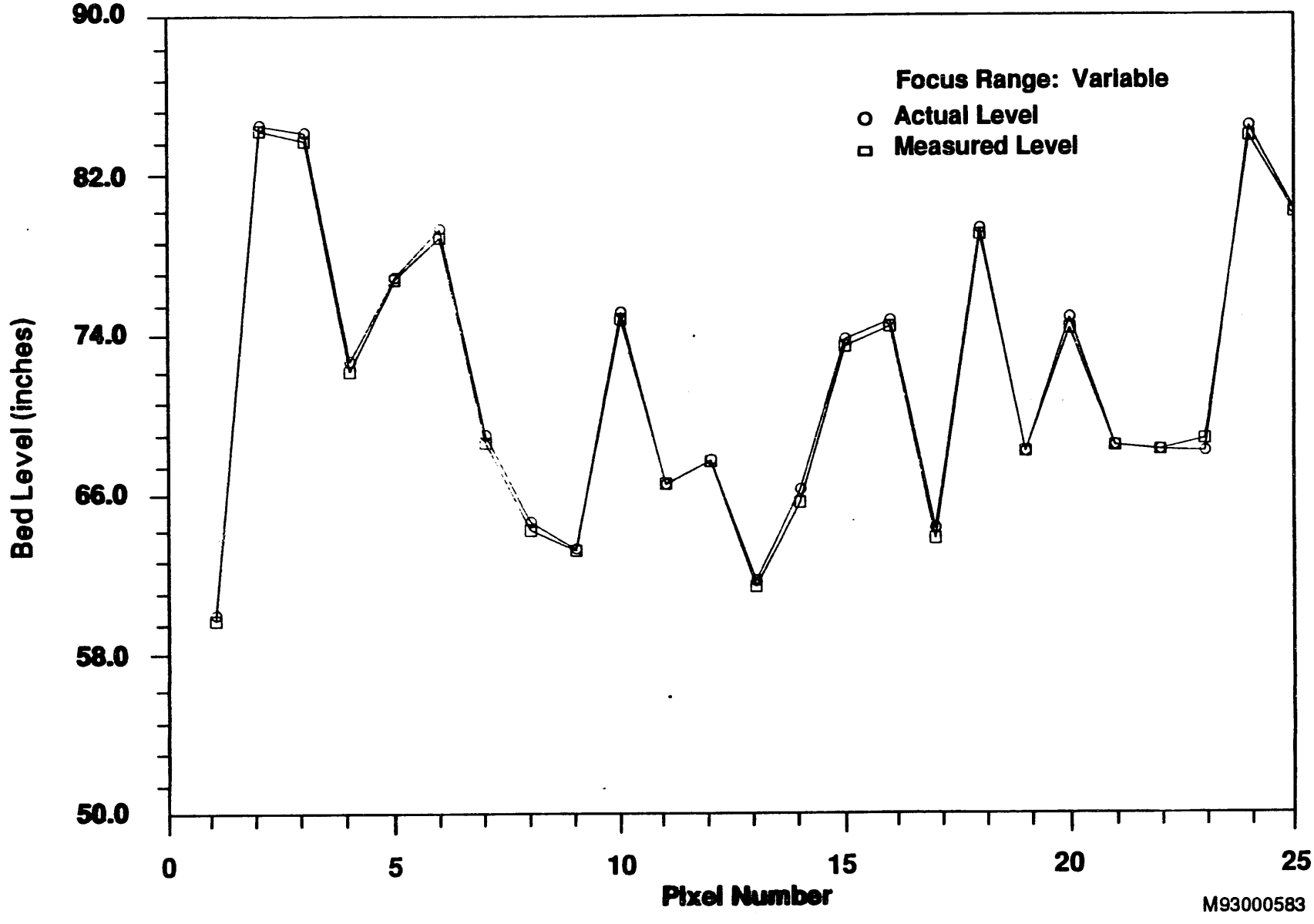

Figure 33. Actual and Measured Bed Levels, All Filters Used, MTA Focus Range: Variable

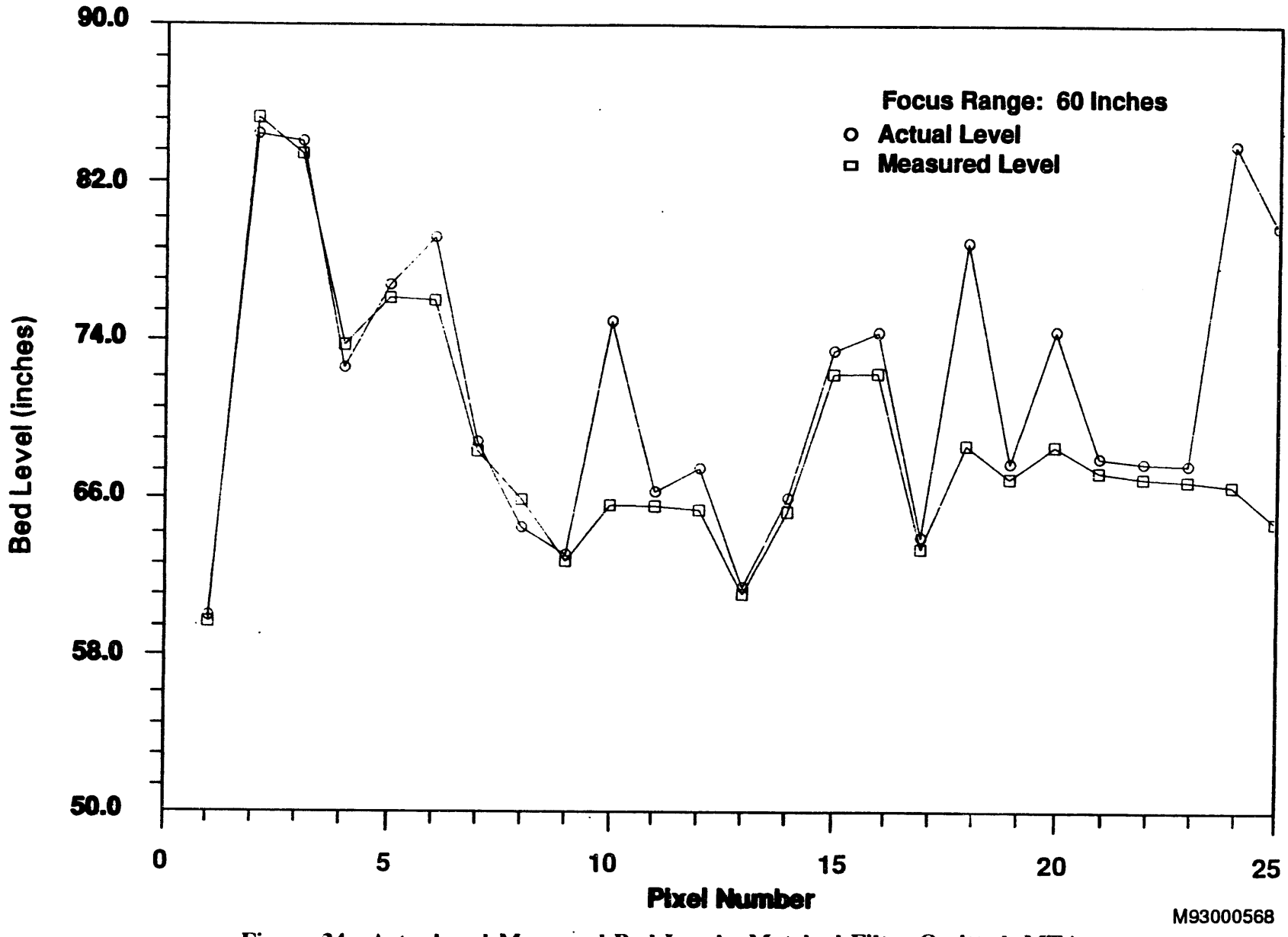

Figure 34. Actual and Measured Bed Levels, Matched Filter Omitted, MTA Focus Range: 60 Inches

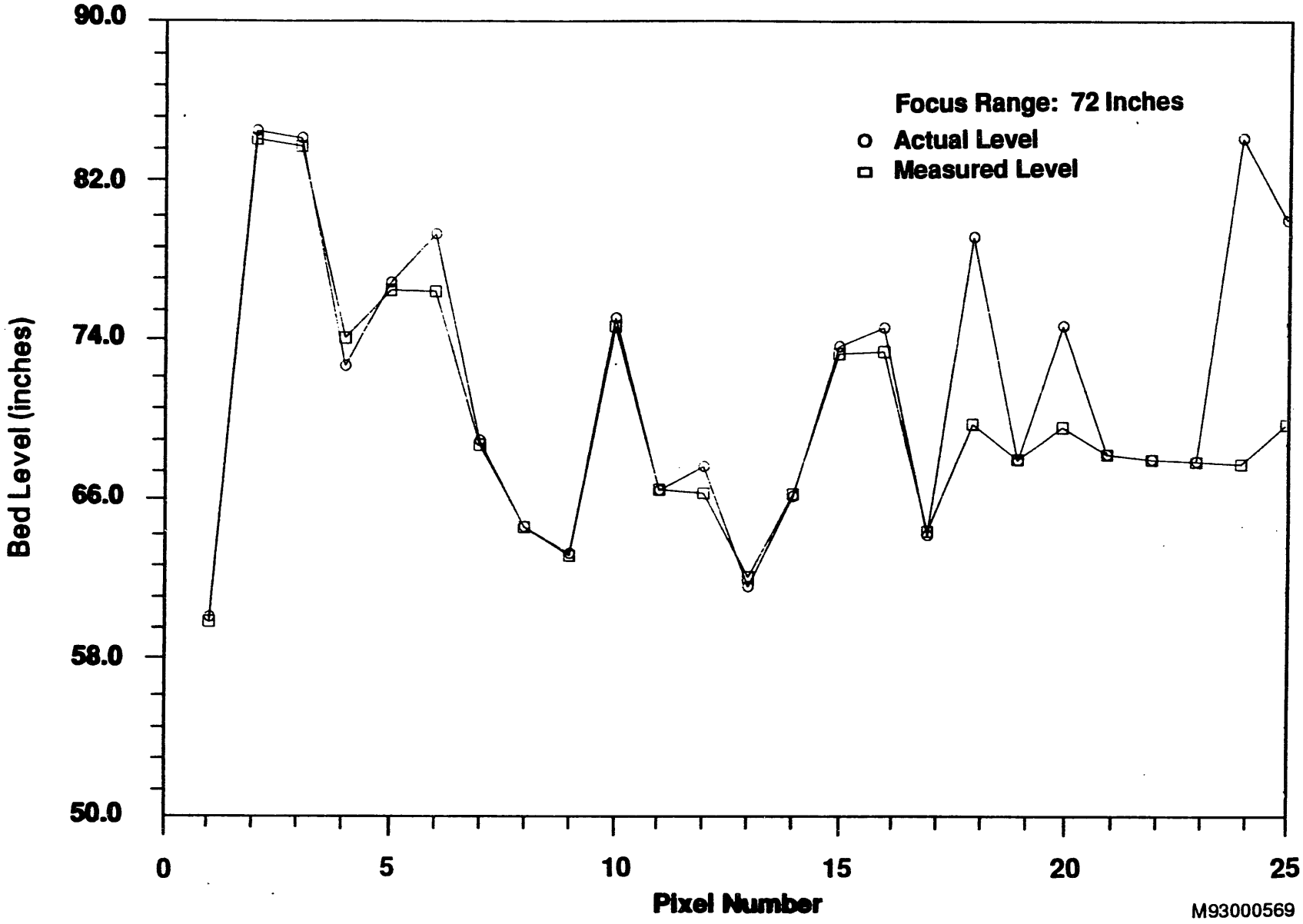

Figure 35. Actual and Measured Bed Levels, Matched Filter Omitted, MTA Focus Range: 72 Inches

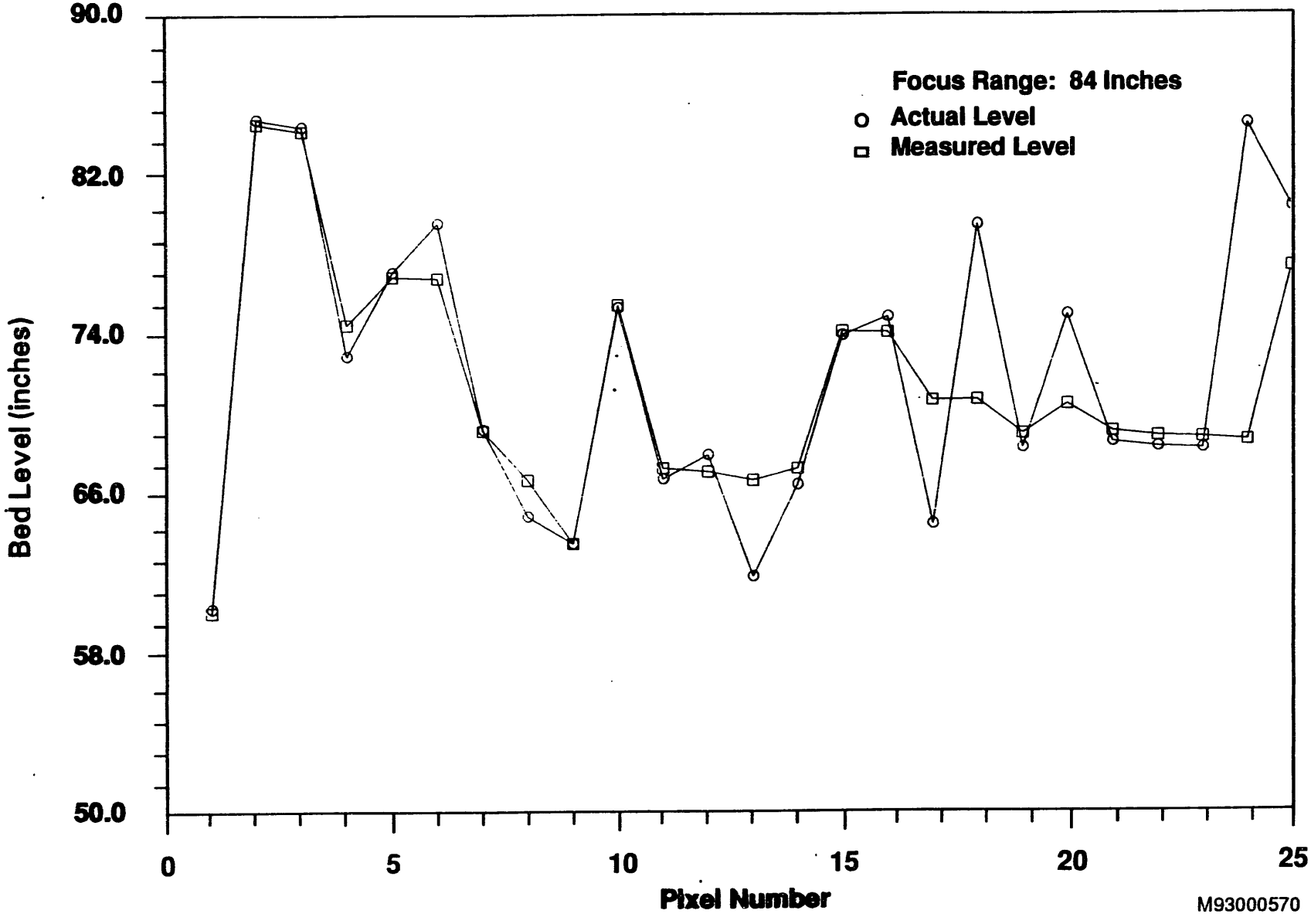

Figure 36. Actual and Measured Bed Levels, Matched Filter Omitted, MTA Focus Range: 84 Inches

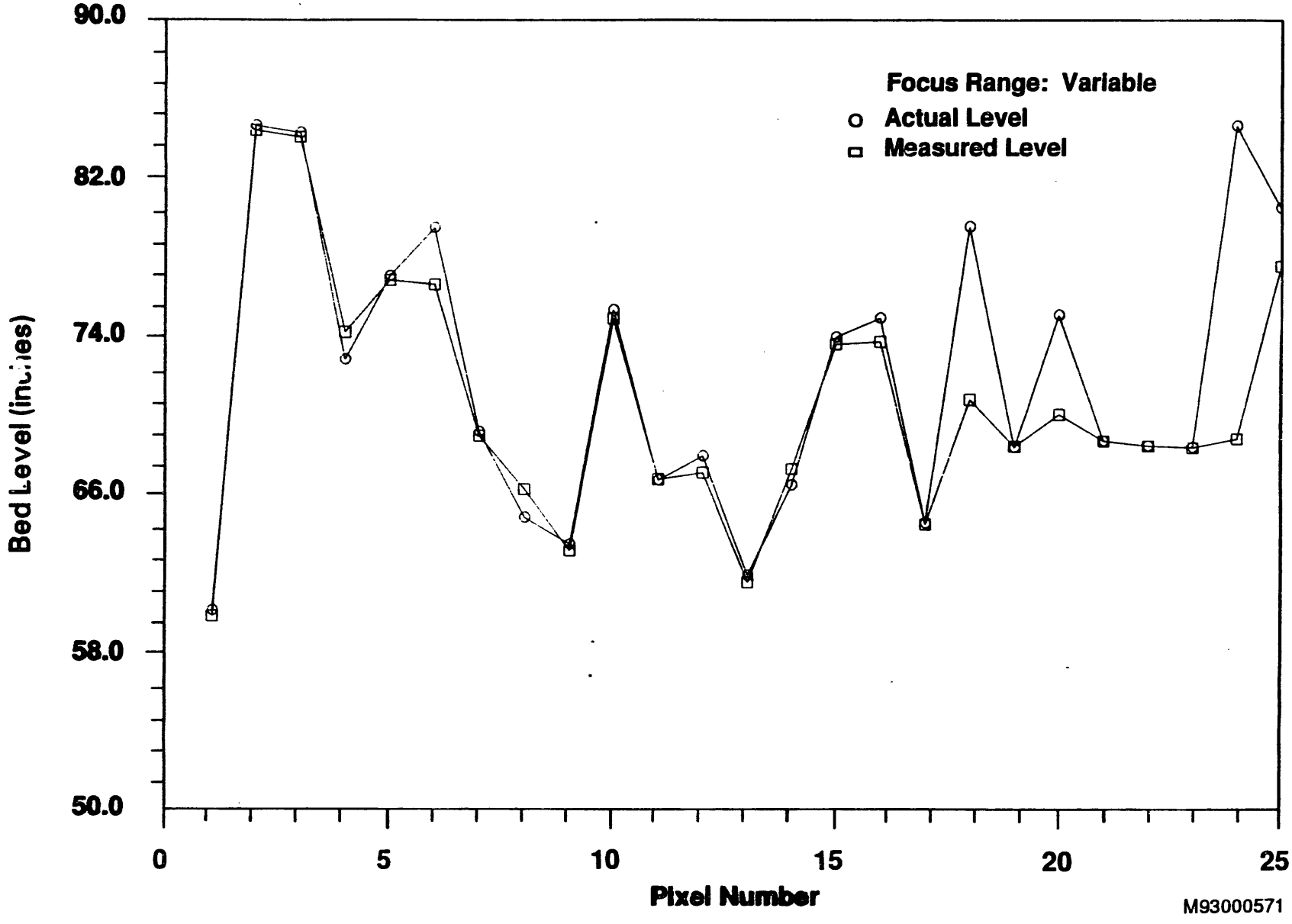

Figure 37. Actual and Measured Bed Levels, Matched Filter Omitted, MTA Focus Range: Variable

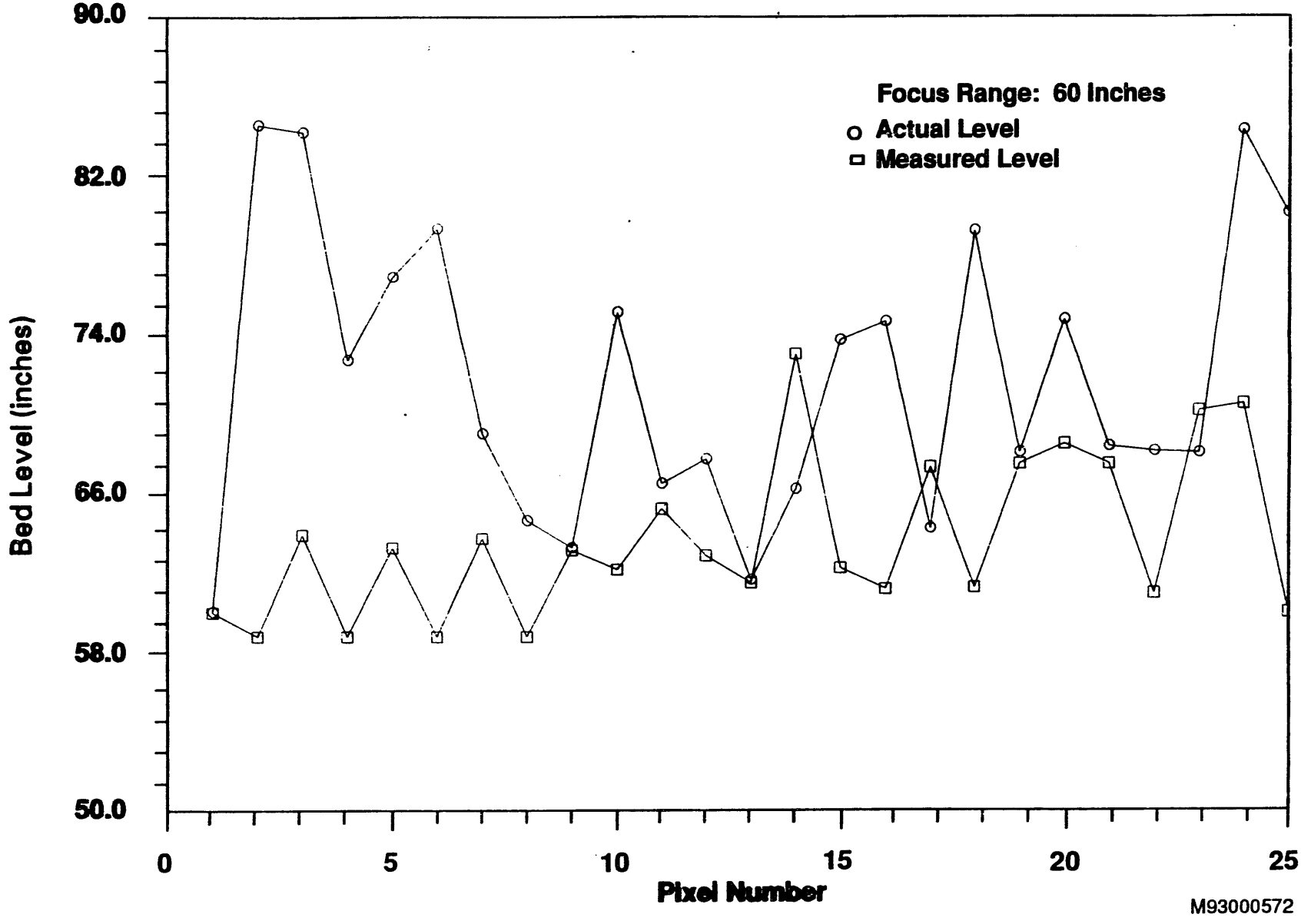

Figure 38. Actual and Measured Bed Levels,
Matched and 2 Low-Pass Filters Omitted, MTA
Focus Range: 60 Inches

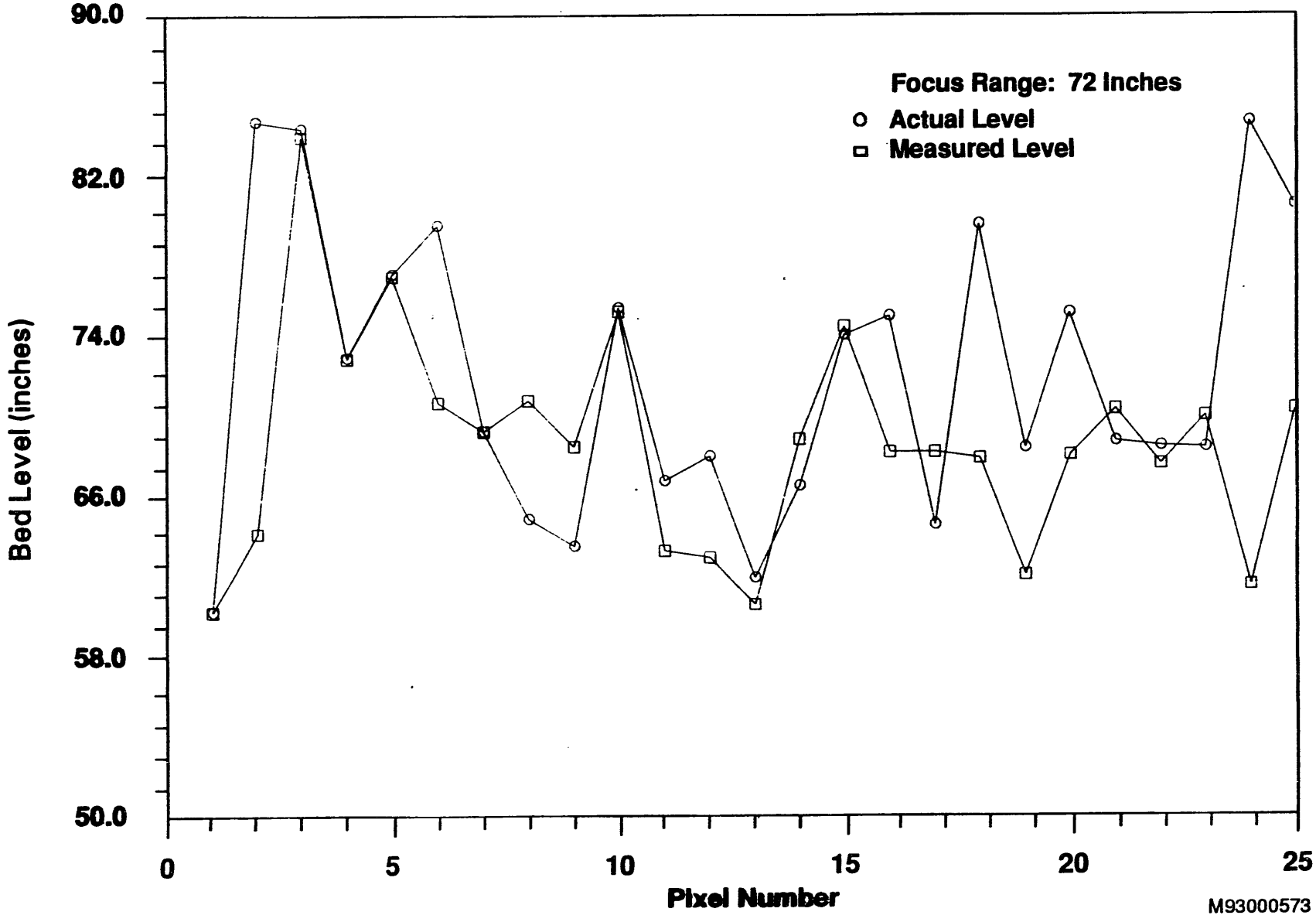

Figure 39. Actual and Measured Bed Levels,
Matched and 2 Low-Pass Filters Omitted, MTA
Focus Range: 72 Inches

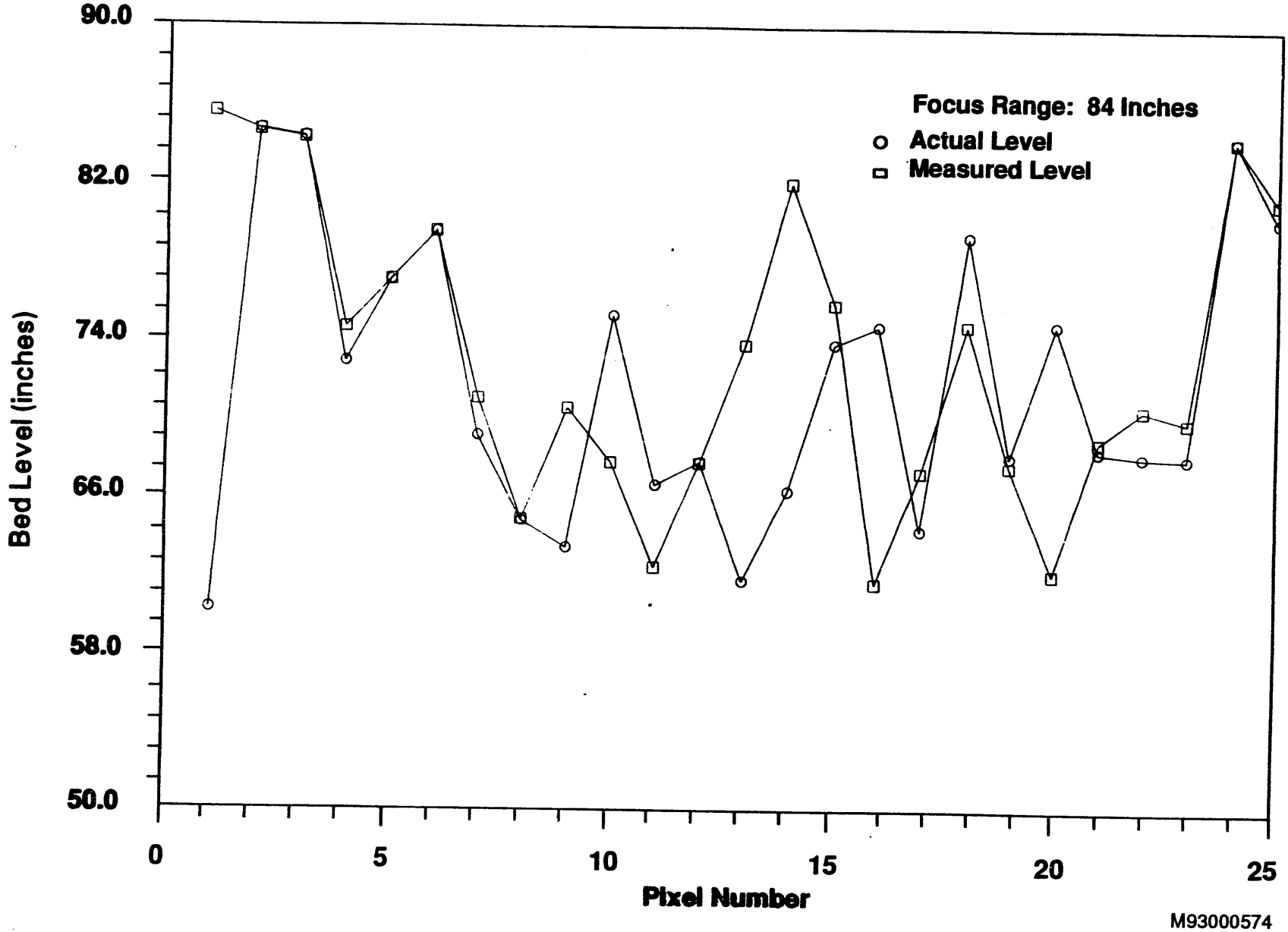

Figure 40. Actual and Measured Bed Levels, Matched and 2 Low-Pass Filters Omitted, MTA Focus Range: 84 Inches

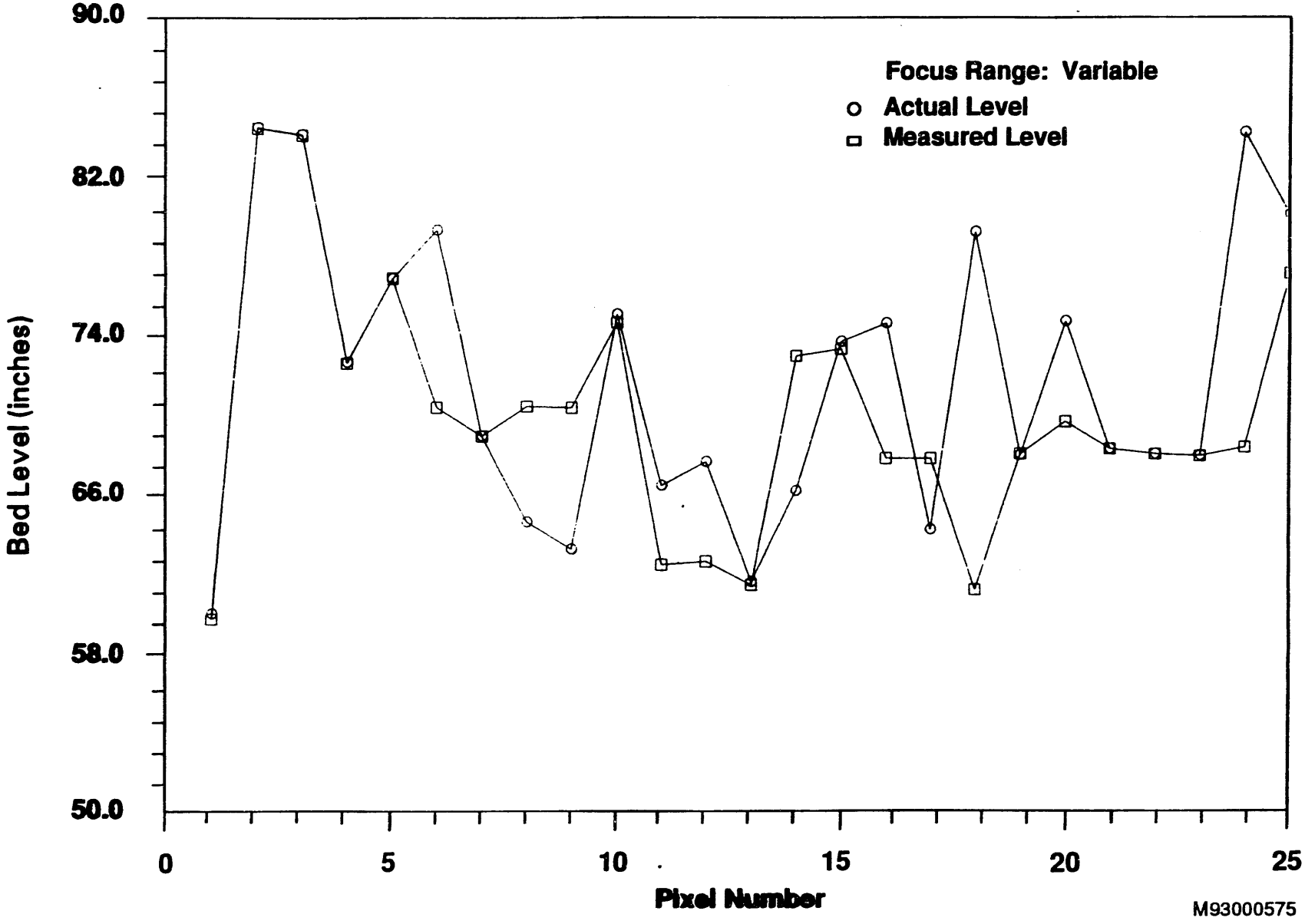

Figure 41. Actual and Measured Bed Levels,
Matched and 2 Low-Pass Filters Omitted, MTA
Focus Range: Variable

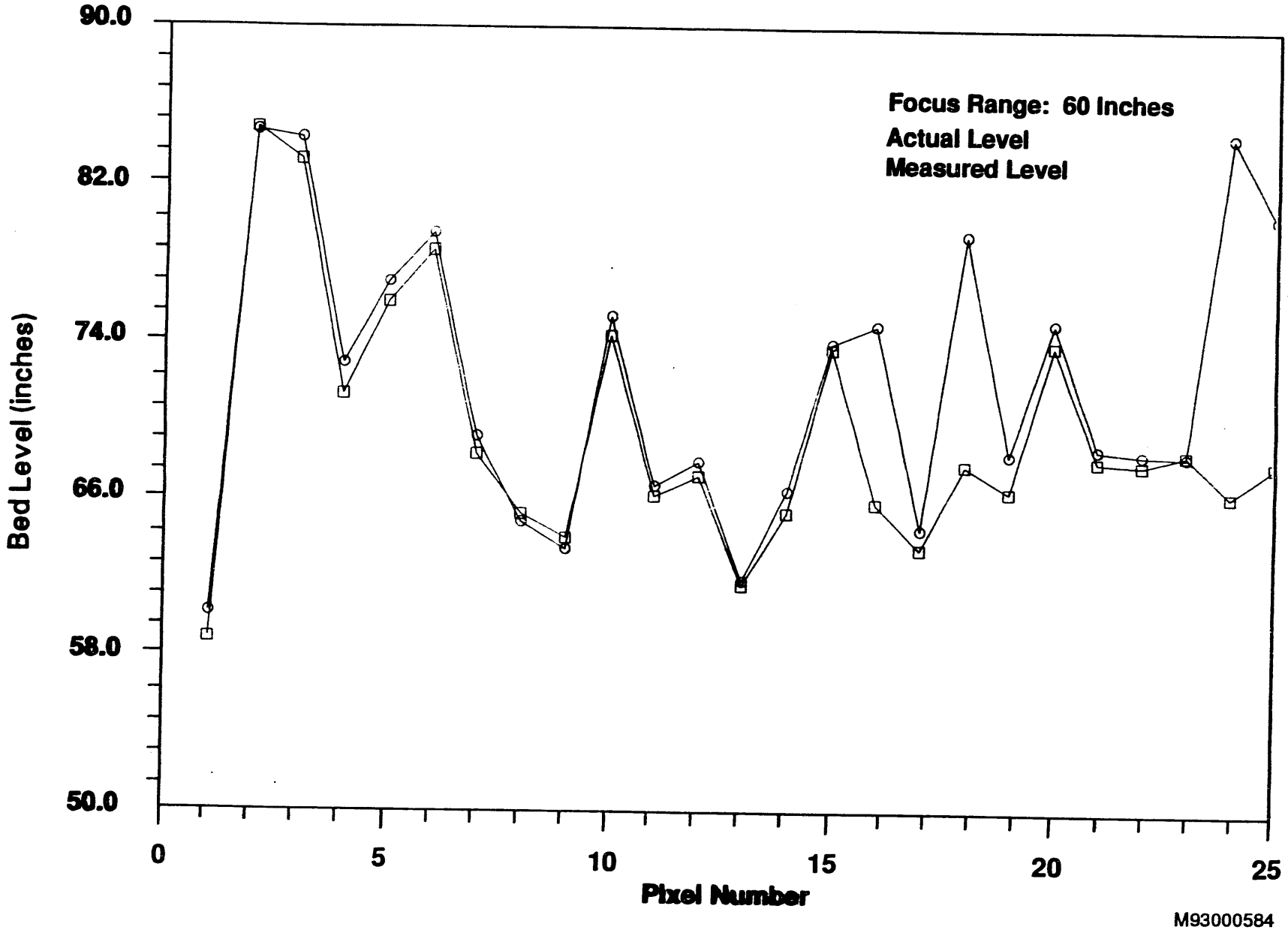

Figure 42. Actual and Measured Bed Levels, All Filters Used, MTB
Focus Range: 60 Inches

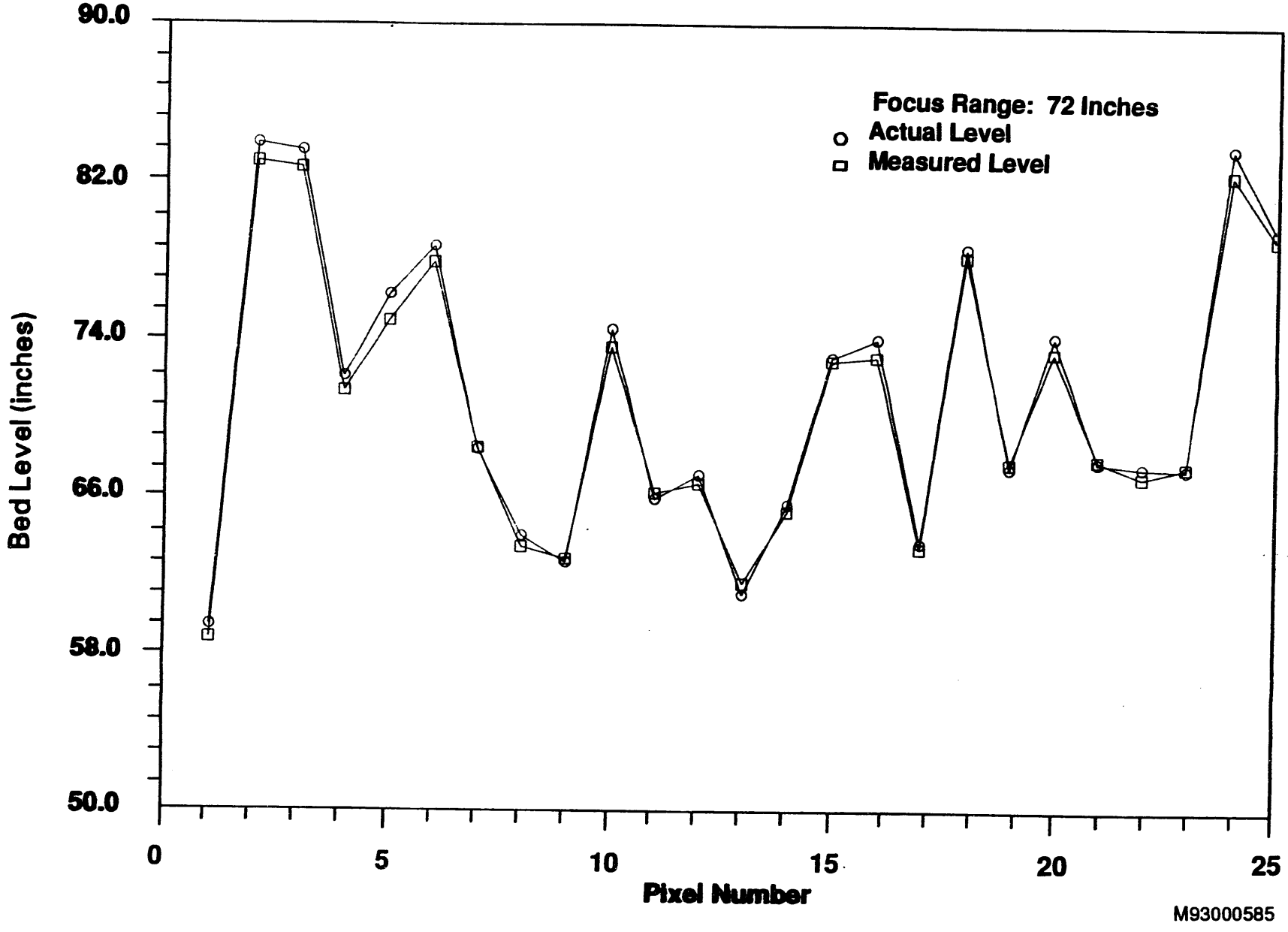

Figure 43. Actual and Measured Bed Levels, All Filters Used, MTB
Focus Range: 72 Inches

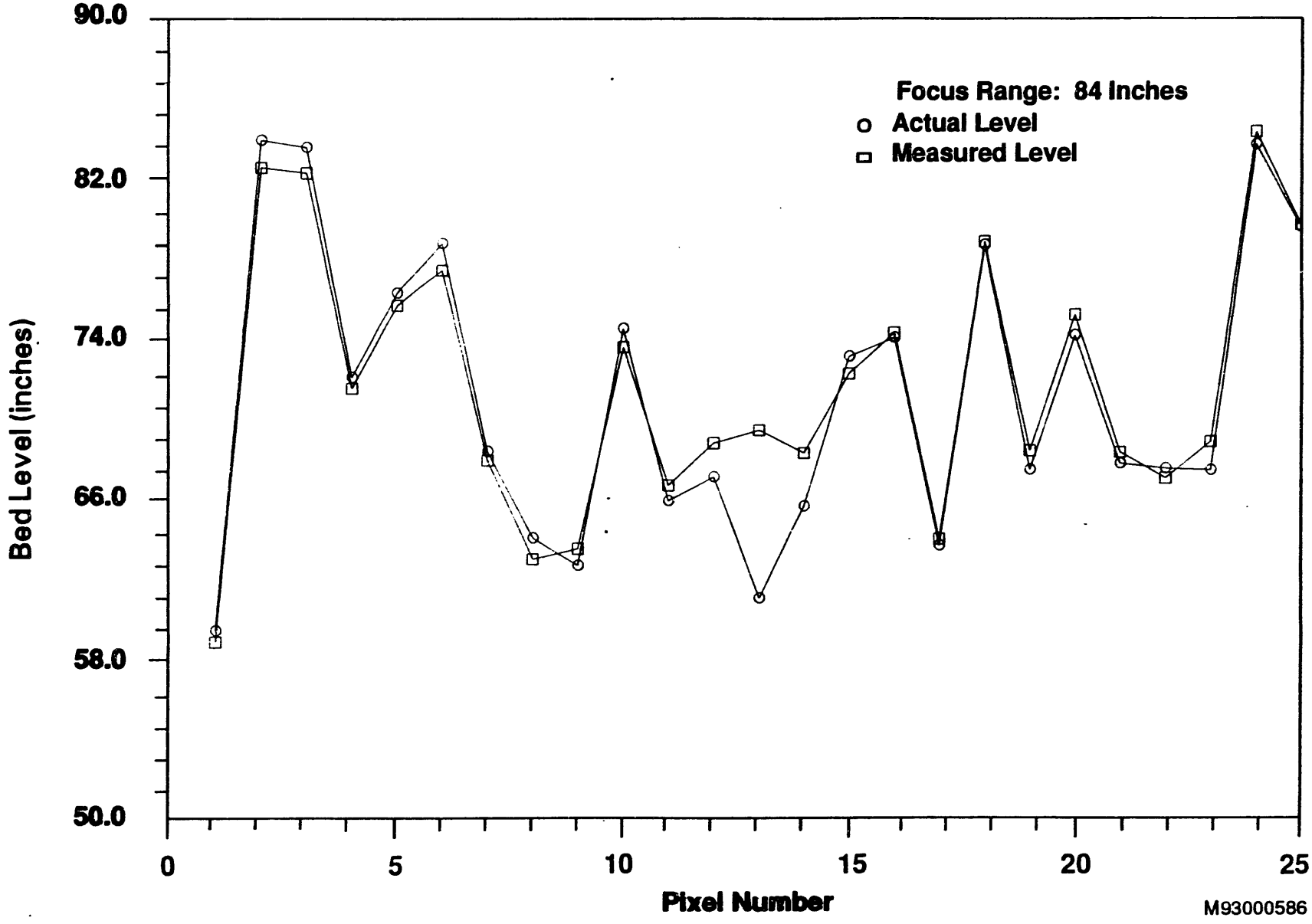

Figure 44. Actual and Measured Bed Levels, All Filters Used, MTB
Focus Range: 84 Inches

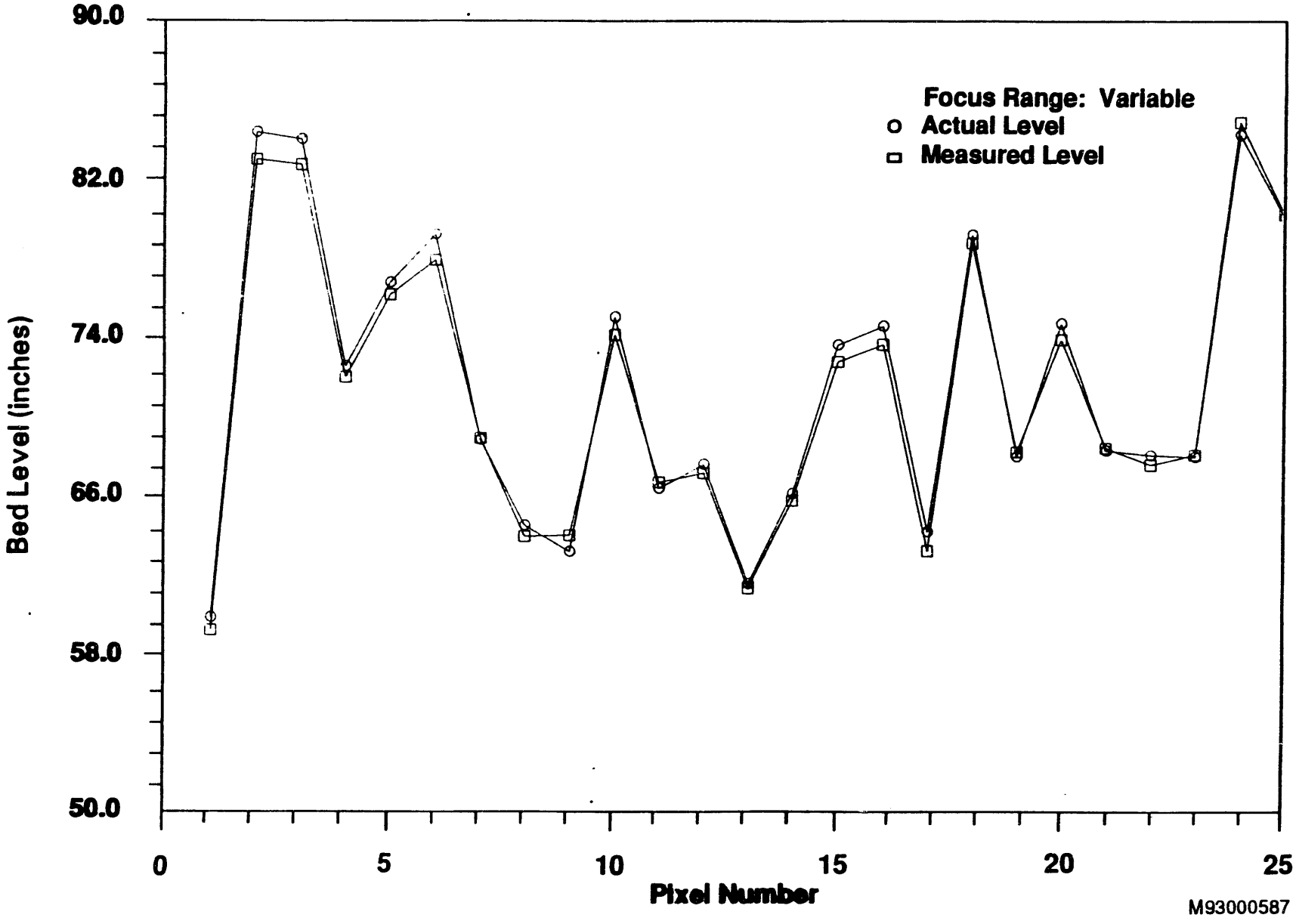

Figure 45. Actual and Measured Bed Levels, All Filters Used, MTB
Focus Range: Variable

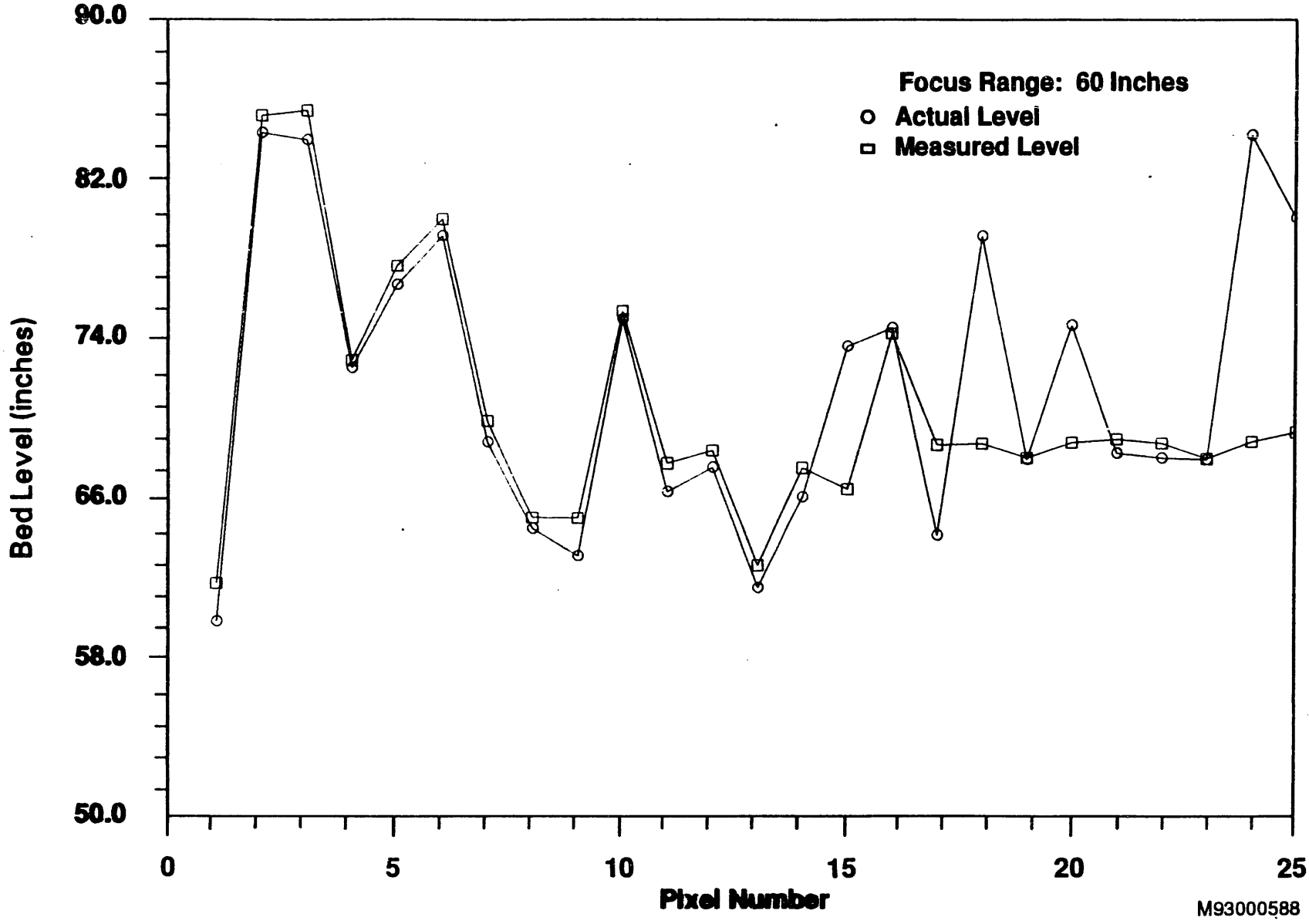

Figure 46. Actual and Measured Bed Levels, Matched Filter Omitted, MTB Focus Range: 60 Inches

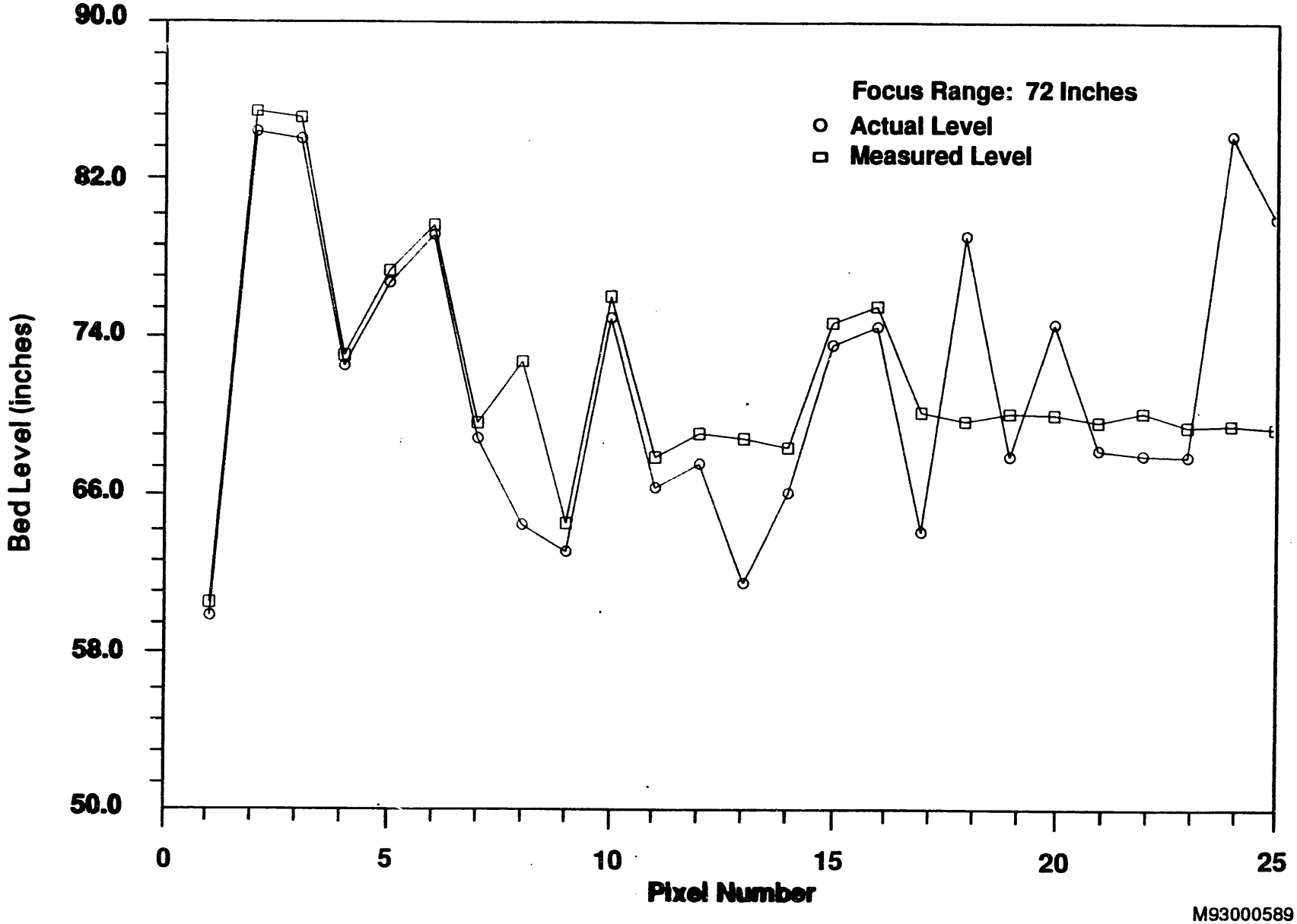

Figure 47. Actual and Measured Bed Levels, Matched Filter Omitted, MTB Focus Range: 72 Inches

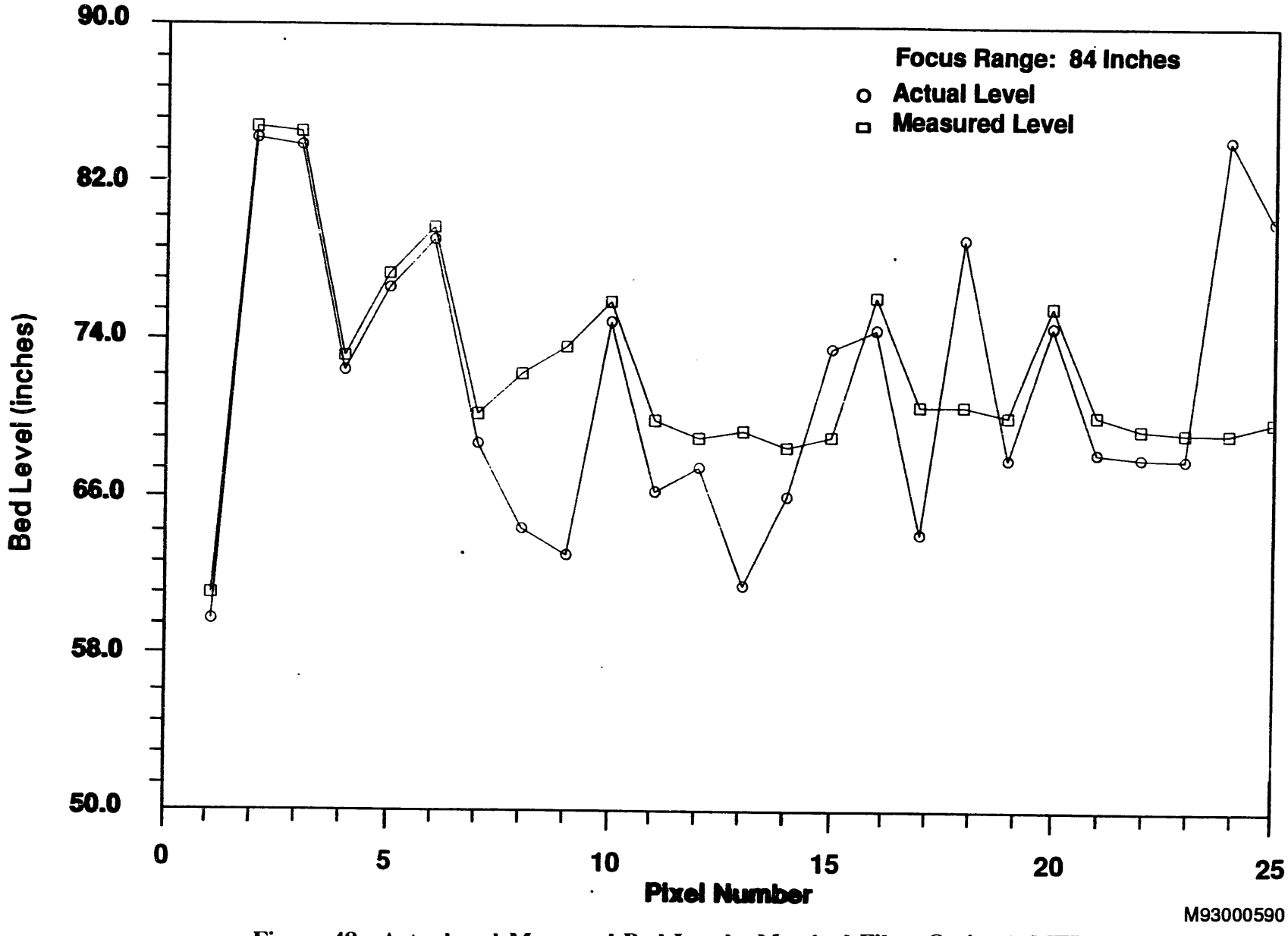

Figure 48. Actual and Measured Bed Levels, Matched Filter Omitted, MTB Focus Range: 84 Inches

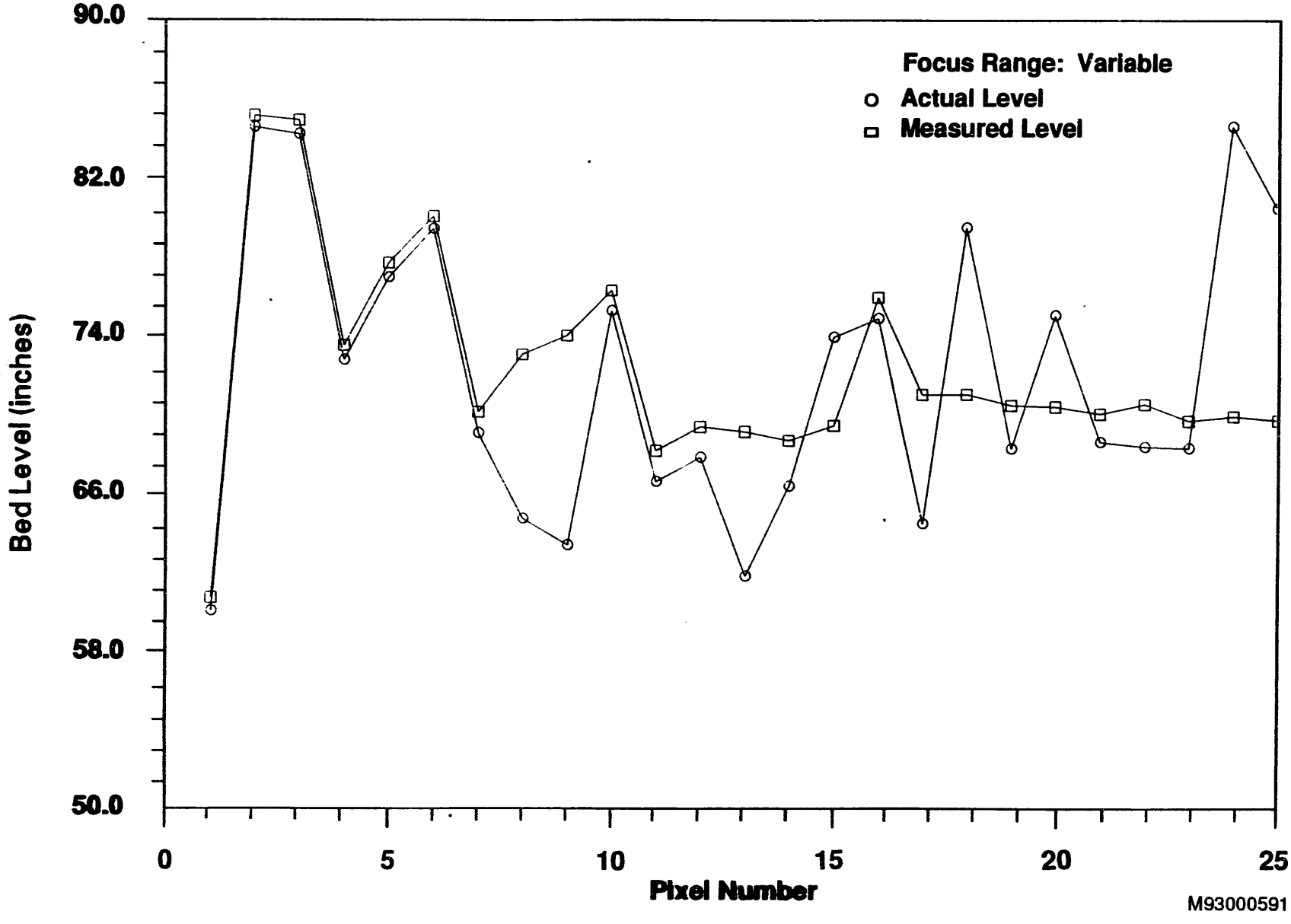

Figure 49. Actual and Measured Bed Levels, Matched Filter Omitted, MTB Focus Range: Variable

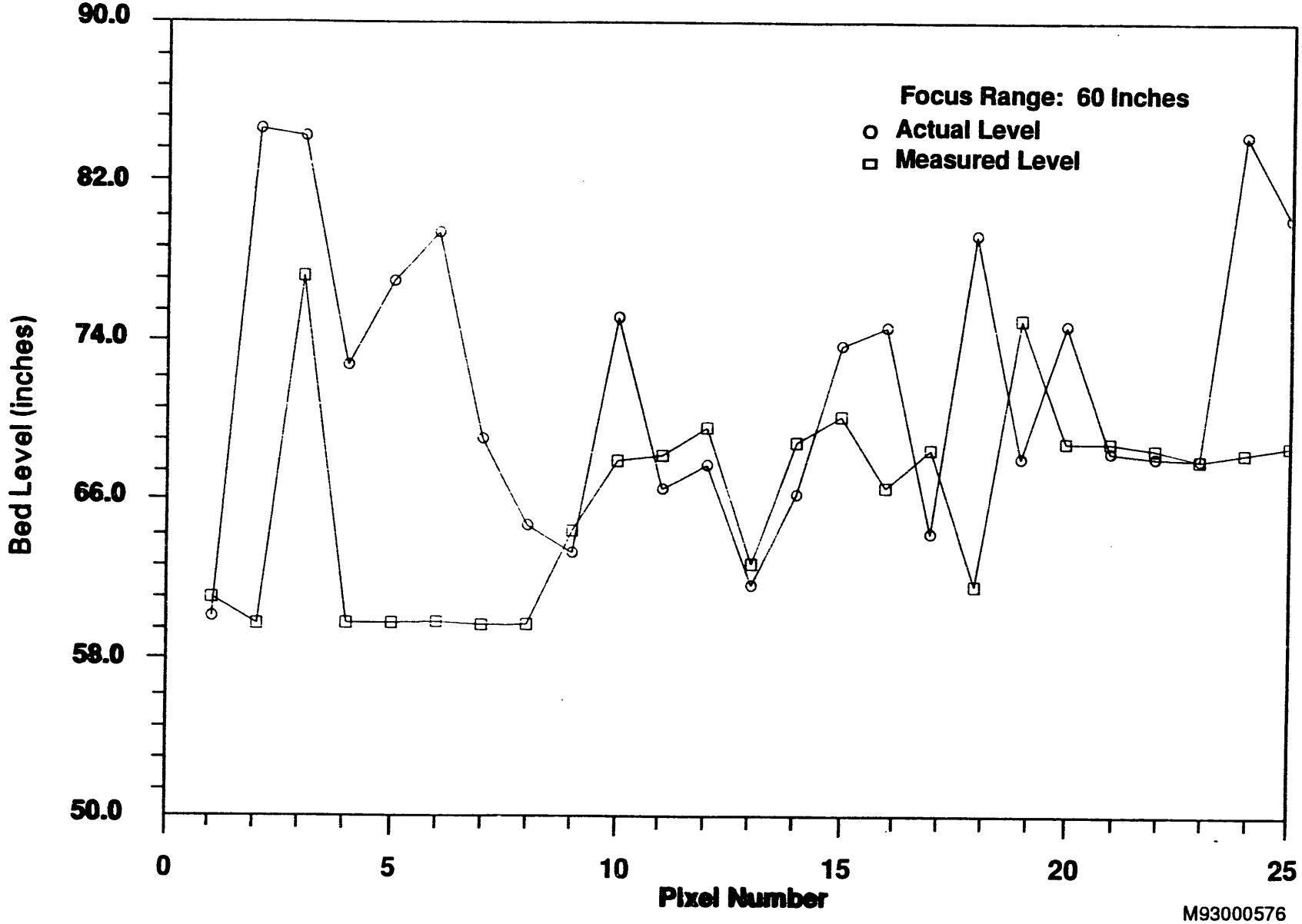

Figure 50. Actual and Measured Bed Levels,
Matched and 2 Low-Pass Filters Omitted, MTB
Focus Range: 60 Inches

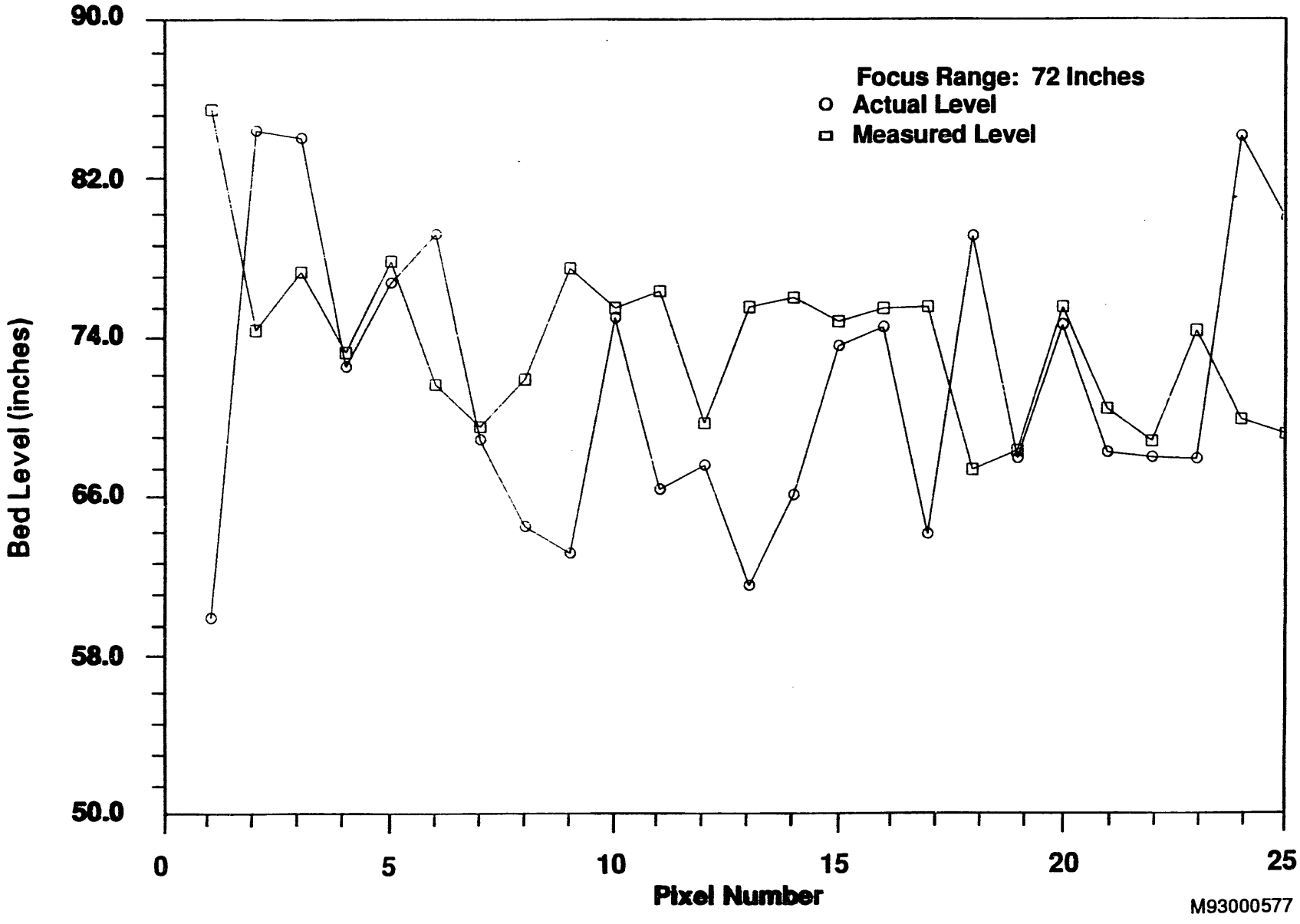

Figure 51. Actual and Measured Bed Levels,
Matched and 2 Low-Pass Filters Omitted, MTB
Focus Range: 72 Inches

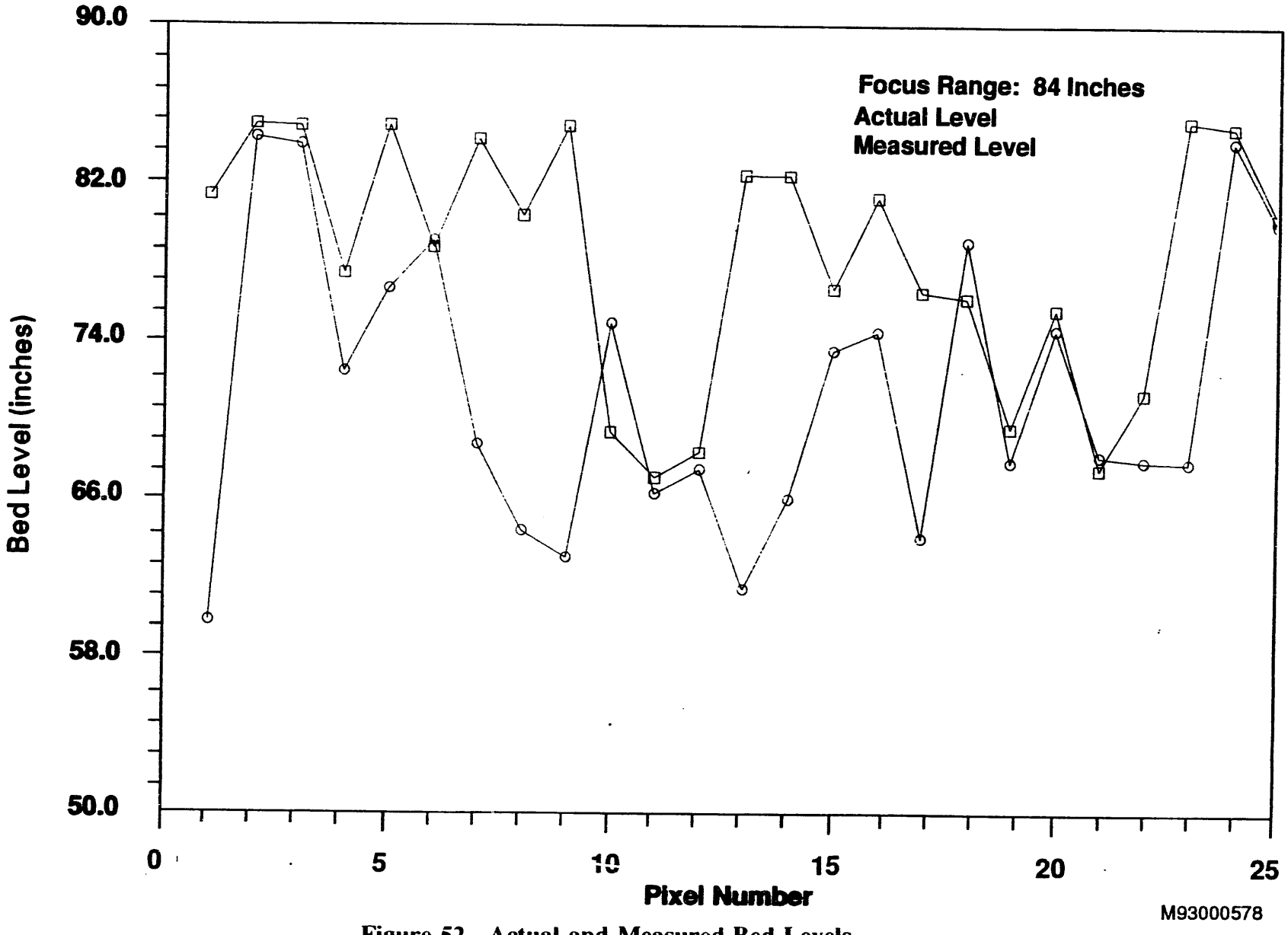

Figure 52. Actual and Measured Bed Levels,
Matched and 2 Low-Pass Filters Omitted, MTB
Focus Range: 84 Inches

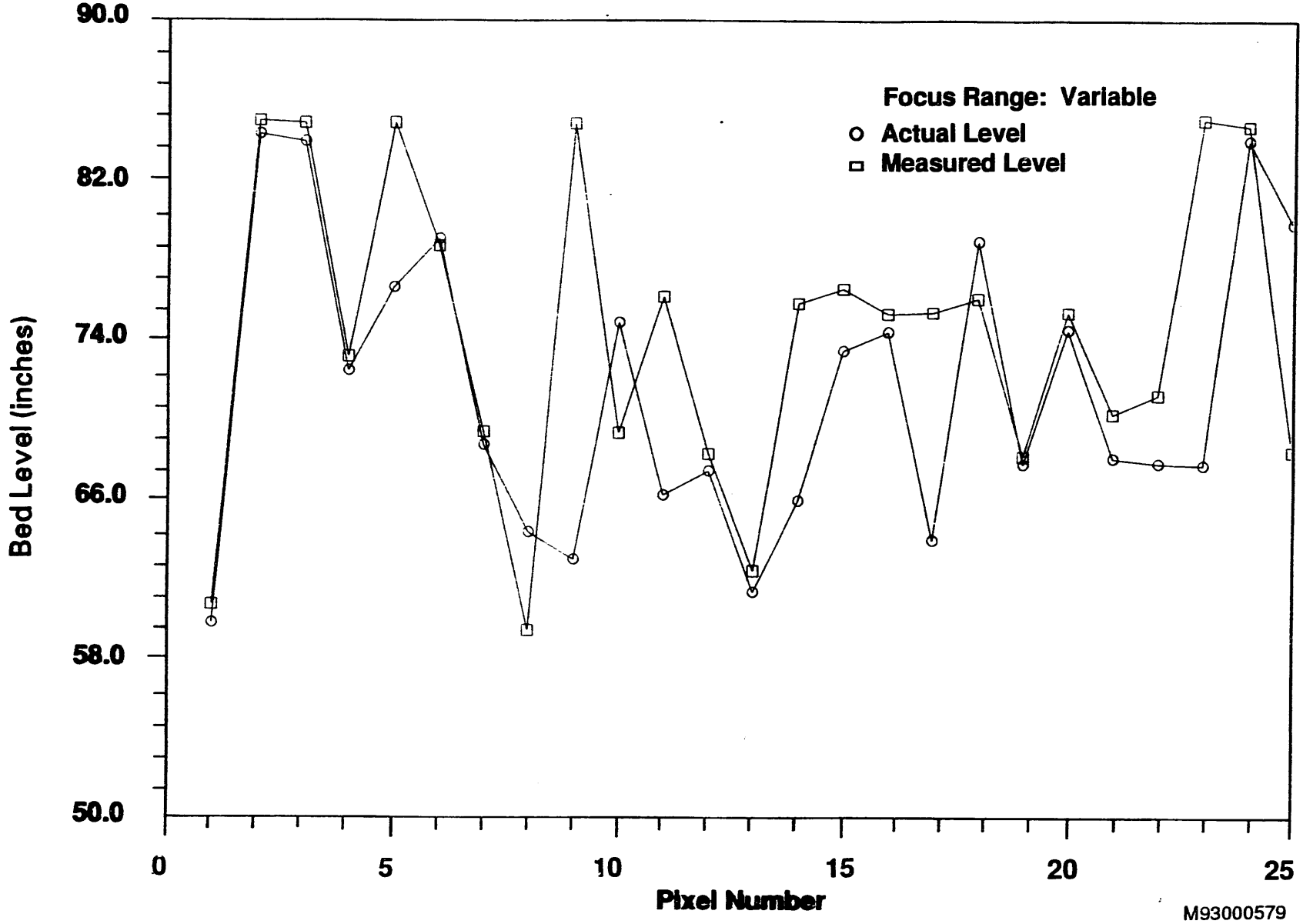

Figure 53. Actual and Measured Bed Levels,
Matched and 2 Low-Pass Filters Omitted, MTB
Focus Range: Variable

END

DATE FILMED

10/6/93